A Methodology for Estimating the Parameters of Steam Turbine Generator Shaft Systems for Subsynchronous Resonance Studies

by

Krishna Sambarapu

A dissertation submitted to the Graduate Faculty of
Auburn University
in partial fulfillment of the
requirements for the Degree of
Doctor of Philosophy

Auburn, Alabama
August 4, 2012

Keywords: Steam Turbine Generator, Parameter Estimation,
Prony's Method, Subsynchronous Resonance, SSR, Electrical Power Systems

Approved by

Mark S. Halpin, Chair, Alabama Power Company Distinguished Professor
R. Mark Nelms, Professor and Chair of Electrical & Computer Engineering Department
Charles A. Gross, Professor Emeritus, Square D Power Professor
University Reader, P. K. Raju, Thomas Walter Distinguished Professor of Mechanical Engineering

Abstract

The increase of coal and nuclear power steam turbines over the past few decades combined with transmission line series capacitors creates a potential drawback known as subsynchronous resonance (SSR) by increasing the risk of interaction between electrical power systems and turbine-generators' rotor torsional systems. Current work presented here adds to a growing body of solutions and preventive measures developed by power industry professionals to address this problem by proposing a new methodology to estimate the shaft spring constants non-intrusively using measurement signals from the shaft systems.

A significant contribution of this work has been in determining, after a thorough investigation of eigen properties of several steam turbine generator shaft systems, which of the non-intrusively available measurement signals, is the best candidate to be used for extracting the shaft torsional modes. The finding that the use of the high-pressure rotor section speed signal is significantly better than the instantaneous power signal in extracting the torsional modes through modal decomposition has been verified using measurement signals obtained from simulations, as well as real measurements. The modal components, which were extracted using Prony's method, were later used along with rotor section moment-of-inertia values to successfully estimate the shaft spring constants of steam turbine generator shaft systems that were simulated in ATP. In addition, an algorithm has been developed to reorder the output modes of Prony's method to identify the power system modes.

Acknowledgments

I would like to express my deepest gratitude to my advisor and mentor, Dr. Mark S. Halpin, without whom this dissertation would not have been possible. I have greatly benefited from his expert guidance, support and owe him immensely for shaping my professional identity. I would also like to thank my committee members Dr. Mark Nelms, Dr. Charles Gross and Dr. P. K. Raju for their inestimable advice and guidance. I am also greatly indebted to Dr. John Hung & Late. Dr. Scott Hodel for their invaluable tutelage in state space control systems.

Most of all, I would like to thank my parents Mr. Sambarapu Narayana and Mrs. Yadamma for their unconditional love, support and countless sacrifices. It is my life's profoundest blessing to have been born as their child. I would also like to express my gratitude to my grandparents, Late. Mr. Madanala Balakistaiah and Mrs Pochamma and Late. Mr. Sambarapu Chennaiah & Mrs. Laxmi. I would also like to thank my brother-in-law & sister, Mr. Botla Maheshwar & Mrs. Anuradha for their constant support and encouragement. I am also greatly indebted to my brothers & sisters-in-law: Mr. Narender Kumar & Mrs. Vani and Mr. Chandra Mohan & Mrs. Pallavi. I would also like to acknowledge my nieces & nephews for making my life richer: Rohith & Haritha, Shashaank & Ojo, Karthik & Nishaant. I would also like to thank all my friends at Auburn University & Mississippi State University and all my relatives for their wonderful support.

Table of Contents

List of Tables

List of Figures

List of Abbreviations

SSR   Subsynchronous resonance

LTI   Linear time invariant

IEEE   Institute of Electrical and Electronics Engineers

FBM   First Benchmark Model

SBM   Second Benchmark Model

STG   Steam turbine generator

STGS   Steam turbine generator shaft

RSV   Rotor section velocity

PM   Prony's Method

GUI   Graphical user interface

HP   High pressure

IP   Intermediate pressure

LPA   Low pressure-A

LPB   Low pressure-B

GENR   Generator

CHAPTER 1

INTRODUCTION

Series capacitor compensation is a scheme used in power systems to alleviate problems that arise because of high reactance of long transmission lines. By reducing effective reactance, it increases transient stability and improves the load carrying capability of these lines. By controlling this reactance it allows better control over load sharing between parallel transmission lines. Because of the advantages it provides economically, it has been used widely in power systems. However, with the increase of coal and nuclear power steam turbines over the past few decades, series capacitors have become a potential drawback by increasing the risk of interaction between electrical power systems and turbine-generators' rotor torsional systems- a phenomenon known as subsynchronous resonance (SSR) or subsynchronous oscillation. "Subsynchronous oscillation is an electric power system condition where the electric network exchanges significant energy with a turbine-generator at one or more of the natural frequencies of the combined system below the synchronous frequency of the system following a disturbance from equilibrium [1]." When these energy interchanges manifest themselves in rotors as pulsating torques, they have the potential to cause irreversible damage to rotor shaft systems such as cracks and fractures. Two such severe incidents occurred in the early 1970s in Nevada's Mohave Generating Station resulting in damaged rotor shafts [2]. As a result, power industry professionals began building a framework of solutions and preventive measures. They developed

definitions [1,3] of the SSR problems, identified the different aspects of SSR, developed the IEEE First Benchmark Model (FBM) [4] and the IEEE Second Benchmark Model (SBM) [5] and performed tests on some turbo-generating (TG) units.

Building preventive measures around SSR frequencies using test simulations requires accurate input data. This data consists of steam turbine rotor shaft system parameters such as moments of inertia, shaft spring constants and the effective dampings due to mechanical hysteresis and system loads. In most cases, the damping is negligible. While moments of inertia can be determined with considerable accuracy, the spring constants are not always precisely known. Traditionally, turbo-generator manufacturers do not provide this information. When requested, the manufacturers estimate or compute these parameters by performing extensive simulations based on the rotor's material composition and physical dimensions and other design parameters. These simulations and tests can also be performed by a third party. Because of the extent of effort and time required, determining spring constants is usually an expensive task. The main focus of this research is to develop a measurement-based methodology to estimate these spring constants without necessitating expensive and intrusive tests. A key advantage of this online measurement method is that it does not require the unit to be taken offline for testing procedures.

This methodology consists of a two-step approach:

- Monitor and record measurements of the instantaneous power at the generator terminals (or available rotor velocity signals) whenever a fault or disturbance occurs. When a large disturbance occurs, it tends to excite all the torsional modes resulting in sustained rotor shaft oscillations at these frequencies for a few seconds. These oscillations can be detected in the measured signals. This recorded ring-down signal is fed to a Prony based

algorithm to extract the modal information - amplitude, phase, frequency and exponential damping - from the signal.

- Using the extracted frequencies and known TG system rotor masses, the necessary shaft spring constants are estimated using a non-linear least squares algorithm.

The different types of SSR phenomena and the types of analysis available to detect these phenomena are reviewed in Chapter 2. Various techniques available to model the entire shaft system will be examined after reviewing the mechanical features of the STG shaft system. One of the main features of this work is the use of Prony's method for modal decomposition instead of the FFT because of its various advantages over the FFT. In Chapter 3 is provided a thorough review, analysis and implementation of Prony's method.

During the course of this work, it was observed that there tend to exist certain general characteristics of STG torsional modes when measured in rotor speed signals or instantaneous power signals. This observation led to the development of a new algorithm, which reorders the output modes of Prony's method and enables the user to differentiate these torsional modes from extraneous signals such as noise etc. This algorithm is presented in Chapter 4.

There are many advantages of Prony's method over the FFT. For instance, it provides modal damping information whereas the FFT does not. However, there are some disadvantages in using Prony's method. The accuracy of its results is compromised by a sensitivity to noise. Moreover, as with any system identification tool, its parameters have to be chosen carefully. These practical issues and their solutions are examined in Chapter 5.

Before the proposed methodology is tested using field data and data obtained from simulations of fully connected test systems consisting of the STG shaft systems and electrical machine models of generators and connected electrical networks, it is very beneficial to study the properties of isolated STG shaft systems. Treating the isolated lumped spring mass model of the STG shaft system as an LTI system, the following three analysis are performed on it:

- Right eigen vector analysis,

- Participation factor analysis, and

- Analysis of impulse response determined by time-domain simulation.

These three analyses are illustrated with the aid of an example shaft system in Chapter 6. The results of a thorough investigation of these three analyses on four STG shaft systems whose data was provided in the literature are presented in Chapter 7. All these STG shaft systems have very similar configuration and overall general characteristics with respect to rotor section moments-of-inertia. This has revealed some extremely useful information that has direct implication to the methodology presented.

In Chapter 8, two test cases will be utilized to illustrate and validate the proposed methodology. These test cases have been built and simulated in ATP and ATPDraw software, which are used by power industry professionals to perform time-domain simulations.

In Chapter 9, the analyses of real field data and the results of modal extraction performed using Prony's method are presented. The real field data consists of instantaneous three-phase power measurements that were obtained from a steam turbine generator unit whose shaft system consists of six rotor sections. It is important to note that this was the only type of field data available for this dissertation work. Rotor section speed signals were not available.

CHAPTER 2

SUBSYNCHRONOUS RESONANCE REVIEW

Although subsynchronous resonance was first mentioned in the literature in 1937 while discussing series capacitors in transmission lines and studying negative damping of electrical machinery [6][7], there were no issues/problems regarding SSR, so it was ignored until 1971. In that year, SSR caused the shaft failure of a turbine-generator shaft in the Mohave Generating Station in Nevada.

Tacoma Narrows bridge (Washington, US) collapsed in 1940 because of resonance induced by wind, which coincided with the bridge's natural frequency, causing extremely large amplitude swings and ultimately the collapse of the bridge. SSR is a similar dynamic phenomenon which involves the TG mechanical shaft system and the electrical network that contains series capacitors coupled electromagnetically to the generator described by Park's equations. Electrical quantities in any electrical circuit can be classified into two components, (1) forced and (2) natural, as follows:

$$i(t) = A_1 \cos(\omega_1 t + \phi_1) + A_2 e^{-\alpha_2 t} \cos(\omega_2 t + \phi_2)$$

While the ω_1 frequency is determined solely by the network's driving or active sources, the ω_2 frequency is dependent completely on the network parameters. In a transmission system, these network parameters include the transmission line reactance, capacitance and the sub transient reactance of the generator. These currents flowing through the generator armature create slip

frequency torques in the TG rotor because of Park's equations. When the frequencies of these slip frequency torques nearly coincide with any of the natural frequencies of the TG shaft system, it has the potential to cause serious damage, including loss of fatigue life or even cracks in the rotor. The Mohave incident refers to a TG shaft system failure that occurred in the early 1970s because of self-excited torsional oscillations in the TG shaft system. It occurred in the 500 KV coal-fired Mohave Generating Station in Nevada, U.S.A., which consisted of two 798 MW steam turbine generating units. The generating station was radially connected to the load, and the fault occurred when one of the two radial long transmission lines was opened with the other line containing series capacitors in place. The opening of the line induced heavy currents in the other line, which, along with the generator, transmission line and series capacitor, formed an LC tank circuit and thus induced 29.5 Hz current in the generator armature. These currents in turn induced 30.5 Hz undamped torques in the TG shaft. The resulting damage included circumferential cracks one inch deep, melting or burning of the TG shaft and burning of collector rings. One of the immediate remedies included removal of series capacitors and installing a TEX type relay, which tripped the unit when SSR current flowed in the armature. But, because of the loss of transient stability, the removal of the series capacitors was not deemed correct, and a permanent solution of installing resistive filters was proposed.

2.1 Types of SSR Phenomena

There are many types of subsynchronous resonance phenomena. Three of them are considered important, namely:

1. Induction generator effect,
2. Torsional interaction, and

3. Transient torque.

As mentioned before, these are SSR phenomenon, i.e. they include series capacitors in lines.

The first two can be considered small signal phenomena (during the initial stages of a fault) and hence can be analyzed using linear analysis tools like Eigen analysis. The third is a non-linear phenomenon which will require a more detailed study. The first one does not include TG modal interaction, i.e. it occurs when the rotor is running at synchronous speed. The latter two involve TG modal interaction.

Induction generator effect

Any disturbance causes transient currents to flow through the electrical network and generator armature at the combined network's natural frequencies, both above and below the synchronous frequency. When the subsynchronous frequency currents flow through the generator armature, they view the synchronously rotating rotor's circuit as negative resistance. If this negative resistance is greater than the positive resistance encountered in the network and generator armature, the net negative resistance will give rise to high amplitude sustained subsynchronous currents.

Torsional Interaction

This phenomenon involves torsional modal interaction. As mentioned previously, any electrical disturbance causes subsynchronous fault currents to flow through generator armature. When these induce subsynchronous torques in the rotor which coincide with the rotor's natural modes, they induce rotor oscillations at these subsynchronous frequencies. These induce voltages in the

generator armature at the subsynchronous frequencies and are sustained when they are in phase. If the magnitudes of these self-excited subsynchronous torques are large enough to overcome the overall mechanical damping involved, they will have the potential to cause large amplitude oscillations that can damage the rotor. This phenomenon was responsible for the Mohave incident.

Transient Torque

This non-linear phenomenon is caused by large short circuit currents that oscillate at one of the system's natural frequencies (resulting from system disturbances). Because resultant rotor torques induced are directly proportional to these disturbance currents, the resulting peak torques can be quite large and have the potential to cause irreversible damage to the rotor.

2.2 SSR Analysis Methods

Frequency Scanning Technique

The frequency scanning technique is a small signal analysis tool that computes the reactance and resistance as a function of frequency looking into the network from behind the stator winding. It is especially suitable for detecting IGE conditions. When, at a particular frequency, the computed reactance is nearly equal to zero and the resistance is less than zero, i.e. negative, then IGE induced stator currents can be expected. It can also aid in detecting torsional interaction and transient torque phenomenon, which could occur when there is series resonance or a reactance minimum. Because of its simplicity, it is widely used in preliminary studies in North America.

Eigen Analysis

Another popular method of studying SSR problems is eigen analysis. In this method, the entire system is mathematically modeled using a single set of linear differential equations. These linear equations are solved using numerical analysis tools like singular value decomposition (SVD) to yield the eigen values of all system components involved. This has the advantage over frequency scanning techniques in that the eigen values provide damping as well as frequency values; any positive real values of eigen values will immediately inform the engineer of a potential unstable mode in the system.

EMTP/ATP/ATPDraw analysis

The EMTP/ATP simulation program is a very powerful software tool for analyzing SSR conditions. Because it uses stepwise numerical integration of differential equations, it allows the user to enter into the program detailed attributes of each component in the system. Instead of using linear approximations (like eigen analysis and frequency scan), this software models all the non-linear attributes of complex components involved in the system study. Also, in comparison to other stability programs, which use per phase or positive sequence models, it uses three-phase information allowing simulation/modeling of unbalanced events. Because it can model non-linear phenomenon it is most suitable for transient torque analysis. The resulting plots of the simulation results yield amplitude information of electrical quantities, in addition to frequency and damping.

2.3 Steam Turbine Description

The invention of steam turbine is attributed to Carl Gustav de Laval of Sweden and Charles Parson of Great Britain during the 1880s independently. Over the decades, steam turbines have grown in size and complexity. Whereas, the typical ratings for large steam turbines prior to the 1950s was less than 200 MW, modern large ST ratings can exceed 1200 MW. In contrast to older units, most modern STs rarely contain gear boxes and so their total length can exceed 150 ft (in the case of tandem units) and their weight can be in the range of several hundred tons [8]. The rotors are usually made of Cr.Mo.V steel and are either forged or welded. The entire rotor system can contain, in addition to the rotor, a multitude of other parts such as turbine blades, discs, retaining rings, etc.. As a result, the rotor system might contain an infinite number of modes of torsional vibration [8]. However, most of these modes interact with higher frequency electrical torques and can be safely ignored for SSR studies. Because of the extremely large power output (>1000 MW), the system is divided into multiple stages of turbine cylinders and shafts, each producing a part of the total output. There are generally two such types of compound units (1) Tandem-compound and (2) Cross compound units. In tandem compound units, all the cylinders are on a single shaft. Consequently, the total length of the shaft can be very large, since it includes many stages (sometimes exceeding 10 stages) in addition to the generator and exciter. The cross-compound unit contains two shafts which allow for lesser rating and reduced total shaft length. However, they have a disadvantage in that they need two separate sets of generator and exciter controllers, one for each shaft.

2.4 TG Shaft System Modeling

SSR is caused by series capacitors in transmission lines. This compensation is such that the total capacitive reactance is less than the total line reactance (usually less than 70%). This leads to SSR frequencies less than 60 Hz. This, in turn, greatly helps simplify the modeling requirements of the TG shaft.

There are three types of TG system models. They are:

1.   Lumped spring mass models,

2.   Advanced continuum models, and

3.   Finite element analysis (FEA) models.

While the first two are theoretical analytical models, the third one is a computational/numerical model. All three models lead to methods which involve assembling sets of linear differential equations and applying equations of equilibrium based on Hooke's law and Newton's laws of dynamics to determine eigen values and eigen vectors (mode shapes).

In the lumped spring mass model, each stage of the turbine (HP, IP etc) as a whole is modeled as a rigid rotating mass, which is connected by massless springs representing the shaft sections. In the advanced continuum model, each rotor disk in each turbine stage is modeled as a rigid mass. Thus, the entire model might contain hundreds of linear differential equations. This fact is further confirmed in FEA analysis.

Finite element analysis is a computational technique generally used by manufacturers for mechanical design purposes. Here, all the rotor's segments, such as turbine blades, retaining

rings, etc, are modeled as discrete regions linked in a geometric model representing the entire turbine generator shaft. The results of these models reasonably match those of the basic lumped spring mass model. This allows us to use the lumped mass model in SSR analysis methods.

2.5 Conclusion

In conclusion, the history, the theory of SSR and the different types of analysis tools commonly used in power industry are reviewed in this chapter. Eigen analysis and time-domain simulation methods using ATP/EMTP have been used extensively to examine the characteristics of the shaft torsional and electrical systems involved. While FEA and advanced continuum models are useful, this work, like most SSR analysis in power industry, uses lumped spring-mass models, which yields sufficient information to aid in analysis and building of SSR preventive measures. Prony's method, reviewed in the next chapter, is then used for modal decomposition of signals obtained from time-domain simulations of lumped spring-mass models.

CHAPTER 3

REVIEW OF PRONY'S METHOD

Prony's method used in this work is an exponential parameter estimation technique. It is used to fit a linear combination of exponential terms to a uniformly sampled signal, thereby extracting the four parameters for each mode from the signal: amplitude, phase, frequency and exponential damping [9][10][11]. This technique was developed in the 1790s by Baron de Prony. However, because it was computationally expensive, it was not applied until the advent of modern fast and efficient computers. Ever since, it has been a practical tool in the field of modern spectrum analysis [11]. However, it is only during the last two decades that it found practical use in power system applications, such as extracting modal information from transient stability programs and system field tests [10]. Because this method also extracts modal damping coefficients, it has an advantage over Fourier analysis for the analysis of electromechanical oscillations that routinely involve exponentially decreasing (or increasing) waveforms.

3.1 History and Literature Review

Prony's Method was invented by Gaspard Clair François Marie Riche de Prony, who was a French mathematician at École Polytechnique in the 18th century. He used the method as described in [12], which fitted a sum of exponentials to a set of equally spaced data points, in his work on expansion of gases. After the original paper by Prony, [9] is one of the earliest texts on

the subject in the 1900s. Hildebrand wrote this in the 1950s as part of describing other approximation procedures in this numerical analysis book. It is presented as an exponential approximation technique, which simplifies the solution of a set of non-linear equations into a much simpler three-step process involving two least-squares solutions and one polynomial root-finding process. After that, Prony's analysis (PA), was considered a good tool among the 11 tools used for spectrum analysis, along with Blackman-Tukey, ARMA etc.

Different interpretations were provided for PA. It was considered that the exponential approximation is the homogenous solution of a non-homogenous constant coefficient linear difference equation. It was found that pre-filtering vastly improved the accuracy of PA results because PA is found to be highly sensitive to noise. In one application it was used after applying a moving average smoothing filter to the extraction of modal parameters in South African tie-line power swings and German faulty neutral-to-ground resonant voltage measurements.

Kumaresan showed that it was possible to create a pre-filter out of the data samples themselves and used it to pre-filter the data samples. In [10] Prony's method was introduced to the field of power systems. In it, the authors introduce Prony's method to the field of power system computations as a complement to eigen analysis and Fourier analysis. Also in the paper, the authors describe the method mathematically, list the strategic issues and shortcomings, and partially validate, with test cases, its viability as a modal analysis tool for transient stability program output.

3.2 Prony's Method Description

Prony's method is an exponential approximation technique that is used to fit a function consisting of a linear combination of exponentially damped sinusoids to a given linearly spaced

data sample set [9,10,11]. Extensive developments during the past few decades in linear prediction theory, especially in speech processing, have provided new interpretations to the original method [13,14,11].

Prony's method can be best explained using the example of an LTI system such as the lumped spring-mass model of the turbo-generator rotor shaft shown in Figure 3-1. Its dynamics are represented by the differential equation for the jth rotor mass shown in (3.1)

$$J_j \frac{d\Delta\omega_j}{dt} = \Delta T_j - K_{ij}\left(\Delta\theta_i - \Delta\theta_j\right) - K_{jk}\left(\Delta\theta_j - \Delta\theta_k\right)$$

$$- D_j\Delta\omega_j - D_{jk}\left(\Delta\omega_j - \Delta\omega_k\right) - D_{ji}\left(\Delta\omega_j - \Delta\omega_i\right) \tag{3.1}$$

In (3.1), J_i and K_{ij} represent the moment of inertia of the ith rotor section and the spring constant of the shaft connecting the ith and j[th] rotor sections, respectively. D_i and D_{ij} represent the damping coefficients. $\Delta\omega_i$, $\Delta\theta_i$ and ΔT_i represent the incremental angular velocity, angular displacement and input torque of the ith rotor mass, respectively.
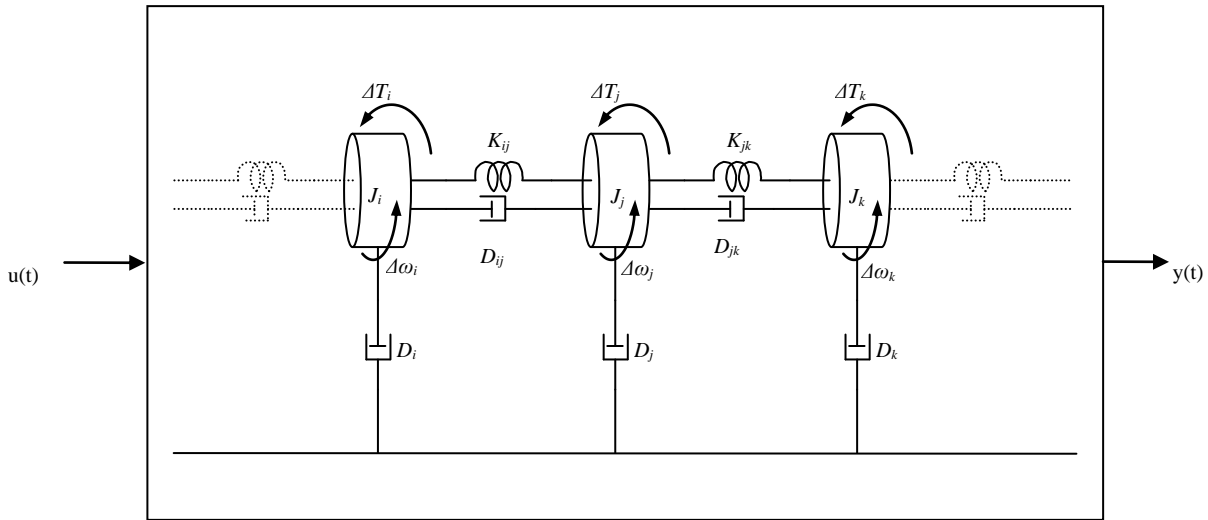
Figure 3-1. Lumped Spring-Mass Model of the Turbine-Generator Shaft [15]

These dynamics can be rewritten in state space form as given in (3.2).

$$\frac{d\tilde{x}(t)}{dt} = [A]\tilde{x}(t) \tag{3.2}$$

In (3.2), the $\tilde{x}(t)$ are the states of the system consisting of n states ($\Delta\omega_i$ & $\Delta\theta_i$) and $[A]$ is the state transition matrix. Assuming the states of the system are brought to an initial state $\tilde{x}_0(t)$ and any further disturbances or inputs (ΔT_i) are removed, then the states of the system can be described by (3.3).

$$\tilde{x}(t) = \sum_{i=1}^{n}\left(\tilde{q}_i^T\tilde{x}_0(t)\right)\tilde{p}_i e^{\lambda_i t} = \sum_{i=1}^{n}\left([R_i]\tilde{x}_0(t)\right)e^{\lambda_i t} \tag{3.3}$$

In (3.3), λ_i, $\tilde{p}_i$ and $\tilde{q}_i$ are the ith eigen value, right eigen vector and left eigen vector, respectively [10].

The output of this system $y(t)$ is given by (3.4).

$$y(t) = [C]\tilde{x}(t) = [C]\sum_{i=1}^{n}\left(\tilde{q}_i^T\tilde{x}_0(t)\right)\tilde{p}_i e^{\lambda_i t} = [C]\sum_{i=1}^{n}\left([R_i]\tilde{x}_0(t)\right)e^{\lambda_i t} \tag{3.4}$$

In (3.4), $[C]$ and $[R_i]$ are the output matrix of the LTI system and its ith residue matrix.

Let $y(k)$ be the measured signal for $y(t)$ consisting of N equally spaced samples at intervals $k=0,1,2,...N-1$. The $y(t)$ equation shows this exponential nature of individual components in the output. Prony's method tries to address this nature by fitting a similar structure to the measured output as shown in (3.5).

$$\hat{y}(t) = \sum_{i=1}^{p}B_i e^{\lambda_i t} \tag{3.5}$$

This exponential structure, which can also be presented as a sum of exponentially damped sinusoids shown in (3.6), is thus suitable to estimate the individual properties like frequencies and dampings of modes in the turbo-generator shaft's output signals.

16

$$\hat{y}(t) = \sum_{i=1}^{Q} A_i e^{\sigma_i t} \cos(2\pi f_i t + \varphi_i) \tag{3.6}$$

In (3.6), A_i, σ_i, f_i, φ_i are the amplitude, exponential damping, frequency and phase values of the ith modal component.

The discrete-time version $\hat{y}(k)$ for $\hat{y}(t)$ can be written in a convenient form as shown in (3.7).

$$\hat{y}(k) = \sum_{i=1}^{P} B_i z_i^k \tag{3.7}$$

In (3.7), z_i is the exponential part of the modal component as shown in (3.8).

$$z_i = e^{\lambda_i \Delta t} \tag{3.8}$$

Expanding (3.7) for sample instants $k=0,1,2\ldots N-1$ gives (3.9).

$$y(0) = B_1 + B_2 + B_3 + \cdots + B_n$$

$$y(1) = B_1 z_1 + B_2 z_2 + B_3 z_3 + \cdots + B_n z_n \tag{3.9}$$

$$y(2) = B_1 z_1^2 + B_2 z_2^2 + B_3 z_3^2 + \cdots + B_n z_n^2$$

$$\ldots$$

$$y(N-1) = B_1 z_1^{N-1} + B_2 z_2^{N-1} + B_3 z_3^{N-1} + \cdots + B_n z_n^{N-1}$$

Rewriting (3.9) in matrix form gives (3.10).

$$\begin{bmatrix} y(0) \\ y(1) \\ \vdots \\ y(N-1) \end{bmatrix} = \begin{bmatrix} B_1 z_1^0 + \cdots + B_n z_n^0 \\ B_1 z_1^1 + \cdots + B_n z_n^1 \\ \vdots \\ B_1 z_1^{N-1} + \cdots + B_n z_n^{N-1} \end{bmatrix} = \begin{bmatrix} z_1^0 & z_2^0 & \cdots & z_n^0 \\ z_1^1 & z_2^1 & \cdots & z_n^1 \\ \vdots & \vdots & \vdots & \vdots \\ z_1^{N-1} & z_2^{N-1} & \cdots & z_n^{N-1} \end{bmatrix} \begin{bmatrix} B_1 \\ B_2 \\ \vdots \\ B_n \end{bmatrix} \tag{3.10}$$

$$[Y]=[Z][B] \tag{3.11}$$

In (3.11), Y, B and Z represent matrices as shown in (3.12).

$$Y = \begin{bmatrix} y(0) \\ y(1) \\ \vdots \\ y(N-1) \end{bmatrix}, \ B = \begin{bmatrix} B_1 \\ B_2 \\ \vdots \\ B_n \end{bmatrix}, \ Z = \begin{bmatrix} z_1^0 & z_2^0 & \cdots & z_n^0 \\ z_1^1 & z_2^1 & \cdots & z_n^1 \\ \vdots & \vdots & \vdots & \vdots \\ z_1^{N-1} & z_2^{N-1} & \cdots & z_n^{N-1} \end{bmatrix} \tag{3.12}$$

The procedure for Prony's method formulated in linear prediction theory to solve the linear equations (3.10) for B_i's and z_i's can be summarized in the following steps [10]:

(1) Build a linear prediction model (LPM) for $y(k)$ where the nth sample is a function of n past samples and unknown prediction coefficients $\{\alpha_1, \alpha_2, ...\alpha_n\}$

$$y(n) = \alpha_1 y(n-1) + \alpha_2 y(n-2) + \cdots + \alpha_n y(0) \tag{3.13}$$

Apply this model for all successive samples as shown in (3.14).

$$y(n+1) = \alpha_1 y(n) + \alpha_2 y(n-1) + \cdots + \alpha_n y(1)$$

$$\cdots \tag{3.14}$$

$$y(N-1) = \alpha_1 y(N-2) + \alpha_2 y(N-3) + \cdots + \alpha_n y(N-n-1)$$

Rearranging (3.14) in matrix form gives (3.15)

$$\begin{bmatrix} y(n-1) & y(n-2) & \cdots & y(0) \\ y(n-0) & y(n-1) & \cdots & y(1) \\ y(n+1) & y(n-0) & \cdots & y(2) \\ \vdots & \vdots & \ddots & \vdots \\ y(N-2) & y(N-3) & \cdots & y(N-n-1) \end{bmatrix} \begin{bmatrix} \alpha_1 \\ \alpha_2 \\ \vdots \\ \alpha_n \end{bmatrix} = \begin{bmatrix} y(n+0) \\ y(n+1) \\ y(n+2) \\ \vdots \\ y(N-1) \end{bmatrix} \tag{3.15}$$

(2) Solve the LPM shown in (3.15) to find the predictor coefficients $\{\alpha_1, \alpha_2, ...\alpha_n\}$.

The α's in the linear equations shown in (3.15) can be solved directly if $N=2n$ or by the method of least squares if $N>2n$

(3) Construct the LPM's associated characteristic polynomial $P(z)$ using the predictor coefficients as shown in (3.16)

$$P(z) = z^n + \alpha_1 z^{n-1} + \alpha_2 z^{n-2} + \cdots \alpha_n \tag{3.16}$$

(4) Determine the roots of the polynomial $P(z)$. These roots are the required complex frequencies z_i [9] [10].

(5) Substitute z_i and $y(k)$ in (3.10) and solve the resulting linear equations by using the least squares method to determine B_i.

 (6) Substitute z_i in (3.8) to find λ_i.

MATLAB Implementation of Prony Analysis

The basic Prony's method has been implemented in MATLAB the following way.

```
| 1 |   function [ vrMagn_n_PhaseRad, vrFreqRad_n_Decay, Dc_offset ] = PronySimple3( t, fn_data,
timestep, numModes )
| 2 |
| 3 |   N = length(fn_data);
| 4 |   init_f = fn_data(1);
| 5 |   fn_data = fn_data(2:N)-fn_data(1:N-1);
| 6 |   numDataPoints = length(fn_data);
| 7 |
| 8 |   % A : #cols = number of modes
| 9 |   % A : #rows = number of data points - number of modes
|10 |
|11 |   A = zeros( numDataPoints-numModes, numModes);
|12 |
|13 |   for r = 1:numDataPoints-numModes
|14 |       for c = 1:numModes
|15 |           A(r,numModes-c+1) = fn_data(c+r-1);
|16 |       end
|17 |   end
|18 |
|19 |   % B is always a column vector (only one column)
|20 |   % #rows = number of data points - number of modes
|21 |   B = zeros( numDataPoints-numModes, 1);
|22 |
|23 |   for r = 1:numDataPoints-numModes
|24 |       B(r,1) = -fn_data(numModes+r);
|25 |   end
|26 |
|27 |   X = A\B;
|28 |
|29 |   mu_ =roots([ 1 transpose(X)]);
|30 |
|31 |
|32 |   vrFreqRad_n_Decay = log(mu_)/timestep;
|33 |
|34 |   % M : #cols = number of modes
|35 |   % M : #rows = number of data points
|36 |   M = zeros(numDataPoints, numModes);
|37 |
|38 |   for r = 1:numDataPoints
|39 |       for c = 1:numModes
|40 |           M(r,c) = (mu_(c)-1)   *   (mu_(c) )^(r-1);
|41 |       end
|42 |   end
|43 |
|44 |   % F is always a column vector (only one column)
|45 |   % #rows = number of data points
|46 |
```

```
|47 |   vrMagn_n_PhaseRad = M \ transpose(fn_data)  ;
|48 |
|49 |
|50 |   Dc_offset = init_f - sum(vrMagn_n_PhaseRad);
|51 |
|52 |
|53 |   return
|54 |
|55 |
```

The original PA fits a sum of complex sinusoids to a given f(t). But, when a dc offset is present

in the signal the algorithm needs some modifications. These modifications are done in the lines

4, 5 and 50 as follows:

```
| 4 |   init_f = fn_data(1);
| 5 |   fn_data = fn_data(2:N)-fn_data(1:N-1);
…
|50 |   Dc_offset = init_f - sum(vrMagn_n_PhaseRad);
|51 |
```

The overall structure of the code can be be divided into mainly 3 parts:

1: Solution of N>n linear equations in the form of AX=B to determine α's in (3.15);

2: Solving for the roots of an nth degree polynomial; and

3: Solution of N>n linear equations in the form of AX=B to determine magnitudes and phase

angles.

In both the cases of solving the linear equations, it is necessary to use the SVD method (svd()

command in MATLAB) to accurately compute the solution for these equations. The main reason

for that is because the matrices are essentially Vandermonde matrices and hence they are highly

singular relative to a computer's working precision. These changes are shown as follows:

```
|11 |   A = zeros( numDataPoints-numModes, numModes);
|12 |
|13 |   for r = 1:numDataPoints-numModes
|14 |       for c = 1:numModes
|15 |           A(r,numModes-c+1) = fn_data(c+r-1);
|16 |       end
|17 |   end
|18 |
|19 |   % B is always a column vector (only one column)
```

```
|20 |  % #rows = number of data points - number of modes
|21 |  B = zeros( numDataPoints-numModes, 1);
|22 |
|23 |  for r = 1:numDataPoints-numModes
|24 |      B(r,1) = -fn_data(numModes+r);
|25 |  end
|26 |
|27 |  X = A\B;
|28 |


|34 |  % M : #cols = number of modes
|35 |  % M : #rows = number of data points
|36 |  M = zeros(numDataPoints, numModes);
|37 |
|38 |  for r = 1:numDataPoints
|39 |      for c = 1:numModes
|40 |          M(r,c) = (mu_(c)-1)  *  (mu_(c) )^(r-1);
|41 |      end
|42 |  end
|43 |
|44 |  % F is always a column vector (only one column)
|45 |  % #rows = number of data points
|46 |
|47 |  vrMagn_n_PhaseRad = M \ transpose(fn_data)  ;
```

The only non-linear process is the finding of the roots of the polynomial to determine the z_i.

3.3 Example

In this section, Prony's method will be illustrated with the aid of a numerical example. Assume that it is required to fit to the record given in Table 3-1 a function of the form (3.17). The data samples are recorded at equally spaced intervals of 1 second beginning at 0 seconds. The actual form and the sinusoidal parameters of the function $f(x)$ are shown in (3.18)

$$f(x) = C_1 e^{a_1 x} + C_2 e^{a_2 x}$$

(3.17)

Table 3-1 A 6-Sample Record To Illustrate Prony's Method

x	f(x)
0	1.085950012
1	-0.017837743
2	-0.244420304
3	-0.024960803
4	0.051582021
5	0.011677152

21

$$f(x) = 1.1e^{-0.75x}\cos(2\pi(0.23)x + 0.16) \tag{3.18}$$

It is more convenient to represent these computations if the quantities are converted using the

identities given in (3.19a) & (3.19b) to that shown in (3.20).

$$e^{a_1} \to \mu_1 \tag{3.19a}$$

$$e^{a_2} \to \mu_2 \tag{3.19b}$$

(3.18) can now be written in the form of (3.20)

$$f(x) = C_1\mu_1^x + C_2\mu_2^x \tag{3.20}$$

Substituting the data samples for $x = 0,1,2,3,4,5$ gives the following equations (3.21a) through
(3.21f)

$$C_1 + C_2 = f(0) = 1.085950012 \tag{3.21a}$$

$$C_1\mu_1 + C_2\mu_2 = f(1) = -0.017837743 \tag{3.21b}$$

$$C_1\mu_1^2 + C_2\mu_2^2 = f(2) = -0.244420304 \tag{3.21c}$$

$$C_1\mu_1^3 + C_2\mu_2^3 = f(3) = -0.024960803 \tag{3.21d}$$

$$C_1\mu_1^4 + C_2\mu_2^4 = f(4) = 0.051582021 \tag{3.21e}$$

$$C_1\mu_1^5 + C_2\mu_2^5 = f(5) = 0.011677152 \tag{3.21f}$$

Rewriting these equations in matrix form gives (3.22)

$$\begin{bmatrix} 1 & 1 \\ \mu_1 & \mu_2 \\ \mu_1^2 & \mu_2^2 \\ \mu_1^3 & \mu_2^3 \\ \mu_1^4 & \mu_2^4 \\ \mu_1^5 & \mu_2^5 \end{bmatrix} \begin{bmatrix} C_1 \\ C_2 \end{bmatrix} = \begin{bmatrix} f(0) \\ f(1) \\ f(2) \\ f(3) \\ f(4) \\ f(5) \end{bmatrix} \tag{3.22}$$

22

Before C_1 and C_2 are determined using (3.22), μ_1 and μ_2 need to be determined first. Let us assume that μ_1 and μ_2 are the roots of a polynomial shown in (3.23)

$$\mu^2 + \alpha_1\mu + \alpha_2 = 0 \qquad (3.23)$$

or

$$(\mu - \mu_1)(\mu - \mu_2) = 0 \qquad (3.24)$$

Multiplying (3.21a) by α_2, (3.21b) by α_1 and adding the result to (3.21c) gives (3.25)

$$\alpha_2(C_1 + C_2) = f(0)\alpha_2 = 1.085950012\alpha_2$$

$$\alpha_1(C_1\mu_1 + C_2\mu_2) = f(1)\alpha_1 = -0.017837743\alpha_1$$

$$C_1\mu_1^2 + C_2\mu_2^2 = f(2) = -0.244420304$$

$$\left(\mu_1^2 + \alpha_1\mu_1 + \alpha_2\right)C_1 + \left(\mu_2^2 + \alpha_1\mu_2 + \alpha_2\right)C_2 = f(2) + \alpha_1 f(1) + \alpha_2 f(0) \qquad (3.25)$$

Because μ_1 and μ_2 are roots of the polynomial, the left hand side of the equations computes to

zero. Repeating the same process using (3.21b), (3.21c) and (3.21d) gives (3.26b). Repeating

again gives (3.26c) and (3.26d).

$$-0.244420304 + \alpha_1(-0.017837743) + \alpha_2(1.085950012) = 0 \qquad (3.26a)$$
$$-0.024960803 + \alpha_1(-0.244420304) + \alpha_2(-0.017837743) = 0 \qquad (3.26b)$$
$$0.051582021 + \alpha_1(-0.024960803) + \alpha_2(-0.244420304) = 0 \qquad (3.26c)$$
$$0.011677152 + \alpha_1(0.051582021) + \alpha_2(-0.024960803) = 0 \qquad (3.26d)$$

Rearranging these equations in matrix form yields (3.27)

$$\begin{bmatrix} -0.017837743 & 1.085950012 \\ -0.244420304 & -0.017837743 \\ -0.024960803 & -0.244420304 \\ 0.051582021 & -0.024960803 \end{bmatrix} \begin{bmatrix} \alpha_1 \\ \alpha_2 \end{bmatrix} = \begin{bmatrix} 0.244420304 \\ 0.024960803 \\ -0.051582021 \\ -0.011677152 \end{bmatrix} \qquad (3.27)$$

This is in the form of AX=B. The solution, X, can be found using the least squares method as

shown in (3.28). However, because of the nature of the numerical values involved it was

observed that using singular value decomposition (SVD) resulted in considerably better results. The solution vector, X, found in Matlab using SVD (3.29) is shown in (3.29).

$$X = \left[A^T A\right]^{-1} A^T B \tag{3.28}$$

$$X = A \backslash B \tag{3.29}$$

Solving (3.29) gives α_1 and α_2 as shown in (3.29b)

$$\begin{bmatrix} \alpha_1 \\ \alpha_2 \end{bmatrix} = \begin{bmatrix} -0.11840645496531 \\ 0.22313016014843 \end{bmatrix} \tag{3.29b}$$

Substituting α_1 and α_2 in (3.23) and determining its roots, yields μ_1 and μ_2 values as:

$$\mu_1 = 0.05920322748265 + 0.46864180138360i \text{ and}$$
$$\mu_2 = 0.05920322748265 - 0.46864180138360i.$$

The exponential parameters of (3.18), a_1 and a_2, are then determined as:

$$a_1 = \log(\mu_1) = -0.75 + 1.44513262065131i \text{ and}$$
$$a_2 = \log(\mu_2) = -0.75 - 1.44513262065131i.$$

Substituting μ_1 and μ_2 in (3.22) gives (3.30).

$$\begin{bmatrix} 1 & 1 \\ (0.059203 + 0.468641i) & (0.059203 - 0.468641i) \\ (-0.216120 + 0.055490i) & (-0.216120 - 0.055490i) \\ (-0.038800 - 0.097997i) & (-0.038800 + 0.097997i) \\ (0.043628 - 0.023985i) & (0.043628 + 0.023985i) \\ (0.013823 + 0.019026i) & (0.013823 - 0.019026i) \end{bmatrix} \begin{bmatrix} C_1 \\ C_2 \end{bmatrix} = \begin{bmatrix} 1.08595 \\ -0.01783 \\ -0.24442 \\ -0.02496 \\ 0.05158 \\ 0.01167 \end{bmatrix} \tag{3.30}$$

The overly determined least square problem, (3.30), is solved in Matlab using SVD to obtain C_1 and C_2 as:

$$C_1 = (0.542975 + 0.087625i) \text{ and}$$
$$C_2 = (0.542975 - 0.087625i).$$

24

Substituting a_1, a_2, C_1 and C_2 in (3.18) gives (3.31).

$$f(x) = (0.542975 + 0.087625i)e^{(-0.7500+1.4451)x} +$$
$$...(0.542975 - 0.087625i)e^{(-0.7500-1.4451)x} \qquad (3.31)$$

Using the complex exponential identities for cosine, (3.31) is converted to its sinusoidal form as shown in (3.32). The parameters of this sinusoid are equal to those of the specified function in (3.17). Thus, we have seen that by using Prony's method on a record consisting of six samples, we have been able to determine the original parameters of the function used in constructing the record.

$$f(x) = 1.1e^{-0.75x} \cos(2\pi(0.23)x + 0.16) \qquad (3.22)$$

3.4 Conclusion

The mathematical analysis of Prony's method and its implementation in MATLAB are reviewed in this chapter. Prony's method, an exponential parameter estimation technique that is used widely in communications as a signal analysis tool, has been chosen over the FFT in this work because of it many advantages. It is ideally suited to extract modal information from transient stability programs' outputs and STG shaft signal measured data.

While Prony's method faithfully fits a specified number of modal components to a given signal, it is necessary to reorder the output resultant modes of Prony's method to distinguish the signal modes from the noise modes. The next chapter presents the details of a reordering algorithm developed during the course of this work. The practical issues such as choosing the proper parameters of Prony's method to obtain better results are examined in Chapter 5.

CHAPTER 4

REORDERING ALGORITHM

In this work, Prony's analysis is used to perform modal decomposition of a given function. When the noise in the signal is low or negligible, the specified modal order can be set equal to the true order. However, usually there is noise or nonlinearities in the signal. In those cases, the modal order should be specified many times larger than the true internal modal order. Prony's analysis is then performed to extract the modes in the given function. The resulting output of Prony's analysis is in no particular order. Therefore, it is hard to distinguish the true modes from noise. A separate sorting algorithm is required for that purpose. One could employ any kind of sorting algorithm based on the constituent parameters: (1) magnitude, (2) frequency, or (3) exponential decay. However, these have their own limitations. Therefore, for torsional modes, it was observed during the course of this work, that a least-squares-error norm based sorting algorithm gives much better results. A weighting factor is computed for each constituent sinusoidal mode. These weighting factors are sorted in descending order to give the final list of modes in which the torsional modes are accumulated at the top of the list. As with Prony's analysis, this reordering algorithm was also coded in MATLAB.

4.1 Proposed Reordering Algorithm

Let $f_T(k)$ be the given linearly sampled signal. Prony's method can be used to extract the constituent modal components by fitting the given signal to a sum of n complex exponentials as shown in (4.1) by computing the complex values B_i and z_i.

$$f_T(k) = B_1 z_1^k + B_2 z_2^k + \cdots B_n z_n^k$$

(4.1)

The output of the Prony algorithm is a list of n complex value pairs where each pair represents an exponentially decaying sinusoid. The complex conjugate pairs can be converted to parameters of sets of exponentially damped sinusoids as shown in (4.2).

$$\{(B_i, z_i), (B_i^*, z_i^*)\} \leftrightarrow \{A_i, \alpha_i, \omega_i, \phi_i\}$$

or

$$\begin{bmatrix} \{A_1, \alpha_1, \omega_1, \phi_1\} \\ \{A_2, \alpha_2, \omega_2, \phi_2\} \\ \vdots \\ \{A_N, \alpha_N, \omega_N, \phi_N\} \end{bmatrix}$$

(4.2)

Let the ith mode be reconstructed to give $f_i(k)$ as shown in (4.3).

$$f_i(k): A_i e^{\alpha_i t} \cos(\omega_i t + \phi_i)$$

(4.3)

The given signal $f_T(k)$ can thus be represented as a sum of individual exponentially damped sinusoids and the error as shown in (4.4) and (4.5).

27

$$f_{_T}(k) = f_1(k) + f_2(k) + f_3(k) + \cdots + f_{_N}(k) + e \tag{4.4}$$

$$f_{_T}(k) = f_{_R}(k) + e \tag{4.5}$$

$$f_i(k) \leftrightarrow \{A_i, \alpha_i, \omega_i, \phi_i\} \tag{4.6}$$

In (4.6), $f_i(k)$ is the signal built using the i$^{\text{th}}$ set of parameters. Let us compute the error norm for the first sinusoid $f_1(k)$. This indicates how much error is generated if this mode were not present in the reconstructed waveform $f_R(k)$.

$$e_1 = \left\| f_{_T}(k) - \left(f_2(k) + f_3(k) + \cdots + f_{_N}(k) \right) \right\| \tag{4.7}$$

$$e_1 = \left\| f_T(k) - \sum_{\substack{i \neq 1 \\ i=1}}^{N} f_{_i}(k) \right\|$$
$$or$$
$$e_1 = \left\| f_1(k) + e \right\| \tag{4.8}$$

$$e_j = \left\| f_T(k) - \sum_{\substack{i \neq j \\ i=1}}^{N} f_{_i}(k) \right\|$$
$$or$$
$$e_j = \left\| f_j(k) + e \right\| \tag{4.9}$$

In this way the error norms for each sinusoid $\{f_1(k), f_2(k), \cdots, f_N(k)\}$ are computed resulting in the list L given in (4.10).

$$L: \{e_1, e_2, \cdots, e_N\} \tag{4.10}$$

28

Sorting the list L in descending order according to magnitude yields the required dominant modes list. The entire algorithm can be summarized in a flowchart as shown in Figure 4-1.
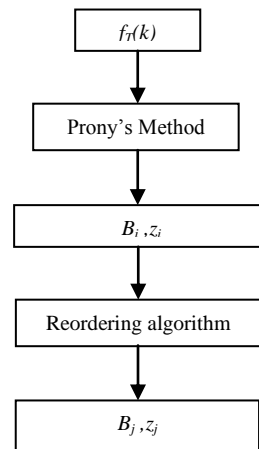
Figure 4-1. Flowchart for Reordering Algorithm

4.2 Example

This method can be illustrated with the aid of the following example. The sampled waveform in this example is constructed out of four modal components (three exponentially decaying sinusoid modes and one exponentially decaying dc mode) and noise ($w(t)$) as shown in (4.11).

$$f(t) = 3.5e^{-0.1t}\cos(2\pi 15t) + 0.1e^{-0.8t}\cos(2\pi 180t) + 9.5e^{-0.02t}\cos(2\pi 2.5t) + 17e^{-0.05t} + w(t) \quad (4.11)$$

The MATLAB code for constructing this signal is listed in Figure 4-2.

```
clearall;clc;
t = 0:0.0001:1;
noise_ = (rand(size(f))-0.5) * 1e-5;
f =  3.5 * exp(-0.1 *t) .* cos(2*pi* 15*t)  +
0.1 * exp(-0.8 *t) .* cos(2*pi*180*t)   + ...
     9.5 * exp(-0.02*t) .* cos(2*pi*2.5*t)  +
17   * exp(-0.05*t)  + noise_ ;
plot( t, f );
```

Figure 4-2. MATLAB Code for Creating the Sample Waveform

29

A plot of f(t) vs time is shown in Figure 4-3.
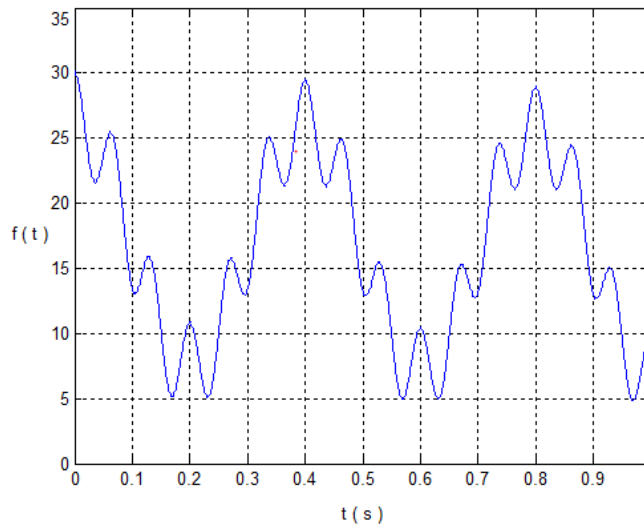
Figure 4-3. Plot of the Sample Waveform.

Prony's method can now be applied on this signal to extract the underlying modal components. Note that while applying the method, it is required to specify the method the number of modes in the signal. Generally speaking, whenever there is noise or any kind of non-linearities in the signal, a modal order much higher than the true estimated modal order needs to be specified. For example, in this case, the modal order is specified as 200 instead of the true modal order, four. Prony's method fits these extraneous modes to noise in the signal. Experience, or trial and error, is usually used to estimate this modal order.

The output, a list of modes, of the MATLAB function implementing Prony's method is given in Table 4-1. Note that these modes are in no particular order. It is difficult to distinguish the real signal modes from the noise modes. Because the signals that are of significance in the current work are slowly decaying lower frequency power system signals, which span the range of 1 Hz to a few 100 Hz, the described method can be applied to separate the signal modes from the noise modes. The MATLAB code shown in Figure 4-4 implements this procedure.

30

Table 4-1. Output of Prony's Method

Mode	Magnitude	decay	f(hz)	Phase
1	17.0672167	-0.050	0.000	0.00
2	2.78E-08	-722.469	0.000	-3.14
3	3.248E-07	-6.565	497.942	-0.94
4	6.276E-07	-3.990	491.587	-2.88
5	8.207E-07	-14.330	485.991	-2.96
6	6.989E-07	-9.757	482.354	2.10
7	6.564E-07	-5.200	477.294	-0.45
8	3.9346E-06	-18.105	471.655	3.11
9	2.7019E-06	-13.365	467.724	1.24
13	1.02827E-05	-17.819	445.327	-2.78
14	9.9657E-06	-14.832	443.801	0.73
…	…	…	…	…
94	0.0000015	-7.454	267.251	-0.69
95	2.0571E-06	-5.710	246.345	2.58
96	1.0887E-06	-7.345	254.272	-2.59
97	1.7877E-06	-8.856	242.250	2.07
98	1.2883E-06	-15.795	259.649	-1.94
99	1.7721E-06	-25.196	262.943	3.14
100	1.63115E-05	-121.743	247.006	-2.58
101	0.000032574	-362.771	283.476	-0.12

```
function [ vrLSE ] = create_vrLSE(    t,
vrMagnFinal, vrDecayFinal, vrFreqHzFinal,
vrPhaseRadFinal, fdiff)
vrLSE = zeros(size(vrMagnFinal));
for k=1:length(vrMagnFinal)
fndata_estk = RebuildFn(t, 0, vrMagnFinal,
vrDecayFinal, vrFreqHzFinal,
vrPhaseRadFinal, k);
lse_k = norm(fdiff+fndata_estk);
vrLSE(k) = lse_k;
% LSE without mode k
end
return
```

Figure 4-4. MATLAB Code for Generating the LSE Norms

The MATLAB function create_vrLSE() shown in Figure 4-4 is used to reorder the list of modes in Table 4-1. Shown in Table 4-2 is the output of this MATLAB function (the reordered list of modes).

Table 4-2. Reordered List of Prony's Method Output Modes

Mode #	LSE	Magnitude	decay	f (hz)	phi
1	5.27E+02	1.71E+01	-0.05	0	0
2	2.10E+02	9.50E+00	-0.02	2.5	0
3	7.45E+01	3.50E+00	-0.1	15	0
4	1.58E+00	1.00E-01	-0.8	180	0.1
5	2.65E-04	1.00E-05	-14.832	443.8	0.7
6	2.65E-04	1.03E-05	-17.819	445.33	-2.8
7	2.64E-04	9.30E-06	-16.161	361.72	-2.7
8	2.64E-04	3.26E-05	-362.771	283.48	-0.1
9	2.64E-04	8.10E-06	-17.014	358.89	1.6
…	…	…	…	…	…
97	2.62E-04	3.00E-07	-6.072	294.37	0.6
98	2.62E-04	3.00E-07	-6.521	97.48	1.9
99	2.62E-04	3.00E-07	-6.565	497.94	-0.9
100	2.62E-04	1.00E-07	-2.333	326.05	-1
101	2.62E-04	0.00E+00	-722.469	0	-3.1

As seen in Table 4-2, the power signal modes are all sorted at the top because of the specific error norm based reordering method.

4.3 Conclusions

An algorithm to reorder the output modes of Prony's method, which was developed during the course of this work, is presented in this chapter. This reordering is performed to help distinguish the signal modes from noise modes in the given signal. A MATLAB implementation is presented along with an example that illustrates the method. In this work, this methodology has been applied every time after modal decomposition is performed using Prony analysis as shown in Chapter 5, 6, 7 and 8. However, this algorithm was not applied to real measurements in Chapter 9 because of reasons discussed in that chapter.

While the issues regarding the output of Prony's method have been dealt with in this chapter, the next chapter deals with the practical issues of choosing the input parameters of Prony's method that aid in getting better results.

CHAPTER 5

EFFECT OF PRONY PARAMETERS

The main focus of the previous chapter was the reordering algorithm for the output modes of Prony's analysis. The focus of this chapter will be the practical issues of applying Prony analysis. These discussions will focus primarily on the effects of varying Prony analysis parameters on the output of Prony analysis. Basically there are three parameters:

- Modal Order (numModes),

- Sampling frequency (nSkipSample), and

- Window parameters - length & position.

These parameters need to be chosen with extreme consideration just like those of other identification methods. The user would set these parameters before running the Prony algorithm. A Matlab GUI has been developed to facilitate changing and setting these parameters in an easy and intuitive way. This careful selection of parameters is especially needed when the data is not explicitly linear or contains significant noise.

5.1 Prony Driver GUI Program Description

This section contains a brief explanation of the Matlab tool that has been developed to run Prony's method. This tool has a GUI shown in Figure 5-1 built using the Matlab GUIDE program. It facilitates setting and modification of Prony parameters and data window properties.
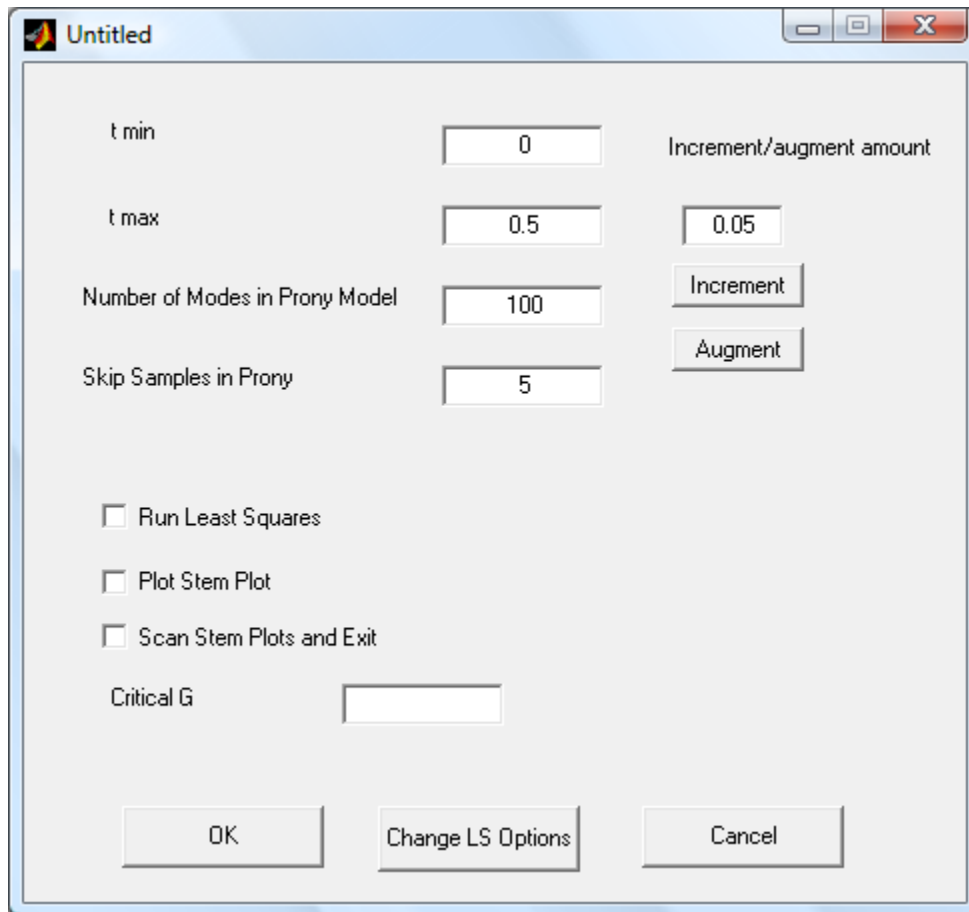
Figure 5-1. GUI Built in Matlab to Allow User Selection of Data Window Properties and Prony

Parameters

The user would enter "PronyDriver" at the ">>" prompt in Matlab command window. A file

open dialog pops up and allows the user to select a data file. This data file contains two columns

which represent time and signal data. Once the program reads the file data, it displays the signal

data in a plot to allow the user to select data window properties such as t_{min} and t_{max}.

The GUI will then pop up and the user can set the required Prony parameters and data window properties. The program will then run Prony's method and display its output in the Matlab command window.

5.2 Effect of Modal Order

The process can be explained with the aid of an example. Shown in Figure 5-2 is the plot of a signal built in Matlab. This signal has three sinusoidal components and noise, i.e., a linear part and a non-linear part.

$$f(t) = 2.5e^{-0.2t}\cos(2\pi \times 1.5t) + 0.5e^{-0.2t}\cos(2\pi \times 5.5t) + 0.15e^{-0.01t}\cos(2\pi \times 11.5t) + w(t) \qquad (5.1)$$

In (5.1) $w(t)$ represents noise.
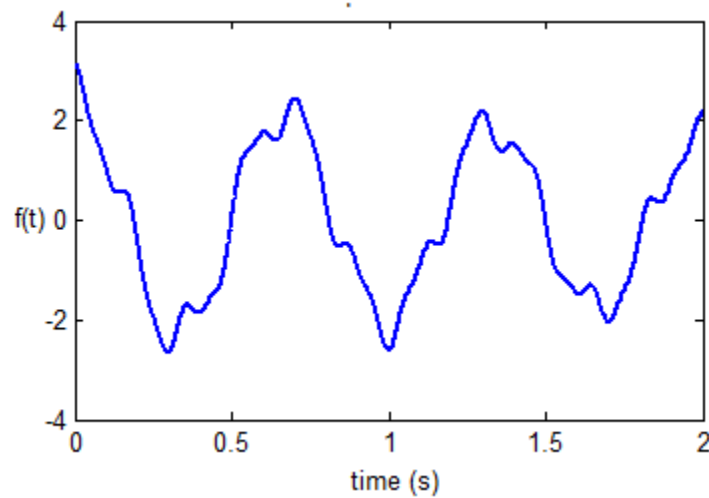
Figure 5-2 Sample Waveform Consisting Of Three Exponentially Decaying Sinusoids and Noise.

Prony's method (PM) is then applied on this signal for modal decomposition. An input parameter to the PM, n, determines the modal order of the constructed model. PM will try to fit this model, a waveform consisting of a linear combination of n sinusoids, to the given signal. Shown in Figure 5-3 is the output of PM. Shown in Figure 5-3a are both the given signal and the

constructed model. The error between these two signals is shown in Figure 5-3b. Shown in Figure 5-3c is the stem plot, which represents the magnitudes of LSE of each individual component in the model. LSE of a sinusoidal component is a kind of weighting factor which represents its 2-norm. Because the signal consists of three sinusoidal components, the stem plot should display only three non-zero stems with the rest being zero magnitudes. However, because of noise in the signal, PM is unable to fit the model to the given data perfectly resulting in error shown in Figure 5-3b. This results in non-zero LSE magnitudes of noise modes.
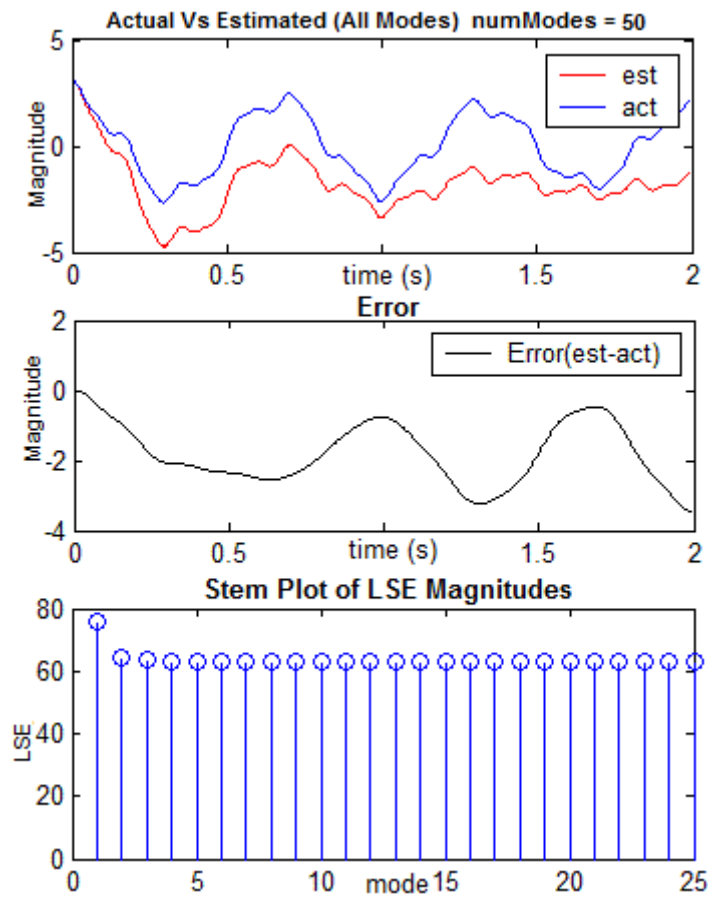
Figure 5-3 Comparison of Actual Signal and PM's Output: Stem Plot Showing the LSE Magnitudes of Constituent Sinusoids.

Repeating this procedure with different values of numModes while keeping all other parameters constant, gives Figures 5-4a through 5-4g. In these figures there are 7 sets of PM results with numModes = {10, 20, 30, 60, 70, 80, 90}.

Figure 5-4a Comparison of Actual Signal and PM's Output Along with Stem Plot of the

Constituent Modes' LSE Magnitudes with numModes Parameter = 10

Figure 5-4b Comparison of Actual Signal and PM's Output Along with Stem Plot of the Constituent Modes' LSE Magnitudes with numModes Parameter = 20

Figure 5-4c Comparison of Actual Signal and PM's Output Along with Stem Plot of the Constituent Modes' LSE Magnitudes with numModes Parameter = 30

Figure 5-4d Comparison of Actual Signal and PM's Output Along with Stem Plot of the Constituent Modes' LSE Magnitudes with numModes Parameter = 60

Figure 5-4e Comparison of Actual Signal and PM's Output Along with Stem Plot of the Constituent Modes' LSE Magnitudes with numModes Parameter = 70

40

Figure 5-4f Comparison of Actual Signal and PM's Output Along with Stem Plot of the Constituent Modes' LSE Magnitudes with numModes Parameter = 80
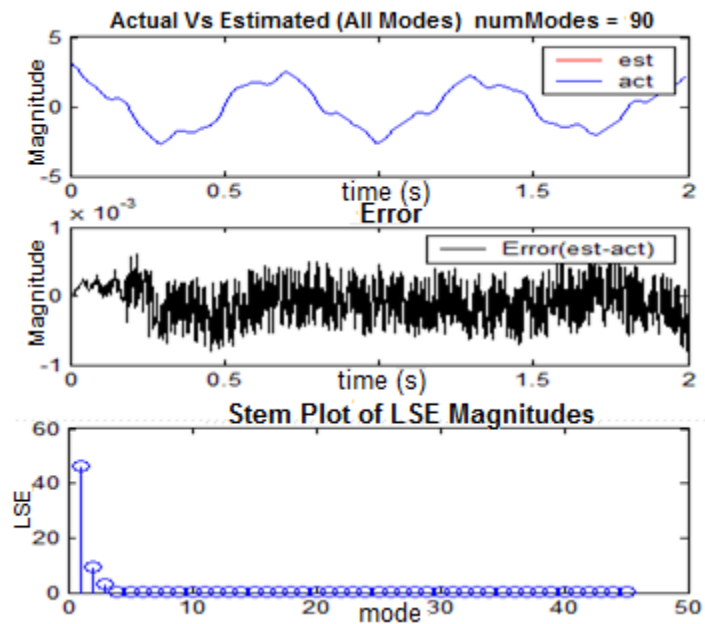
Figure 5-4g Comparison of Actual Signal and PM's Output Along with Stem Plot of the Constituent Modes' LSE Magnitudes with numModes Parameter = 90

From these figures, it is evident that as numModes increases the model waveform increasingly matches the given signal which results in decreasing error magnitude. In other words, the 2-norm of the error signal decreases as numModes increases. Also, the true signal modes' LSEs in the stem plot becomes increasingly obvious, i.e., they stand out from other noise stems more distinctly because as numModes increases the LSE magnitudes of the noise modes will gradually diminish. Comparing the LSE magnitudes of noise modes in set (1) and set (8), the magnitude has decreased from 75 to less than 0.1. This property has been used in creating an LSE based reordering algorithm, discussed in Chapter 4, which reorders the modes based on LSE magnitudes. Thereafter, another algorithm is used to separate the signal modes from the noise modes.

Increasing the numModes usually results in decreased error. However, there is a particular characteristic to this decrease. This characteristic is captured and illustrated in Figure 5-5. It can be observed that the error initially decreases only slightly. However, after a threshold it decreases exponentially. Note that the y-axis is logarithmic.
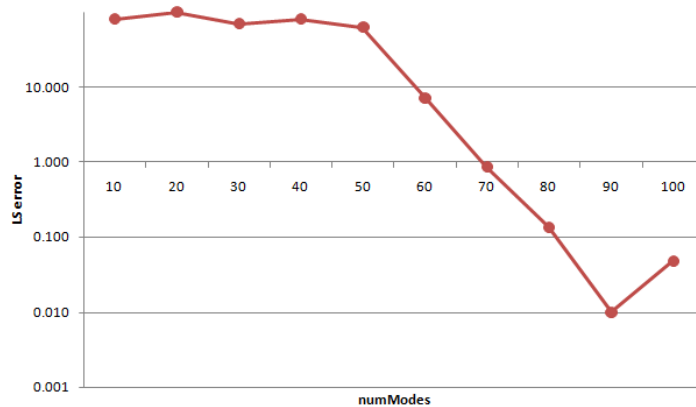
Figure 5-5 Plot of LS Error as a Function of numModes

Next, the same experiment is repeated with the magnitude of noise in the signal as the varying parameter. The relationship between these LSEs and numModes for various noise magnitudes are plotted as shown in Figure 5-6. It can be observed from this figure that as the noise in the signal increases, it takes more numModes for the LSE to fall below a certain specified level.
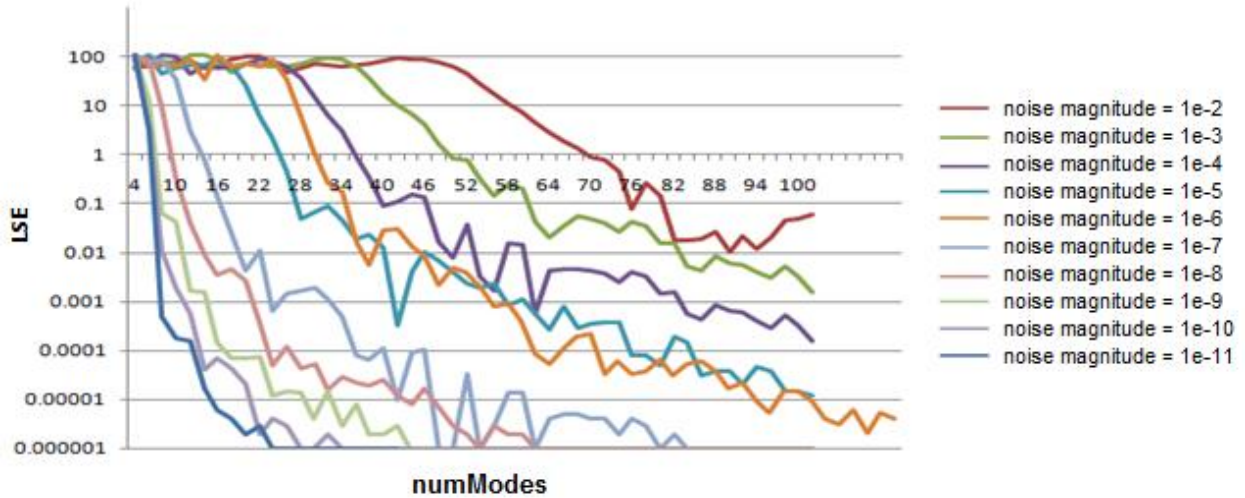
Figure 5-6 Total LSE vs numModes with Noise as Varying Parameter for a 3-Sinusoid Signal

Next, the previous experiment is repeated with a different modal composition in the given signal. This time a signal composed of only one sinusoid instead of three sinusoids is used. The corresponding relationship between LSE and numModes is shown in Figure 5-7.
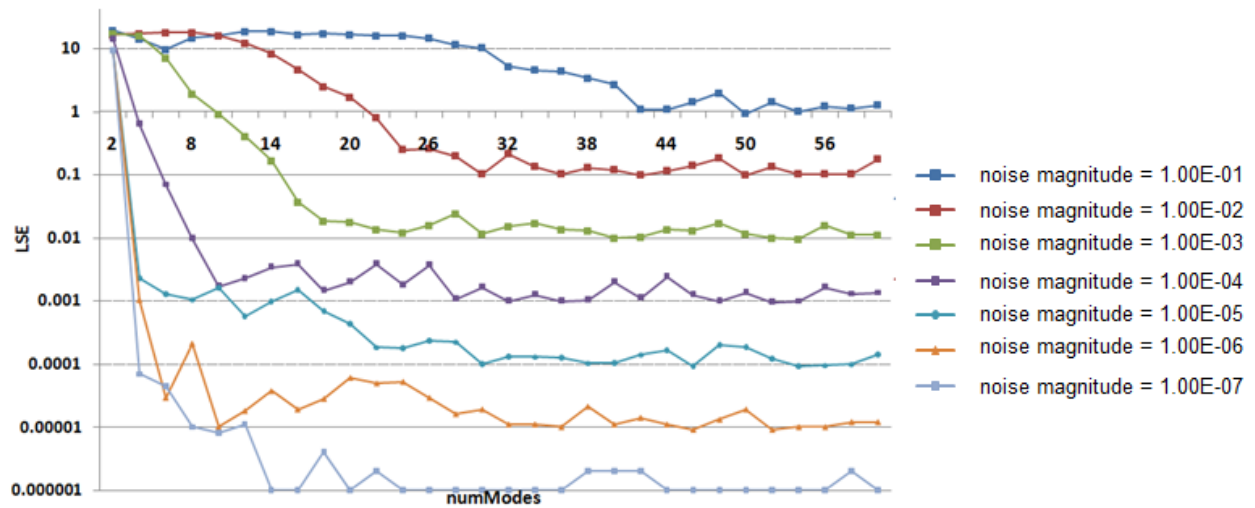
Figure 5-7 Total LSE vs numModes with Noise as a Varying Parameter for a 1-Sinusoid Signal

5.3 Effect of Sliding Window Parameters on Prony's Method's Output

As mentioned previously, the output of the Prony analysis for a given signal depends on three parameters that are chosen by the user. These are the selected modal order, the sampling rate and the data window's size and position. The effects of the window parameters – length and position – on the output of Prony analysis will be discussed in this section. For convenience sake, a new parameter, named nSkipSample, will be used instead of sampling rate. The nSkipSample parameter downsamples the given record by sampling only every n^{th} point. The window size and position are specified by two parameters t_{min}, which specifies the beginning point of the data window, and t_{max}, which specifies the ending point of the data window.

Consider the same signal that was used in the previous chapter as shown in (5.2).

$$f(t) = 3.5e^{-0.1t}\cos(2\pi \times 15t) + 0.1e^{-0.8t}\cos(2\pi \times 180t) + 9.5e^{-0.02t}\cos(2\pi \times 2.5t) + w(t) \quad (5.2)$$

This data record is fed to Prony's method to extract its constituent modes using the following input parameters:

44

Modal Order (numModes) : 50

nSkipSample : 4

Window size and position: $t_{min} = 0$ and $t_{max} = 2.0$

Shown in Figure 5-8 is the output of the Prony's method. As seen in this Figure, the Prony model

matches the actual given data very closely.
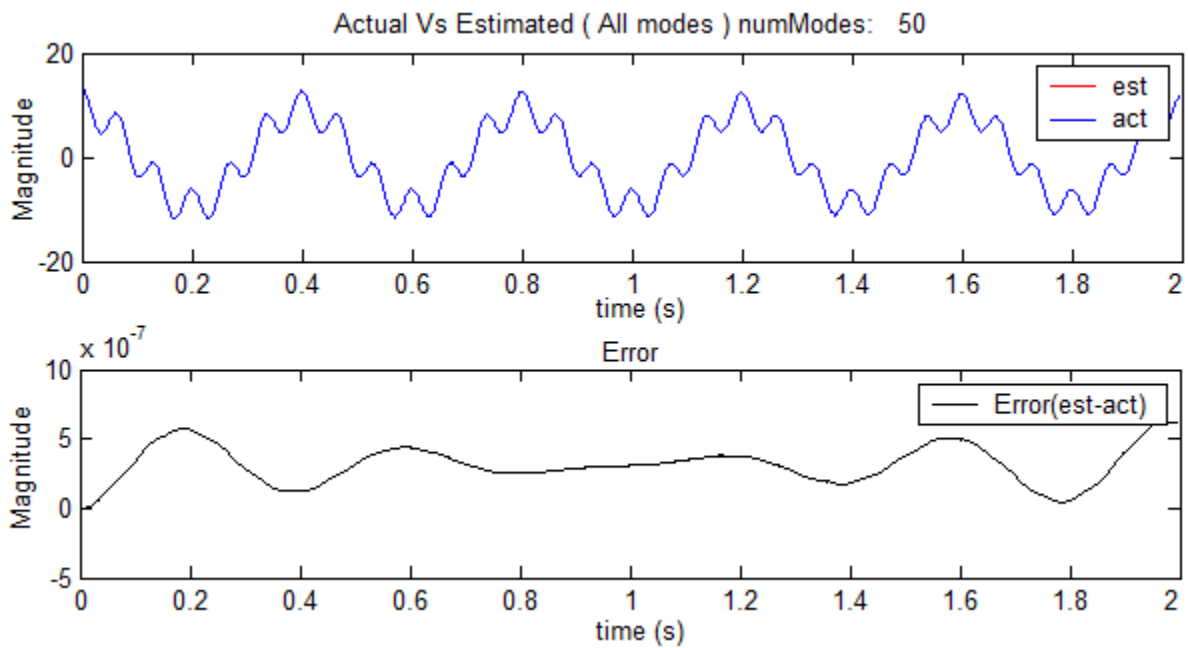
Figure 5-8 Comparison of Given and Estimated Waveforms

The error norm, LSE, for this window is 2.41E-5. Next, the same experiment is repeated while

sliding the window 0.4 seconds every time. The results of these tests are shown in Figures 5-9a

through 5-9c and Tables 5-1 through 5-4. Here, as the very small LSE numbers indicate, the

model matches the given signal very closely.

Table 5-1. The LSE Values for Successive Windows

Window #	t_{min}	t_{max}	LSE
1	0	2	2.41E-05
2	0.4	2.4	7.52E-06
3	0.8	2.8	1.91E-05
4	1.2	3.2	3.67E-05
5	1.6	3.6	4.39E-05
6	2	4	7.92E-06

Table 5-2 Effect of Sliding Window on Frequency of Mode1

Window #	Magnitude	Decay	Frequency (Hz)	Phase
1	9.4999807	-0.02	2.5	0.0015708
2	9.4242842	-0.02	2.5	0.0015708
3	9.3491911	-0.02	2.5	0.0015708
4	9.2746952	-0.0199999	2.5	0.0015708
5	9.2007935	-0.0199999	2.5	0.0015708
6	9.1274815	-0.02	2.5	0.0015708

Table 5-3 Effect of Sliding Window on Frequency of Mode 2

Window #	Magnitude	Decay	Frequency (Hz)	Phase
1	3.499965	-0.1	15	0.0094248
2	3.3627294	-0.1	15	0.0094248
3	3.2308749	-0.1	15	0.0094248
4	3.1041905	-0.1	15	0.0094248
5	2.9824734	-0.1	15	0.0094248
6	2.865529	-0.1	15	0.0094248

Table 5-4 Effect of Sliding Window on Frequency of Mode 3

Window #	Magnitude	Decay	Frequency (Hz)	Phase
1	0.099992	-0.8	180	0.1130973
2	0.0726091	-0.8	180	0.1130973
3	0.052725	-0.8	180	0.1130973
4	0.0382862	-0.8	180	0.1130973
5	0.0278015	-0.8	180	0.1130973
6	0.020188	-0.8	180	0.1130973
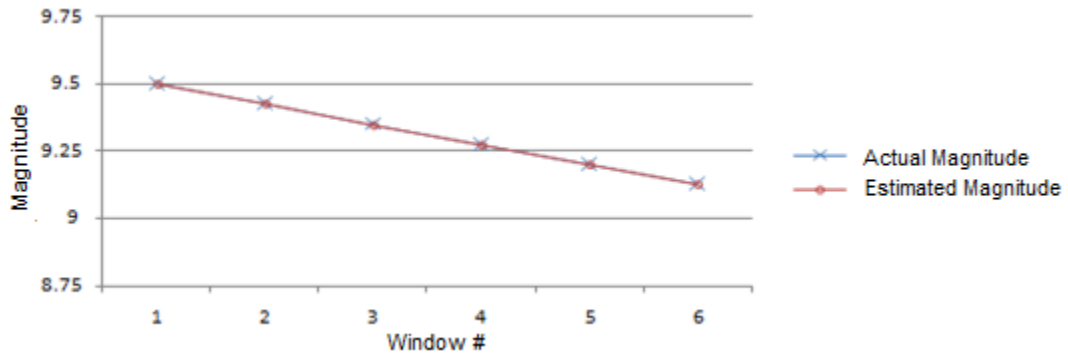
Figure 5-9a Comparison of Estimated and Actual Magnitudes of Mode 1 (2.5 Hz) mode
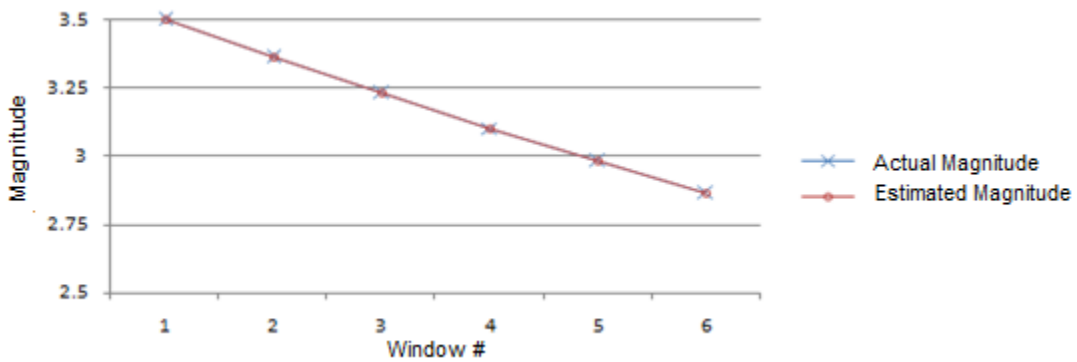
Figure 5-9b Comparison of Estimated and Actual Magnitudes of Mode 2 (15 Hz) mode
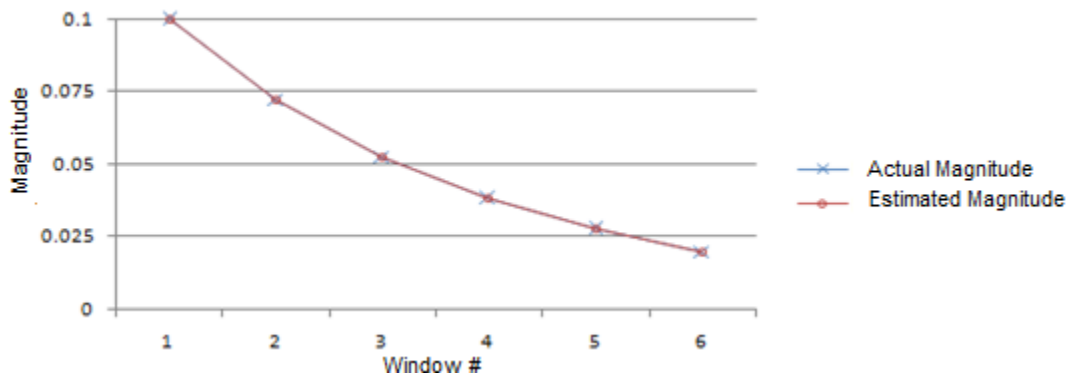
Figure 5-9c Comparison of Estimated and Actual Magnitudes of Mode 3 (180 Hz) mode

5.4 Effect of varying sampling rate parameter on Prony's Method's Output

In this section, the effects of varying the sampling-rate parameter on the PM's output, and consequently its LSE, are observed. As mentioned previously, a new parameter, named nSkipSample, will be used instead of sampling rate. The nSkipSample parameter downsamples the given record by sampling only every nth point. Consider the same data set that was used in previous section. It is given in (5.3).

$$f(t) = 3.5e^{-0.1t}\cos(2\pi \times 15t) + 0.1e^{-0.8t}\cos(2\pi \times 180t) + 9.5e^{-0.02t}\cos(2\pi \times 2.5t) + w(t) \quad (5.3)$$

Because of noise in the signal, the numModes parameter was set to 100 and was kept constant throughout all five test cases i.e., nSkipSample = {1,2,3,4,5}. This data record is originally sampled at 10 kHz and contains two seconds of data. Therefore the maximum number of modes that we could specify to PM as a parameter is 20,000/2 = 10,000. However, because the highest frequency is 180 Hz, we could specify a much lower numModes parameter, usually less than 500. As mentioned previously, experience is often used in this choice. As can be seen in Figure 5-10a through Figure 5-10e, as the nSkipSample parameter increases, the PM fits the model to given data sample more and more completely, i.e., the PM model increasingly matches the given data sample. Consequently, the LSE decreases as seen in Table 5-5.
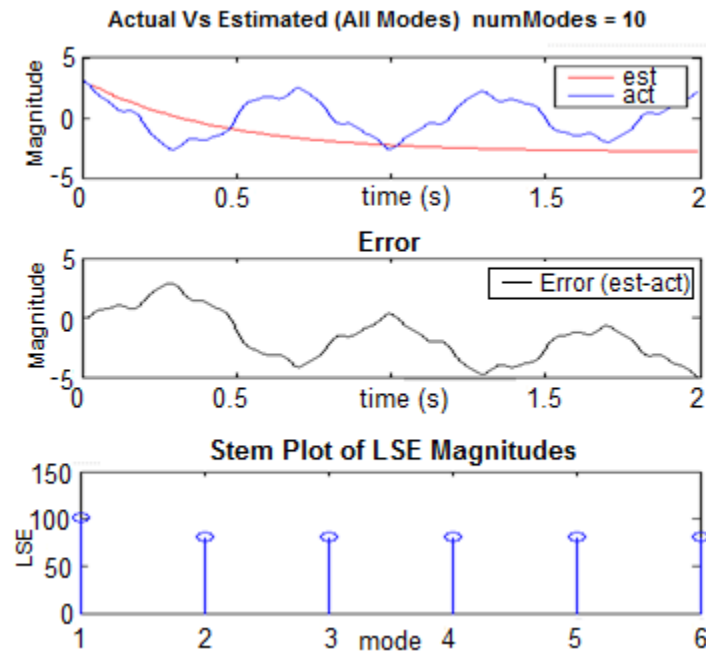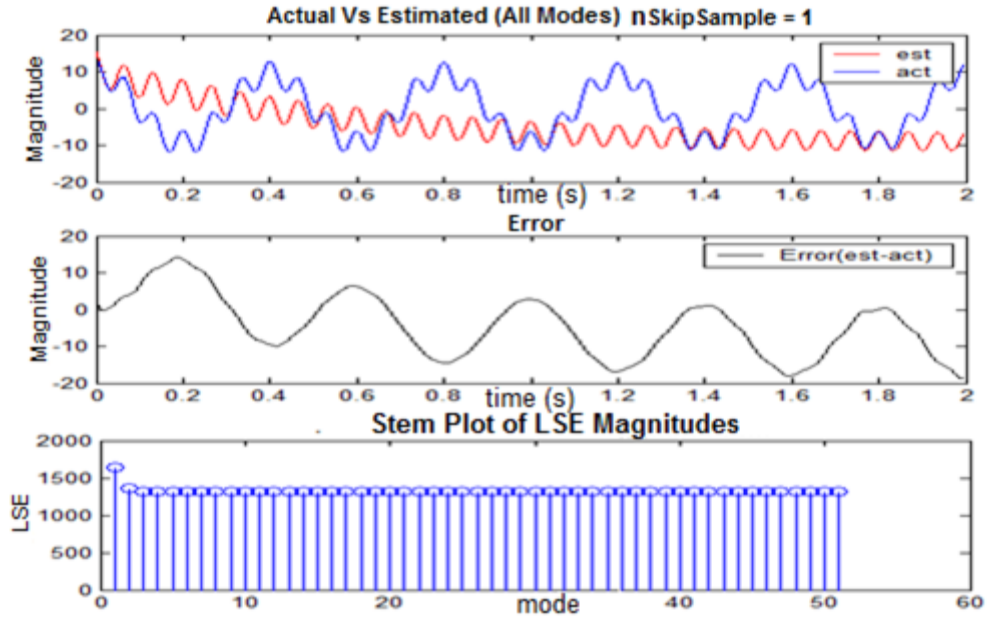
Figure 5-10a Comparison of Actual Signal and PM's Output Along With Stem Plot of the Constituent Modes' LSE Magnitudes with nSkipSample Parameter = 1
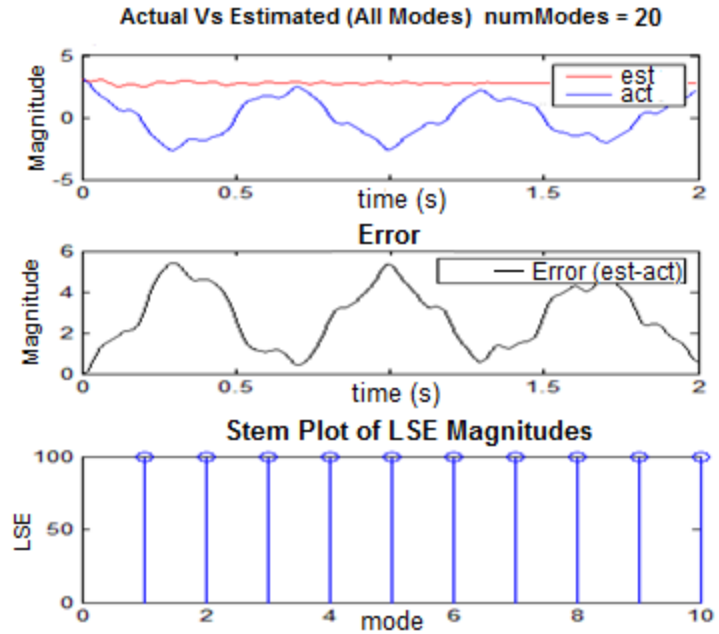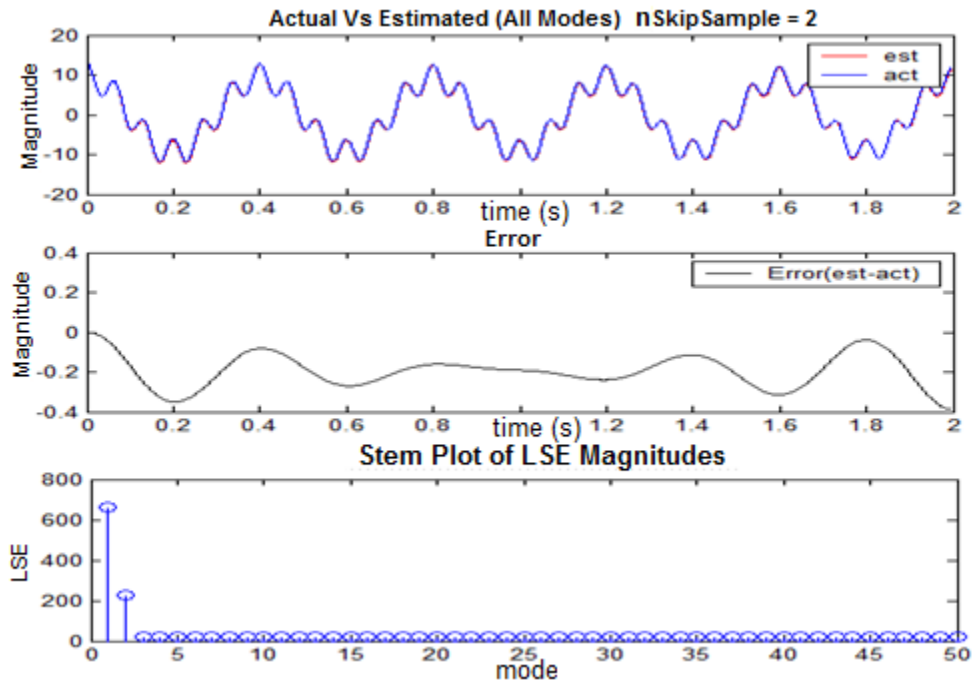

Figure 5-10b Comparison of Actual Signal and PM's Output Along With Stem Plot of the Constituent Modes' LSE Magnitudes with nSkipSample Parameter = 2
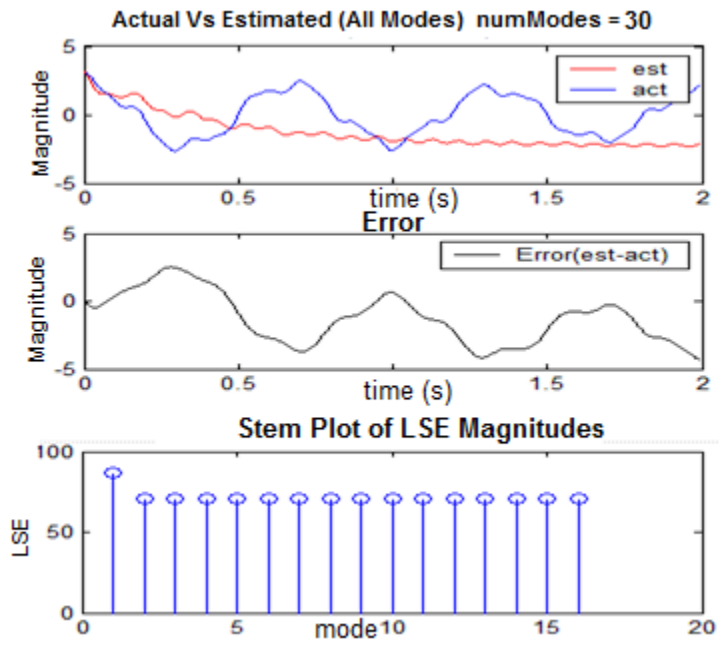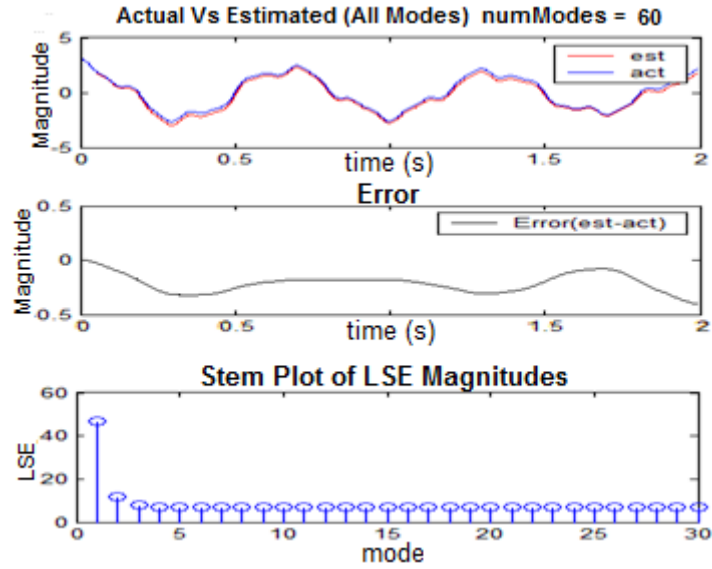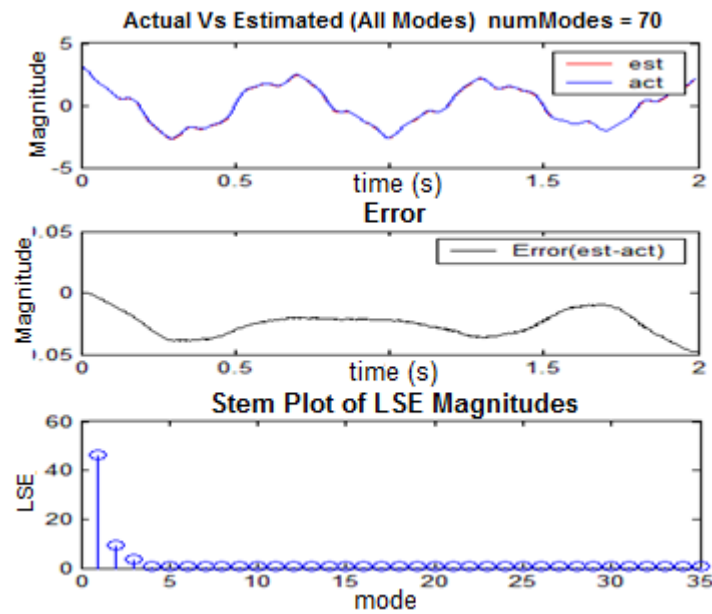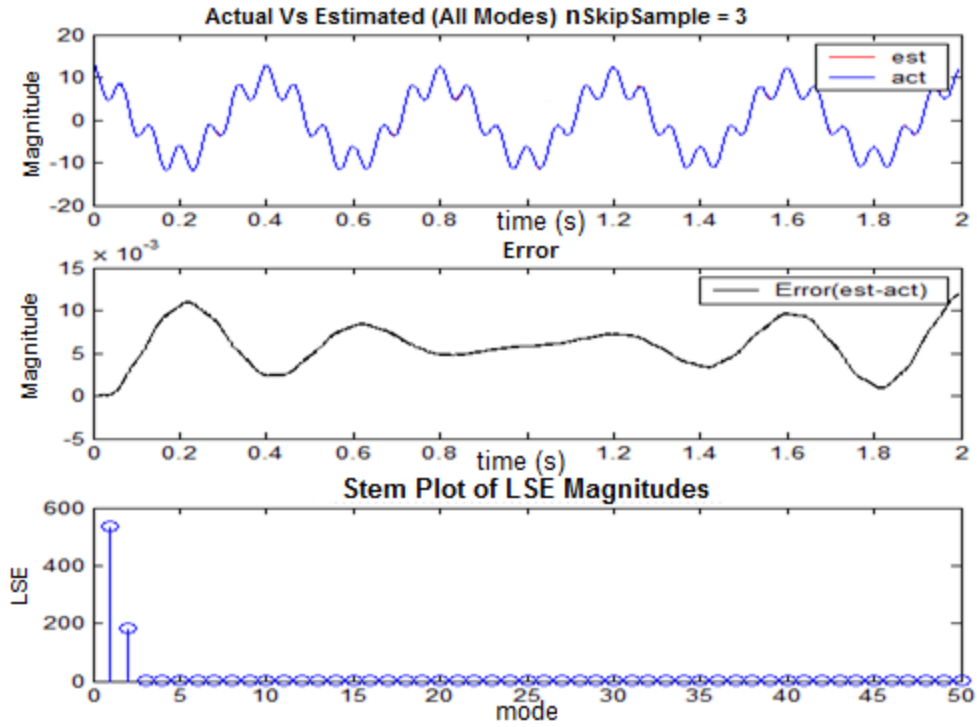
Figure 5-10c Comparison of Actual Signal and PM's Output Along With Stem Plot of the Constituent Modes' LSE Magnitudes with nSkipSample Parameter = 3
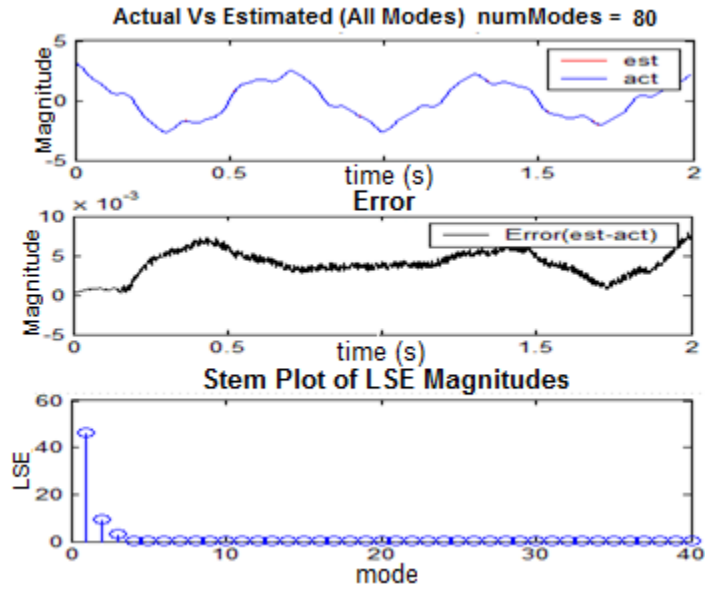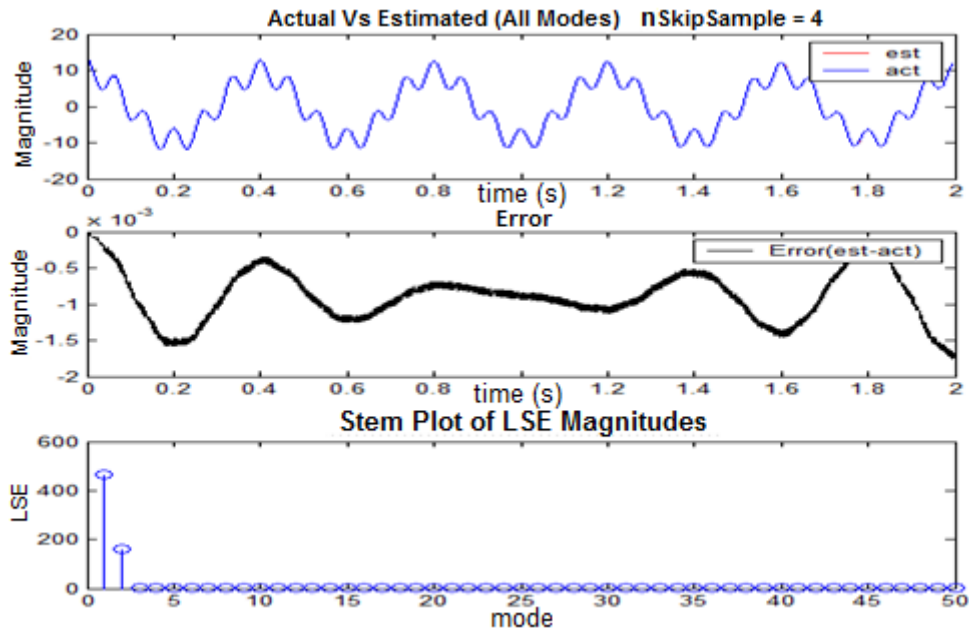

Figure 5-10d Comparison of Actual Signal and PM's Output Along With Stem Plot of the Constituent Modes' LSE Magnitudes with nSkipSample Parameter = 4
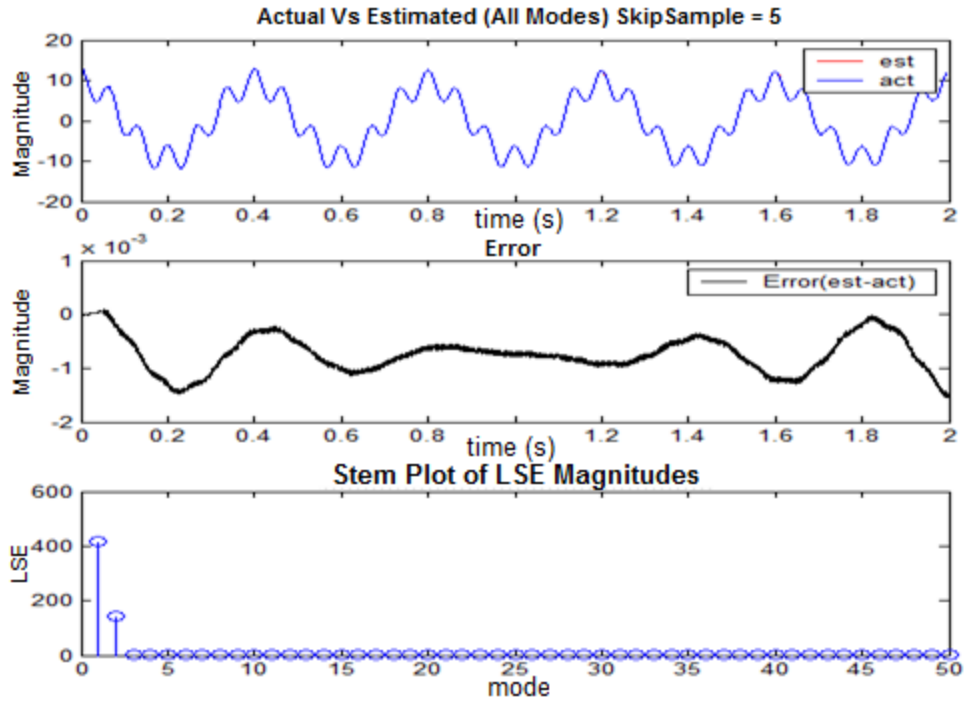
Figure 5-10e Comparison of Actual Signal and PM's Output Along With Stem Plot of the Constituent Modes' LSE Magnitudes with nSkipSample Parameter = 5

Table 5-5 Sampling Rate (nSkipSample) vs LSE - A

nSkipSample	LSE-error
1	1317.27
2	21.1131
3	0.52178
4	0.06744
5	0.05099

It is to be noted that as the nSkipSample parameter rises the resolution decreases, and hence the PM might miss detecting some higher frequencies. In this case, because the highest frequency is 180 Hz and the lowest sampling rate (case nSkipSample = 5) is 2 kHz, there is no such problem.

From Table 5-6 it can be inferred that although the total LSE is decreasing quickly, the individual parameters, i.e., magnitudes, frequencies, etc, converge to their correct values slowly. It requires nSkipSample of greater than or equal to four for the magnitude of the frequency 2.5 Hz mode to converge to its correct value, 9.5.

Table 5-6 Sampling rate (nSkipSample) vs LSE - B

		Mode #	Magnitude	ExpDecay	Frequency(Hz)	Phase(rad)
nSkipSample:	1	1	19.7376133	-1.882675	0	0
		2	3.9084642	-0.2312709	14.9710909	0.1716462
		3	1.1300583	-144.9632392	0	3.1415927
		4	0.1001143	-0.8003881	179.9999787	0.1125296
nSkipSample:	2	1	9.695243	-0.0408697	2.5001401	-0.0012846
		2	3.4998881	-0.0999648	14.9999748	0.0096094
		3	0.1000002	-0.8001528	180.0000277	0.113005
nSkipSample:	3	1	9.4940861	-0.0193665	2.4999749	0.0017882
		2	3.4998786	-0.0999756	15.0000111	0.0093589
		3	0.0999947	-0.8000499	180.0000022	0.1130859
nSkipSample:	4	1	9.5007977	-0.0200874	2.5000007	0.0015574
		2	3.4999868	-0.1000066	15.0000012	0.0094178
		3	0.0999847	-0.7998804	180.000008	0.1130771
nSkipSample:	5	1	9.5007017	-0.0200781	2.5000061	0.0015255
		2	3.4999951	-0.1000082	14.9999978	0.0094376
		3	0.0999979	-0.8001168	179.999992	0.1131259

In the previous example, the numModes parameter was kept constant, while the sampling rate varied. Now the sampling rate is kept constant (nSkipSample = 1) and numModes is increased while keeping the window size and position constant. Next, the LSE for each numMode is recorded. Plotting the corresponding LSE vs. numMode parameter gives us data for one curve. Repeating the same example with varying sampling rate   (nSkipSample = 2, 3) would give the family of curves shown in Figure 5-11.

52
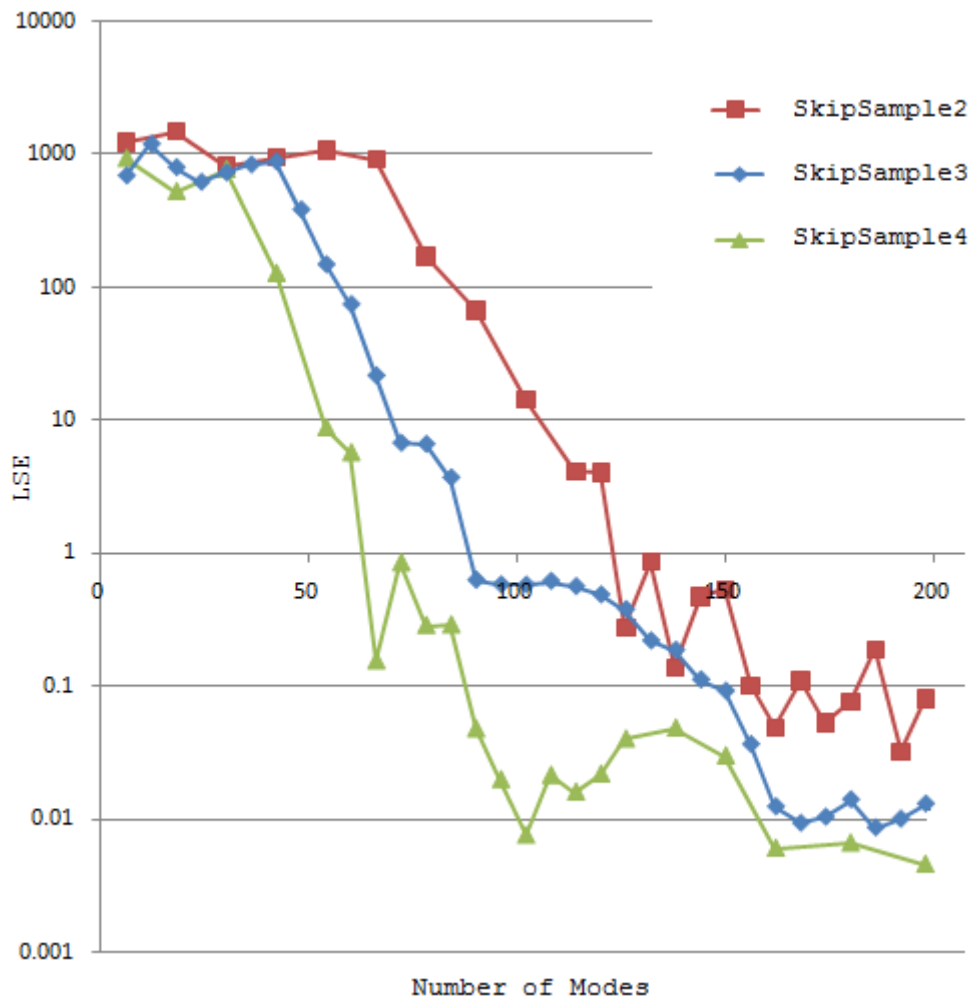
Figure 5-11 Effect of Sampling Rate on the Relationship Between numModes and LSE

It can be observed from these families of curves that while it took about 150 modes/numModes for obtaining sufficiently less final LSE with the SkipSample2 parameter, it took only about 80 numModes for obtaining the final LSE with the SkipSample4 parameter. One inference: in some cases increasing the sampling rate (thereby the number of samples) does not necessarily give us better results. It will take more numModes, and hence, become more computationally expensive and time consuming. In other words, the sampling rate can be

decreased to a certain extent, provided it is much higher than the highest frequency. Additionally, it can also be inferred that, as long as the sampling rate is much higher than the highest signal frequency, we can afford to reduce the sampling frequency to obtain the same result with the same LSE, but much quicker and less computationally expensive.

5.5 Guidelines

Based on the observations working with Prony's method, some general guidelines have been developed for setting these parameters. These mostly apply for extracting power system torsional modal information. The guidelines for real signal measurements are slightly different from those of transient stability program (TSP) output signals, because of the presence of measurement noise and other nonlinearities in real signal measurements.

Setting the modal order parameter (numModes) :

As mentioned earlier, the real signal measurements contain measurement noise and other nonlinearities. To compensate for this, it is required to choose a larger numModes as an input parameter for Prony's method. It is difficult to choose the correct value in a single step [10]. It is usually an iterative process where the user sets the numModes parameter and executes Prony's method. The output modes are used to reconstruct the signal and if it is not a good fit, a higher numModes parameter is set and the process is repeated. However, it was observed that too high a modal order, while resulting in a good fit, could result in incorrect modal results probably because the matrices used in Prony's method's becoming increasingly singular. Therefore, numModes should be increased gradually, until a good fit for TSP output signals or a reasonable enough fit for real measurement signals is obtained.

54

Choosing the window location and size parameters:

When choosing the window position for a given TSP output record, it is advisable to choose later because these torsional modes do not decay quickly in comparison to other short duration modes, such as electrical stator transients. For real measurement records, it is advisable to choose earlier because as the length of the record increases, the probability of non-linear phenomena - switching events or other influences because of corrective measures, such as governors and exciters - distorting the LTI nature of the overall signal increases. Finally, the window size should include at least two cycles of the lowest modal frequency in most cases.

Setting the sampling rate parameter:

Increasing this parameter is another way of modifying numModes and the total record length. The sampling rate should be such that each mode in the signal would at least have four samples per cycle similar to the Nyquist criteria. Increasing the sampling rate parameter thereafter does result in a better fit. However, increasing it too much does not necessarily increase fit quality, because the matrices involved in Prony's analysis tend to become singular and give incorrect results.

5.6 Conclusions

The process of selecting the various parameters for Prony's method is complex. It requires careful consideration as there are many parameters that affect directly the results and their accuracy. Unlike Fourier analysis, each data record must be treated individually. While there are some empirical rules, as discussed in the previous section, the user does need some training/practice before obtaining good results. The most important parameter is numModes, which is used to fit not only the signal modes, but also any noise or non-linearities in the signal.

CHAPTER 6

EIGEN ANALYSIS OF STEAM TURBINE GENERATOR SHAFT SYSTEMS

The main aim of this work, as mentioned earlier, is to estimate the shaft spring constants so that they could be used to build better models for SSR analysis. These shaft spring constants are estimated using rotor mass values and measured modal frequency values obtained from either the rotor speed signals or the power signal p(t). The accuracy of the estimated shaft spring constants is therefore directly dependent on the accuracy of the measured frequencies. This accuracy is in turn dependent on the signal-to-noise ratio of the frequencies in the signal. In other words, it is highly preferable to have a signal where the magnitudes of modal frequencies are large enough that they could be measured reliably. One of the major factors that affects the magnitudes of modal components in a signal is the eigen properties of the concerned shaft system. In this and the next chapter, these aspects, eigen properties of the STG shaft systems, will be investigated to determine their effects on this work. In order to apply eigen analysis, the isolated lumped-spring-mass mechanical model of the STG turbine will be treated as an LTI system. There are certain unique properties of STG shaft systems because of the way the rotor masses and the interconnecting shafts of the lumped-spring-mass model are connected. These properties will be examined with the aid of a few shaft systems whose data is provided in the literature [4][16].

6.1 State-Space Theory Review [17]

One of the main reasons eigen analysis is used here is that it makes it easier to analyze state systems of different sizes in a similar unified manner. Using eigen analysis allows the use of linear algebra principles and well-established computer routines to easily analyze the system characteristic features such as eigen values, eigen vectors and participation factors. A brief review of the relevant state space theory used in this work is provided in the following section. Let the dynamics of an nth order non-linear system be described by the set of first order differential equations given by (6.1) and its outputs be described by (6.2).

$$\frac{dx_i(t)}{dt} = f_i\big(x_1(t), x_2(t) \cdots x_n(t), u_1(t), u_2(t), \cdots u_m(t)\big)$$

(6.1)

$$i = 1, 2, \ldots n$$

$$y_i(t) = g_i\big(x_1(t), x_2(t) \cdots x_n(t), u_1(t), u_2(t), \cdots u_m(t)\big)$$

(6.2)

In (6.1) and (6.2) f_i and g_i are non-linear functions of variables, also known as system state variables $x_1(t), x_2(t) \ldots x_n(t)$, and inputs $u_1(t), u_2(t) \ldots u_m(t)$.

The states, x_i, are a minimal set of linearly independent system variables, either real, physical (such as capacitor voltage and inductor current) or abstract mathematical variables associated with the system equations. Knowledge of these state variables at $t=t_0$ along with the inputs for $t>t_0$ is sufficient to completely determine the system behavior and all other system variables. The selection of state variables is not unique. Any selected set would yield the same information about the state except in a different coordinate system in the dynamic system's n-dimensional euclidean state space. If the number of state variables is chosen greater than the true

order of the system, then not all of them will be linearly independent as shown in the following example.

There are at least two sets of state variables that can be used to represent the system shown in Figure 6-1: (1) v_1, v_2, i_1, i_2 and (2) v_1, v_2, v_3, i_1, i_2. Only the first set one is the correct choice because it is a minimal set, whereas set (2) is not. Set (2) is not a minimal set because any one of the three voltage variables (v_1, v_2, v_3,) can be represented as a linear combination of the other variables.
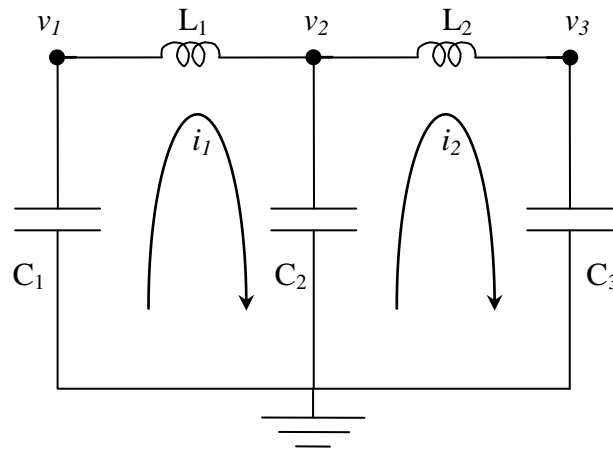
Figure 6-1. Example of a Four State System Consisting of Inductors and Capacitors

In the case of a linear time-invariant system, the non-linear functions f_i and g_i can be replaced by constant coefficient matrices and these equations can be written in vector-matrix form as shown in (6.3a) and (6.3b).

$$\frac{dx(t)}{dt} = Ax(t) + Bu(t)$$

<div align="right">(6.3a)</div>

$$y(t) = Cx(t) + Du(t)$$

<div align="right">(6.3b)</div>

The matrix A is commonly referred to as the system's state matrix. B, C and D are all constant coefficient matrices. Using the traditional transfer function approach, the transfer function of this system can be derived after taking the Laplace transform of the equations and setting the initial conditions to 0. The resulting transfer function is shown in (6.4).

$$G(s) = \frac{C\left[adj(sI - A)B + |sI - A|D\right]}{|sI - A|}$$

<div align="right">(6.4)</div>

Setting the denominator of G(s), also referred to as the characteristic polynomial, to 0 gives the characteristic equation (6.5).

$$|sI - A| = 0$$

<div align="right">(6.5)</div>

6.2 Eigen values

The roots of the characteristic equation shown in (6.5) are called the eigen values, λ_i, of the system. When (6.3a) and (6.3b) are used to describe the dynamics of an isolated linear time-invariant TG shaft system, these eigen values correspond to its natural frequencies or torsional mode frequencies.

6.3 Right eigen vectors

A right eigen vector of matrix A associated with λ_i is any non-zero vector that satisfies equation (6.6).

$$A\phi_i = \lambda_i\phi_i \tag{6.6}$$

$$i = 1, 2, \dots n$$

Rearranging terms in (6.6) gives (6.7).

$$(A - \lambda_i I)\phi_i = 0 \tag{6.7}$$

Because equation (6.7) is a homogenous equation, the eigen vector can only be determined within a scalar multiplier. Generally, this vector is scaled such that it is of unit length. In this current work, for displaying purposes only, these vectors will be occasionally scaled such that the absolute value of the largest element in the vector is 1. In the context of TG rotor system analysis, these right eigen vectors, also called mode-shapes, indicate the fixed relative amplitude and phase of turbine rotor sections, when they are oscillating under steady state conditions at a given natural frequency.

6.4 Left eigen vectors

The left eigen vector, ψ_i, of the state matrix A associated with λ_i, is any non-zero vector that satisfies equation (6.8).

$$\psi_i A = \lambda_i \psi_i \tag{6.8}$$

$$i = 1, 2, \dots n$$

Just like the right eigen vectors, the left eigen vectors, ψ_i, can only be determined within a scalar multiplier and are usually scaled to have unit length.

$$\psi_i \phi_i = 1 \tag{6.9}$$

60

Let us define matrix Λ, shown in (6.10), as a diagonal matrix consisting of eigen values, λ_i, of the state matrix, A.

$$\Lambda = \begin{bmatrix} \lambda_1 & 0 & \cdots & 0 \\ 0 & \lambda_2 & \cdots & 0 \\ \vdots & \vdots & \ddots & \vdots \\ 0 & 0 & \cdots & \lambda_n \end{bmatrix}$$

(6.10)

Let us define matrices Φ and Ψ, shown in (6.11) and (6.12), as consisting of right and left eigen vectors, φ_i and ψ_i, of the state matrix, A.

$$\Phi = \begin{bmatrix} \phi_1 & \cdots & \phi_n \end{bmatrix}$$

(6.11)

$$\Psi = \begin{bmatrix} \psi_1 & \cdots & \psi_n \end{bmatrix}$$

(6.12)

Using (6.6) and (6.11) gives (6.13) and (6.14).

$$A\Phi = \Phi\Lambda$$

(6.13)

$$\Phi^{-1}A\Phi = \Lambda$$

(6.14)

Using (6.9), (6.11) and (6.12) gives (6.15) and (6.16).

$$\Psi\Phi = I$$

(6.15)

$$\Psi = \Phi^{-1}$$

(6.16)

The current work on eigen analysis involves computing these matrices in Matlab. First, the right eigen vector matrix, Φ, is computed from the state matrix, A. Then the left eigen vector matrix, Ψ, is computed by inverting the right eigen vector matrix as shown in (6.16).

The formulae discussed in the previous sections have been used to study the eigen properties of the linear time-invariant TG shaft system. Because of the configuration, physical properties and the differential equations governing the system, the isolated undamped TG shaft

system's state matrix, A, consists of only real elements. Furthermore, all its eigen values occur in complex conjugate pairs with real parts equal to 0, with each of the complex conjugate pairs corresponding to one undamped oscillatory mode of the form given in (6.17).

$$a_i \cos(\omega_i t + \gamma_i)$$

(6.17)

6.5 Participation Factors [16]

An additional important technique of quantifying how strongly the modes and states are associated is participation factors. These combine both the right and left eigen vectors of a mode to create a new vector that shows how this mode is associated with the system states as shown in (6.18).

$$p_i = \begin{bmatrix} p_{1i} \\ p_{2i} \\ \vdots \\ p_{ni} \end{bmatrix} = \begin{bmatrix} \phi_{1i}\psi_{i1} \\ \phi_{2i}\psi_{i2} \\ \\ \phi_{ni}\psi_{in} \end{bmatrix}$$

(6.18)

Collecting the participation vectors of all the modes gives us the participation matrix as shown in (6.19).

$$P = \begin{bmatrix} p_1 & p_2 & \cdots & p_n \end{bmatrix}$$

(6.19)

Because we will be dealing with a lot of TG shaft system analyses, let us first take a look at how they are derived with the aid of one STG shaft system example provided in [16].

6.6 Derivation of State Equations for Kundur 1039 System

These derivations are better illustrated with the aid of a test system whose rotor layout schematic is shown in Figure 6-2 and its electrical equivalent in Figure 6-3. This data belongs to

a 191 MVA 3,600 rpm STG unit. In this equivalent scheme, the rotor section masses are represented by capacitors and shaft spring constants are represented by inverse inductances. The torques transmitted in shaft springs and the rotor section velocities are represented by inductor currents and capacitor voltages respectively.
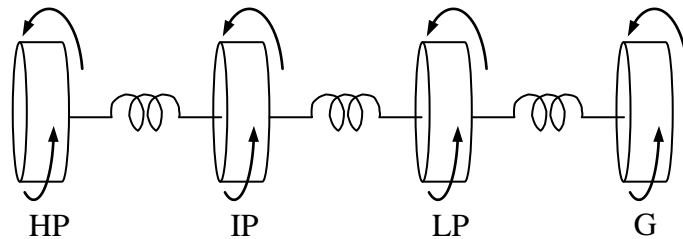
Figure 6-2 Schematic Layout of Rotors and Shafts of Kundur pp. 1039 Problem

Table 6-1 Rotor Inertias

Rotor	H (MW-s/MVA)
HP	0.099
IP	0.337
LP	3.68
G	0.946

Table 6-2 Shaft Spring Constants

Shaft	K (p.u. torque/rad)
HP-IP	37.95
IP-LP	81.91
LP-G	82.74
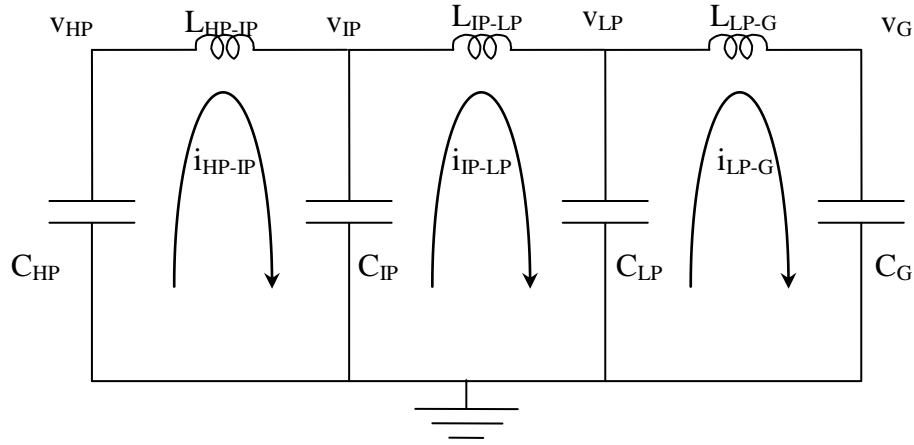
Figure 6-3 Electrical Equivalent of Shaft System

The following differential equations for voltage across an inductor and current through a capacitor will be used to represent the dynamics of the electrical equivalent circuit shown in Figure 6-3.

$$C\frac{dv(t)}{dt} = i(t)$$

$$L\frac{di(t)}{dt} = v(t)$$

Applying Kirchoff's laws on the electrical equivalent circuit shown in Figure 6-3 and using these equations yields equations (6.20) through (6.24).

$$C_{HP}\frac{dv_{HP}(t)}{dt} = -i_{HP-IP}(t) \tag{6.20}$$

$$C_{IP}\frac{dv_{IP}(t)}{dt} = i_{HP-IP}(t) - i_{IP-LP}(t) \tag{6.21}$$

$$C_{LP}\frac{dv_{LP}(t)}{dt} = i_{IP-LP}(t) - i_{LP-G}(t) \tag{6.22}$$

$$C_G \frac{dv_G(t)}{dt} = i_{LP-G}(t) \tag{6.23}$$

$$L_{HP-IP} \frac{di_{HP-IP}(t)}{dt} = v_{HP}(t) - v_{IP}(t) \tag{6.24a}$$

$$L_{IP-LP} \frac{di_{IP-LP}(t)}{dt} = v_{IP}(t) - v_{LP}(t) \tag{6.24b}$$

$$L_{LP-G} \frac{di_{LP-G}(t)}{dt} = v_{LP}(t) - v_G(t) \tag{6.24c}$$

Using equations (6.20), (6.21), (6.22) and (6.23) yields (6.25).
.

$$C_G \frac{dv_G(t)}{dt} = -C_{HP} \frac{dv_{HP}(t)}{dt} - C_{IP} \frac{dv_{IP}(t)}{dt} - C_{LP} \frac{dv_{LP}(t)}{dt}$$

$$C_G v_G(t) = -C_{HP} v_{HP}(t) - C_{IP} v_{IP}(t) - C_{LP} v_{LP}(t) + K \tag{6.25}$$

Because the main concern in this work is eigen values, vectors and participation factors, i.e., dynamics only, the non-transient part, K, can be safely ignored as shown in (6.26).

$$C_G v_G(t) = -C_{HP} v_{HP}(t) - C_{IP} v_{IP}(t) - C_{LP} v_{LP}(t) \tag{6.26}$$

Substituting (6.26) in (6.24c) yields (6.27).

$$L_{LP-G} \frac{di_{LP-G}(t)}{dt} = \left(\frac{C_{HP}}{C_G} \right) v_{HP}(t) + \left(\frac{C_{IP}}{C_G} \right) v_{IP}(t) + \left(1 + \frac{C_{LP}}{C_G} \right) v_{LP}(t) \tag{6.27}$$

Rewriting the differential equations, (6.20), (6.21), (6.22), (6.24a), (6.24b) and (6.27) in matrix form yields (6.28).

$$
\begin{bmatrix}
\left(\dfrac{di_{HP-IP}(t)}{dt}\right) \\[2mm]
\left(\dfrac{di_{IP-LP}(t)}{dt}\right) \\[2mm]
\left(\dfrac{di_{LP-G}(t)}{dt}\right) \\[2mm]
\left(\dfrac{dv_{HP}(t)}{dt}\right) \\[2mm]
\left(\dfrac{dv_{IP}(t)}{dt}\right) \\[2mm]
\left(\dfrac{dv_{LP}(t)}{dt}\right)
\end{bmatrix}
=
\begin{bmatrix}
0 & 0 & 0 & \left(\dfrac{1}{L_{HP-IP}}\right) & \left(\dfrac{-1}{L_{HP-IP}}\right) & 0 \\[3mm]
0 & 0 & 0 & 0 & \left(\dfrac{1}{L_{IP-LP}}\right) & \left(\dfrac{-1}{L_{IP-LP}}\right) \\[3mm]
0 & 0 & 0 & \left(\dfrac{C_{HP}}{L_{LP-G}C_G}\right) & \left(\dfrac{C_{IP}}{L_{LP-G}C_G}\right) & \left(\dfrac{1}{L_{LP-G}}+\dfrac{C_{LP}}{L_{LP-G}C_G}\right) \\[3mm]
\left(\dfrac{-1}{C_{HP}}\right) & 0 & 0 & 0 & 0 & 0 \\[3mm]
\left(\dfrac{1}{C_{IP}}\right) & \left(\dfrac{-1}{C_{IP}}\right) & 0 & 0 & 0 & 0 \\[3mm]
0 & \left(\dfrac{1}{C_{LP}}\right) & \left(\dfrac{-1}{C_{LP}}\right) & 0 & 0 & 0
\end{bmatrix}
\begin{bmatrix}
i_{HP-IP}(t) \\[2mm]
i_{IP-LP}(t) \\[2mm]
i_{LP-G}(t) \\[2mm]
v_{HP}(t) \\[2mm]
v_{IP}(t) \\[2mm]
v_{LP}(t)
\end{bmatrix}
\tag{6.28}
$$

The state matrix of the STG shaft system is now given by (6.29).

$$
A =
\begin{bmatrix}
0 & 0 & 0 & \left(\dfrac{1}{L_{HP-IP}}\right) & \left(\dfrac{-1}{L_{HP-IP}}\right) & 0 \\[3mm]
0 & 0 & 0 & 0 & \left(\dfrac{1}{L_{IP-LP}}\right) & \left(\dfrac{-1}{L_{IP-LP}}\right) \\[3mm]
0 & 0 & 0 & \left(\dfrac{C_{HP}}{L_{LP-G}C_G}\right) & \left(\dfrac{C_{IP}}{L_{LP-G}C_G}\right) & \left(\dfrac{1}{L_{LP-G}}+\dfrac{C_{LP}}{L_{LP-G}C_G}\right) \\[3mm]
\left(\dfrac{-1}{C_{HP}}\right) & 0 & 0 & 0 & 0 & 0 \\[3mm]
\left(\dfrac{1}{C_{IP}}\right) & \left(\dfrac{-1}{C_{IP}}\right) & 0 & 0 & 0 & 0 \\[3mm]
0 & \left(\dfrac{1}{C_{LP}}\right) & \left(\dfrac{-1}{C_{LP}}\right) & 0 & 0 & 0
\end{bmatrix}
\tag{6.29}
$$

Using the generator ratings of 191 MVA and 3600 rpm as base values and choosing a time base value of 1 second establishes the base values for the rest of the relevant parameters as shown:

$\omega_m\text{-}base = 377$ mech-rad/sec,

$VA\text{-}base = 191{,}000{,}000$ VA,

$$H\text{-}base = \frac{2*VA_{base}}{(\omega_{mbase})^2} = 2687.6992 \text{ seconds,}$$

Torque-base = 506631.2997 N.m,

J-base = 1343.849601 kg.m^2, and

K-base = 1343.849601 N.m/mech-rad.

Provided in Tables 6-1 and 6-2 are the rotor sections' moment of inertia values and shaft spring values in seconds and p.u. torque/rad. Using the base values computed, these are converted to S.I values and p.u. values as shown in Tables 6-3 and 6-4.

Table 6-3 S.I. and p.u Values of Kundur 1039 STG Rotor Section Moment of Inertias

J (kg-m^2)	J-p.u	C-p.u (C=J)
266.0822211	0.198	0.198
905.7546314	0.674	0.674
9890.733066	7.36	7.36
2542.563446	1.892	1.892

Table 6-4 S.I. and p.u. Values of Kundur 1039 STG Shaft Spring Constants

K (Nm/m.rad)	K-p.u.	L p.u. (L = 1/K)
19226657.82	14307.15	6.98951E-05
41498169.76	30880.07	3.23833E-05
41918673.74	31192.98	3.20585E-05

These tables also provide the equivalent capacitances and inverse-inductances. Plugging these values into the state matrix, A, gives (6.30).

$$A = \begin{bmatrix} 0 & 0 & 0 & 14307.15 & -14307.15 & 0 \\ 0 & 0 & 0 & 0 & 30880.1 & -30880.1 \\ 0 & 0 & 0 & 3264.38 & 11112.08 & 152535.6 \\ -5.05 & 0 & 0 & 0 & 0 & 0 \\ 1.4836 & -1.4836 & 0 & 0 & 0 & 0 \\ 0 & 0.1358 & -0.1358 & 0 & 0 & 0 \end{bmatrix}$$

(6.30)

The matrix of eigen values (W) and matrix of right eigen vectors (V), shown in Table 6-5, are computed using the Matlab command **eig(A)** on the state matrix, A. The matrix V consists of the right eigen vectors and the diagonal matrix W matrix gives the corresponding eigen values. The eigen values are 52.74, 29.66 and 22.33.

Table 6-5 Right Eigen Vector Matrix of Kundur 1039 STG Shaft System

0.792379	0.792379	0.326785	0.326785	0.068212	0.068212
-0.609188	-0.609188	0.904531	0.904531	0.237142	0.237142
0.028983	0.028983	-0.273741	-0.273741	0.969072	0.969072
0.012077 i	-0.012077 i	0.008856 i	-0.008856 i	0.002455 i	-0.002455 i
-0.006275 i	0.006275 i	0.004600 i	-0.004600 i	0.001786 i	-0.001786 i
0.000262 i	-0.000262 i	-0.000859 i	0.000859 i	0.000709 i	-0.000709 i

Each column in the matrix V gives the eigen vector of one eigen value in a diagonal position of the W matrix. Because we are interested in the rotor section velocities, these are selected and displayed in Table 6-6. Note that in the first column of Table 6-5, which represents the V matrix, there are six elements. These are the row elements in the eigen vector for the 52.74 Hz mode and correspond to the six state variables, $i_{HP-IP}(t)$, $i_{IP-LP}(t)$, $i_{LP-G}(t)$, $v_{HP}(t)$, $v_{IP}(t)$ and $v_{LP}(t)$, respectively. The row element for $v_G(t)$ is obtained using equation (6.26) and the row elements

for the remaining state variables are obtained as in the previous step. From these seven eigen vector elements, the four corresponding to the voltages are selected and normalized such that the maximum absolute value is 1. The resulting eigen vectors for the three modes are shown in Table 6-6.

Table 6-6 Three Right Eigen Vectors of Modes 52 Hz, 29 Hz, and 22 Hz Mode

eigen vector for 52.74 hz :		
v1	HP	1
v2	IP	-0.51962
v3	LP	0.021667
v4	GENR	-0.00383

eigen vector for 29.66 hz :		
v1	HP	1
v2	IP	0.519373
v3	LP	-0.097
v4	GENR	0.087664

eigen vector for 22.33 hz :		
v1	HP	-0.6726
v2	IP	-0.48934
v3	LP	-0.19416
v4	GENR	1

The inverse of matrix V shown in Table 6-5 gives the matrix consisting of left eigen vectors, where each row is the left eigen vector of the corresponding eigen value in the W matrix. Multiplying the ith mode's right eigen vector and left eigen vector gives the column of participation factors for the ith mode and the corresponding states. The participation factors for all the modes are given in Table 6-7.

Table 6-7. Participation Factors of Kundur-pp-1039 System

Rotor	52.73 Hz Mode	29.66 Hz Mode	22.33 Hz Mode
HP	0.258171	0.213546	0.018504
IP	0.237287	0.196085	0.03334
LP	0.004505	0.074687	0.057315
GENR	3.61E-05	0.015682	0.390841

Impulse Response

To obtain the impulse response magnitudes of the modes in individual rotor section velocities, the Kundur shaft system was built and simulated in ATPDraw/ATP software. The schematic for this system is shown in Figure 6-4. In this equivalent electrical circuit, the capacitors represent the rotor sections' moments of inertia and the inductances represent the inverse values of the shaft spring constants.
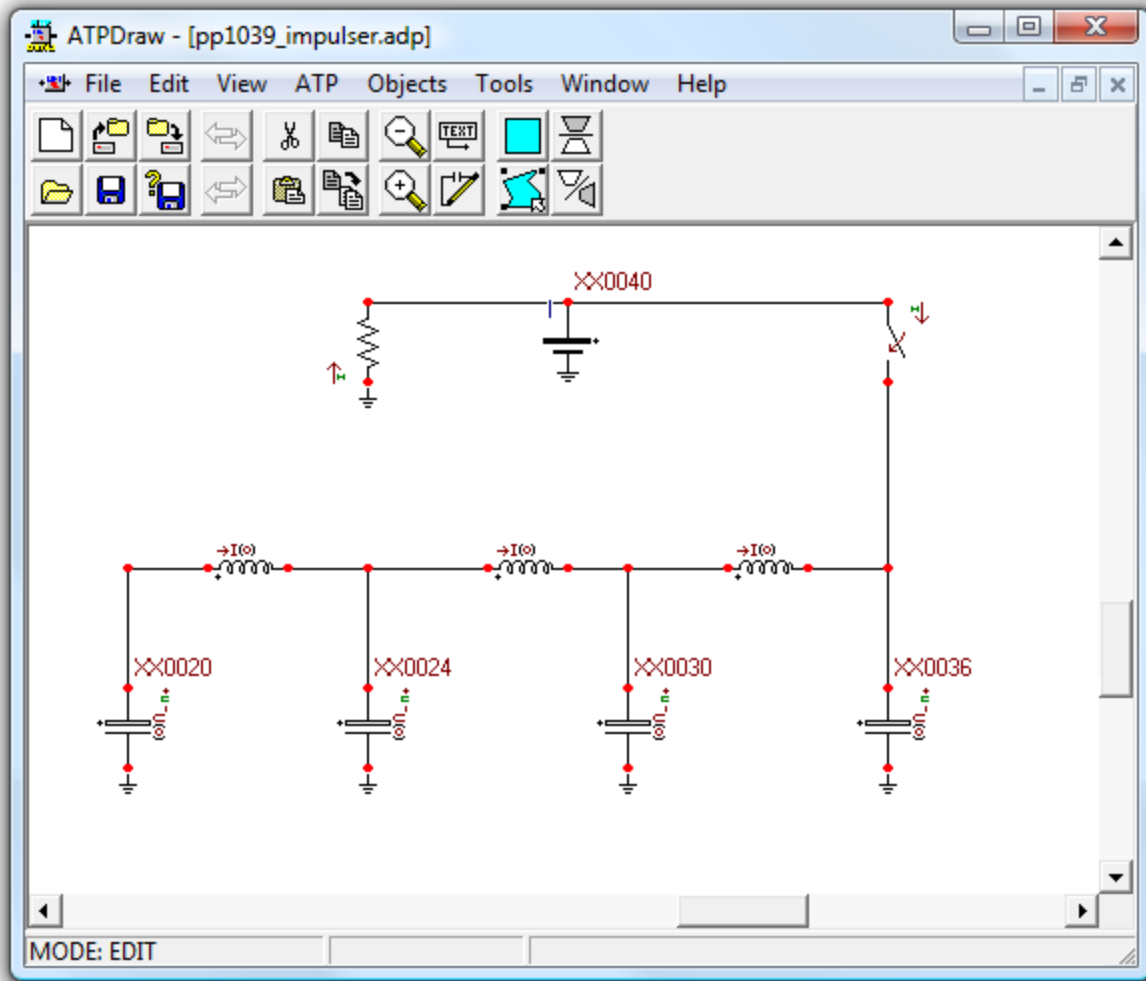
Figure 6-4 ATPDraw Schematic of Simulation of Impulse Response of Kundur 1039 Shaft

System

All the electrical quantities in this circuit are zero when the simulations begin. The impulse signal is applied as a short duration torque into the generator rotor section, which is represented by the capacitor connected to the node labeled XX0036. This causes the quantities to rapidly rise (for the duration of the impulse) and then ring-down back to zero. The ATPDraw/ATP software writes the capacitor voltage signals into a binary output.pl4 file. Another program is used read to the .pl4 output file and display the saved waveforms. Shown in

Figure 6-5 is the plot of the HP rotor section velocity signal. Note that the HP rotor section was represented by the capacitor connected to the node XX0020 in Figure 6-4.
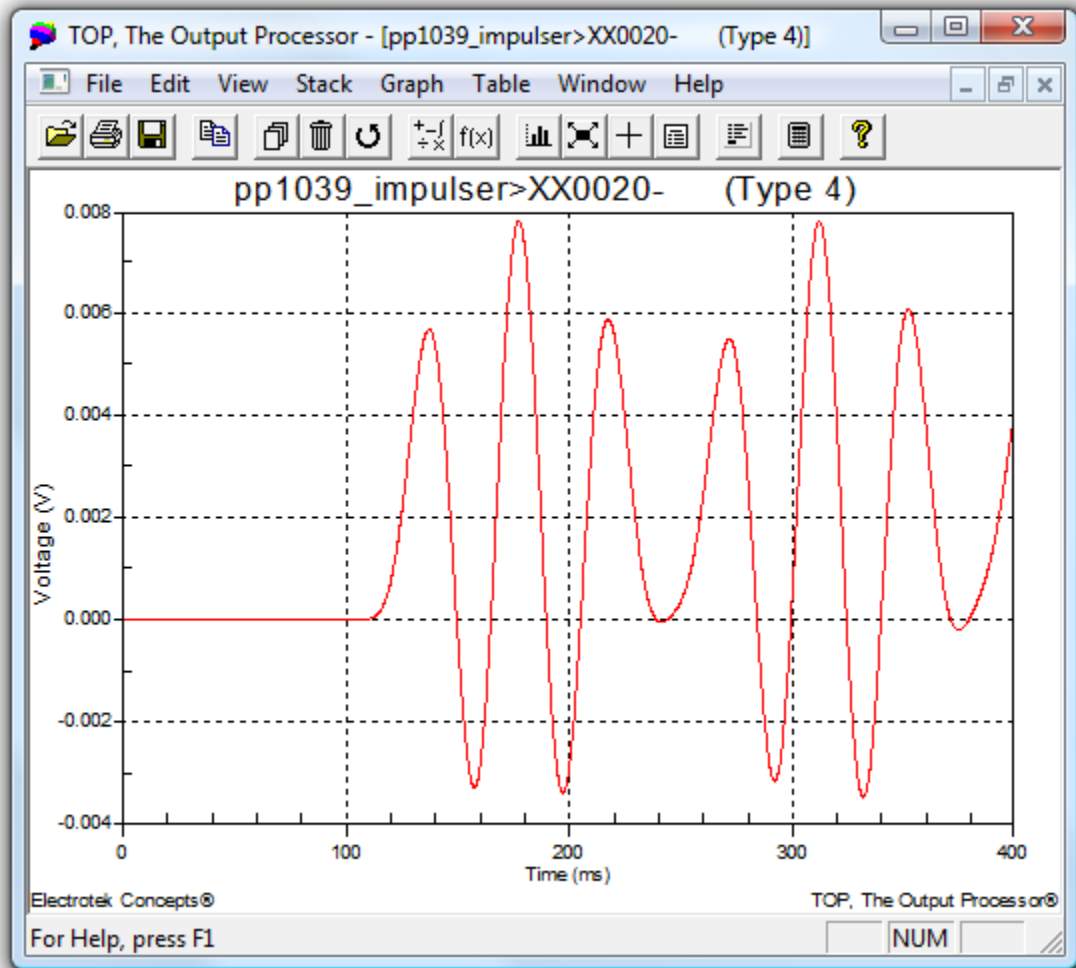
Figure 6-5 Plot of HP Rotor Section Velocity

The software also allows us to convert these waveforms to ascii format and store them in a .txt file. Prony's method and the reordering algorithm presented in Chapter 4 are then used to extract the constituent modes in each rotor section velocity signal. The results are given in Table 6-8. Each column in this table gives the magnitude of the particular mode in a given signal. For

instance, shown in Column 1 (titled HP) are the magnitudes of the 52.7 Hz, 29.7 Hz and 22.3 Hz modes in the HP rotor section velocity signal: 0.0000104, 0.0019394 and 0.0038962 respectively. The purpose of performing this test is to further illustrate the association of different modes and the states of the shaft system. This serves as a good complement to the theoretical analysis involving right eigen vectors and participation factors discussed in the previous sections.

Table 6-8. Impulse Response Modal Magnitudes of Kundur-pp-1039 system

	HP	IP	LP	GENR
Frequency(Hz)	Magnitude	Magnitude	Magnitude	Magnitude
52.7	0.0000104	0.0000054	0.0000002	4.87E-08
29.7	0.0019394	0.0010071	0.0001881	0.0001703
22.3	0.0038962	0.0028337	0.001123	0.0057919

6.7 Conclusions

The basic concepts of state space theory are revisited and reviewed in this chapter in order to aid in analyzing the eigen characteristics of STG shaft systems. An STG system whose data was provided in [16] was used to illustrate the way in which these eigen properties, such as eigen values, right eigen vectors and participation factors are computed. ATPDraw/ATP software was used to simulate the impulse response of this shaft system. The purpose of impulse response analysis is to verify, to a certain degree, the theoretical approximations that were obtained using eigen analysis. These methods are used in the next chapter, in which four STG shaft systems are analyzed, to help reveal general characteristics of all these shaft systems.

73

CHAPTER 7

APPLICATION OF EIGEN ANALYSIS ON TEST CASES

Before the proposed methodology is applied to test a complete system (in the next chapter) consisting of both the mechanical shaft system and the connected electrical power system, it is beneficial to study the behavior of a few typical STG shaft systems whose data is presented in the literature [4,16]. It is hoped that applying eigen analyses on these test cases will help reveal crucial information about how typical STG shaft systems aspects affect the proposed methodology's capabilities in determining the parameters of STG systems.

In this chapter, the concepts of eigen analysis introduced in the last chapter will be applied to four separate systems. These systems will be separately analyzed to help draw conclusions regarding the effect of these eigen properties on the measured magnitudes of rotor speed signals. The four shaft systems presented are:

1. 555 MVA, 3600 rpm STG shaft system (Kundur pp 1036) [16],

2. 960 MVA, 1800 rpm STG shaft system (Kundur pp 1038) [16],

3. 191 MVA, 3600 rpm STG shaft system (Kundur pp 1039) [16], and

4. 892.4 MVA, STG shaft system, IEEE-FBM [4].

7.1 Remarks on Terminology Used

Eigen analysis has proved to be an extremely valuable analysis tool in this work. It has helped reveal some fundamental aspects of the STG shaft systems that directly affect the proposed methodology's performance. While applying these analyses the actual speed signals of various rotor sections will be referred to as state variables in the sense that these are all purely mathematical variables.

However, in real life there are some important constraints. First is that not every state variable in the STG shaft system is measureable. We only have access to speed signals on either end of the shaft system and the instantaneous power p(t) at the generator terminals. In most cases for large systems, the exciter is at the extreme end of the shaft system. Therefore, we do not have access to generator speed in most cases. In those cases we can try to extract the modes using measured instantaneous signal, p(t), but only to a certain extent. The reason for this is if a mode is present with a very small magnitude in the generator-section velocity state, then this small magnitude signal of the mode after passing through the electrical stator and the rotor circuits and the air-gap flux, which tend to attenuate it, becomes even smaller. It is important to consider these constraints as we proceed with the analysis.

Because certain terms and phrases appear very frequently in all the following sections, they are abbreviated to help increase clarity. These terms are as follows:

HPRSV : High pressure rotor section velocity,

GNRSV : Generator section velocity,

HFM : Highest frequency mode,

75

LFM : Lowest frequency mode,

STGS : Steam turbine generator shaft, and

REV : Right eigen vectors.

7.2 System 1: 555 MVA STG System from Kundur pp 1036

The schematic for this STG shaft system is provided in Figure 7-1. This shaft system has five rotor sections and thus has four natural frequencies: {16.3 Hz, 24.1 Hz, 30.3 Hz and 44.0 Hz} that are also provided in [16]. The STG shaft system parameters are presented in tables 7-1 and 7-2. These are first converted to p.u. using proper base quantities as discussed in the previous chapter and they are used to compute the system's state matrix, A. All the relevant eigen properties such as left and right eigen vectors and participation factors are then computed from this state matrix using Matlab.
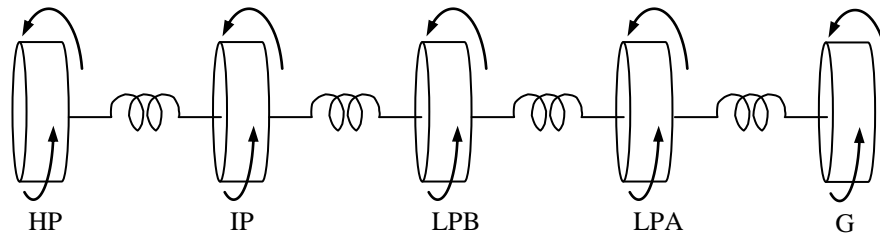
Figure 7-1 Schematic Layout of Rotor and Shaft Sections of Kundur pp. 1036 system

Table 7-1 Rotor Inertias

Rotor	H (MW-s/MVA)
HP	0.124
IP	0.232
LPB	1.155
LPA	1.192
GENR	0.855

Table 7-2 Shaft Spring Constants

Shaft	K (pu. torque/rad)
HP-IP	21.8
IP-LPB	48.4
LPB-LPA	75.6
LPA-GENR	62.3

7.2.1 Right Eigen Vector Analysis

The right eigen vectors (REVs) are shown in table 7-3. Note that these are normalized such that the maximum absolute value of any given vector element is 1. Because we are currently concerned about rotor section velocity states, only the corresponding entries in each eigen vector are shown. These eigen vectors are plotted in Figure 7-2. The y-axis is logarithmic because the values are of different orders of magnitude. Only the absolute values of right eigen vectors are displayed because the logarithmic axis does not allow plotting negative values and, more importantly, we are currently interested in the actual magnitudes (not the signs).

Table 7-3 Right Eigen Vectors for Kundur-pp-1036 System

Rotor	43.99 Hz Mode	30.30 Hz Mode	24.08 Hz Mode	16.22 Hz Mode
HP	-0.76569	1	1	1
IP	1	-0.09383	0.309226	0.686315
LPB	-0.148	-0.50002	-0.18192	0.363603
LPA	0.033732	0.708974	-0.15883	-0.14935
GENR	-0.00739	-0.43252	0.23824	-0.61422
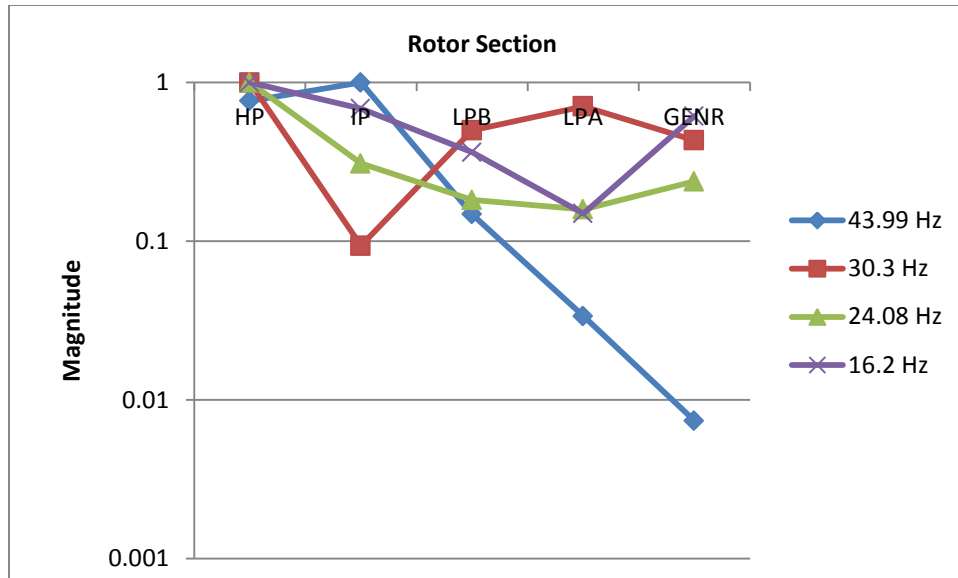
Figure 7-2 Kundur 1036 Right Eigen Vector (mode shape) Absolute Magnitudes Across Rotor Sections

Shown in Figure 7-2 are four curves with each curve illustrating the relationship between a given mode and the five rotor section velocity states in the system. For instance, the first curve shows, in a free response case, the relative magnitudes of the first mode with respect to each other as they appear in different rotor signals. The observed magnitude of the 44 Hz mode in the generator rotor section's speed signal is about 100 times smaller than the observed magnitude in the H.P. rotor section speed signal. It is important to note that these are not indicative of the absolute magnitudes because the right eigen vectors are scaled such that the absolute maximum value is 1. This means that these charts can be used to infer information about relative magnitudes of a given mode in different rotor section speeds, and not regarding magnitudes of various modes in a given rotor section velocity signal. For instance, the relative magnitudes of all modes in the generator rotor section velocity (GRSV) measurements cannot be predicted. However, if the highest frequency modal (HFM) magnitude in one velocity state is known, it can be used to predict the HFM's magnitude in another rotor section velocity state. For instance, in

the next section, in table 7.3 on impulse response tests, it is given that the magnitude of the 44 Hz mode in GNRSV is approximately 2e-7. Looking at REV of the 44 Hz mode in Figure 6-5, it can be predicted that the magnitude of the 44 Hz mode in HPRSV would be 100 times 2e-7 i.e., 2e-5. This prediction is confirmed as indicated in table 7-3 where the magnitude of the 44 Hz is shown to be approximately equal to 2.2e-5. As mentioned earlier, using the REVs, the relative magnitudes of all modes in a given rotor section velocity measurement cannot be predicted. To do that, it is recommended to use participation factors, which will be discussed in the next section.

It can be concluded from Figure 7-2 that the measured magnitude of the highest frequency, 44 Hz, varies significantly across rotor sections. Especially, as mentioned earlier, it appears very small in the generator rotor section velocity signal compared to its measured magnitude in the HP rotor section velocity signal. As mentioned in section 7.1, this small magnitude mode in the generator rotor section velocity signal would appear even smaller in the instantaneous power, p(t) signal. It can also be inferred that there is only modest variation in measured magnitudes of lower frequencies across rotor sections when compared to the highest frequency. Thus, it can be deduced that the HP rotor section velocity signal is a much better candidate than p(t) for detection of STG shaft torsional modes, especially for higher frequency modal identification.

7.2.2 Participation Factors

Right eigen vectors provide valuable information about the manner in which the modes show up in different velocity states. But, they do not represent the complete picture of how the modes and states are connected. To do that, it is also necessary to take into account the left eigen vectors, which depict how the initial conditions on states impact the magnitudes of the modes of

the system in a free response behavior. Participation factors combine both these vectors to illustrate completely how the states and modes are associated. Participation factors for the Kundur 1036 STGS system computed using (6.18) are given in Table 7-4 and illustrated in Figure 7-3. Just like in right eigen vectors charts, the y-axis in this chart is logarithmic because the values are of different orders of magnitude.

Table 7-4. Participation Factors of Kundur-pp-1036 System

Rotor	43.9 Hz	30.3 Hz	24.0 Hz	16.2 Hz
HP	1.097E-01	5.281E-02	2.357E-01	8.434E-02
IP	3.500E-01	8.700E-04	4.217E-02	7.433E-02
LPB	3.817E-02	1.230E-01	7.267E-02	1.039E-01
LPA	2.046E-03	2.552E-01	5.717E-02	1.808E-02
GENR	7.047E-05	6.813E-02	9.226E-02	2.194E-01
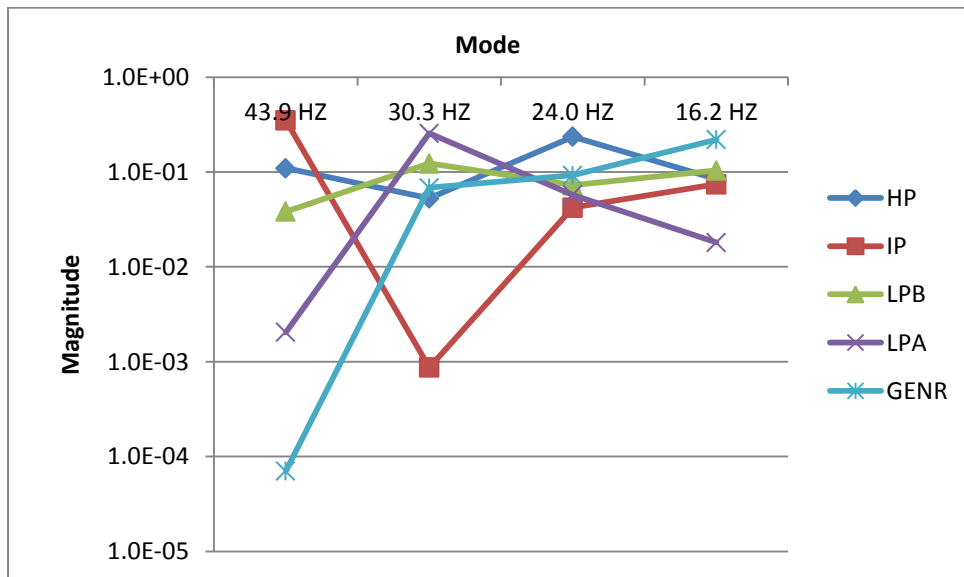
Figure 7-3 Kundur 1036 System's Participation Factors Across All Rotor Sections

Each curve in this chart illustrates how strongly a given rotor velocity state is associated with the different modes in the system. The participation factor for the 44 Hz mode across various RSV states varies tremendously. The lower frequency modes participate approximately the same amount across all RSV states. Mode 2 (30 Hz) participates approximately the same amount across all RSV states except in the IP RSV. These Figures indicate there will be difficulties measuring mode 4 in the generator rotor section velocity signal. To compensate for this, the HP rotor section velocity signal could be used as a measurement signal, because in this state all the modes participate equally and sufficiently well.

7.2.3 Impulse Response Analysis

The third analysis that will be performed on the Kundur 1036 STG shaft system is the impulse response test. As discussed in the previous chapter, instead of using frequency domain methods to obtain the transfer function, the impulse response includes a time domain simulation of the shaft system to obtain the modal magnitudes in different rotor velocity states. This is in contrast to the first two analyses, which used right eigen vectors and participation factors, i.e., eigen properties of the shaft system. This allows us to compare not only the magnitude of a particular mode across rotor sections but also different modal magnitudes in given rotor sections. This allows us the opportunity to test the theoretical inferences made using right eigen vectors and participation factors analyses.

The isolated shaft system is simulated in ATP using an equivalent LC tank circuit where the rotor section mass inertias are represented by capacitors, and shaft spring constants are represented by inverse inductance values. Just as in full simulations, where the main disturbance torque enters the shaft system in the generator-section through an electrical torque signal, here

too the disturbance enters the generator rotor section in the form of a short impulse that represents a disturbance torque. Prior to the disturbance, all the states, capacitor voltages and inductor currents, are equal to zero. The effect of the disturbance, a short current pulse for about 20 milliseconds, is that capacitor voltages and inductor currents states display free-response type behavior decaying down to zero. These speed signals are measured in all rotor sections and modal decomposition is performed using Prony's method to determine the resulting modal frequencies and magnitudes. These results are shown in table 7-5 and Figure 7-4. As predicted earlier from eigen analysis, the 44 Hz mode magnitude is very small in the generator rotor section velocity signal, as compared to the HP rotor section velocity signal. In addition, as mentioned in section 7.1, this small magnitude mode in the generator rotor section velocity signal would appear even smaller in the instantaneous power, p(t) signal. Also, all the modes appear well in the HP rotor section velocity signal.

Table 7-5. Impulse Response Modal Magnitudes of Kundur-pp-1036 system

	HP	IP	LPB	LPA	GENR
Frequency (Hz)	Magnitude	Magnitude	Magnitude	Magnitude	Magnitude
43.9975	2.26E-05	2.96E-05	4.4E-06	0.000001	2E-07
30.31358	0.001817	0.000172	0.000909	0.001292	0.000787
24.08246	0.005947	0.001838	0.001083	0.000944	0.001415
16.22699	0.006954	0.004773	0.002529	0.001039	0.004274
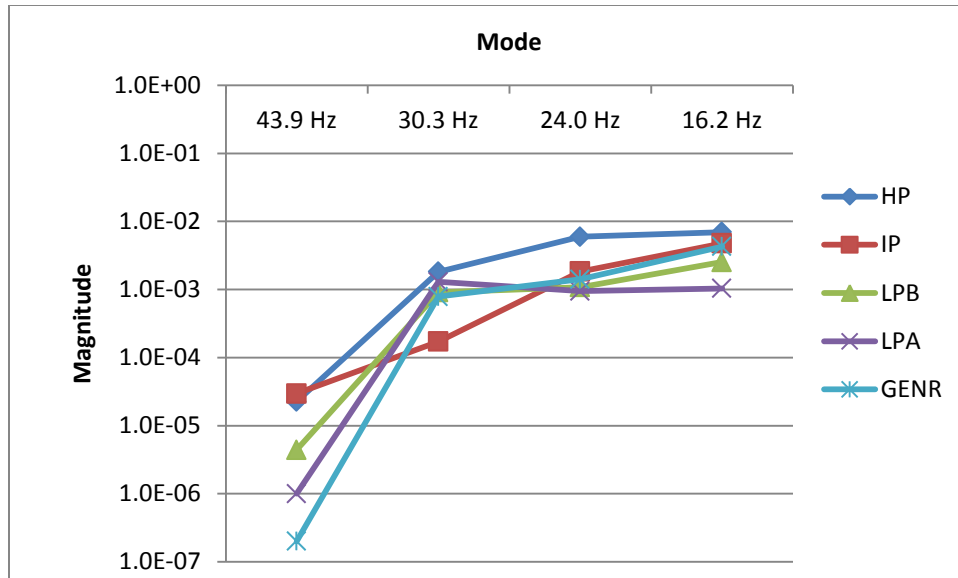
Figure 7-4 Kundur 1036 System Impulse Response Results

7.2.4 Conclusions for Kundur 1036 System

Looking at the chart for participation factors in Figure 7-3, it can be inferred that the highest frequency mode (HFM) does not participate sufficiently well in the generator rotor section velocity state. This fact was confirmed by impulse response test results shown in Figure 7-4 where the measured magnitude of the 44Hz mode (HFM) was 10,000 times smaller than the 16 Hz mode. In real-life situations, this would mean that it would be extremely hard to detect the 44 Hz mode in the generator rotor section velocity signal. Moreover, it would be even harder to detect in the instantaneous power, p(t) signal. However, there is a solution to this problem. The REV or mode shapes, shown in Figure 7-2, indicate that the 44 Hz mode would be 100 times stronger in the HP rotor section velocity signal. Moreover, the rest of the modes participate sufficiently well in the HPRSV. This indicates that the HP rotor section velocity signal is a much

83

better candidate for detecting these torsional modes when compared to the generator rotor section velocity signal and a better candidate than the associated instantaneous power signal.

7.3 System 2: 960 MVA STG shaft system from Kundur 1038

This 960 MVA STG shaft system is identical to the previous STG shaft system with respect to the layout. Consequently, it also has four natural torsional frequencies. They are 8.4 Hz, 15.2 Hz, 20.3 Hz and 23.6 Hz. Just as in the previous section, all the eigen properties were computed using the system's state matrix built using the converted p.u. data.
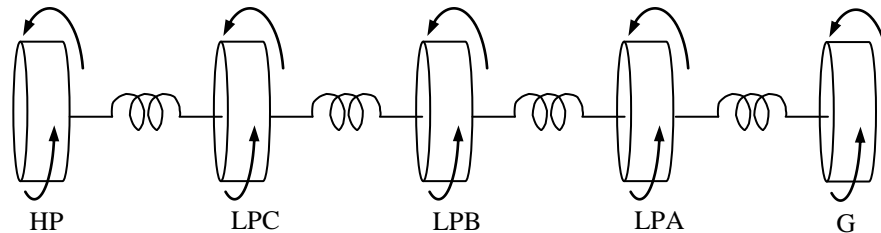
Figure 7-5 Schematic Layout of STG Shaft System of Kundur pp. 1038 Problem

Table 7-6 Rotor Section Inertias

Rotor	H (MW-s/MVA)
HP	0.176
LPC	1.427
LPB	1.428
LPA	1.428
GENR	0.869

Table 7-7 Shaft Spring Constants

Shaft	K (pu. torque/rad)
HP-LPC	17.78
LPC-LPB	27.66
LPB-LPA	31.31
LPA-GENR	37.25

7.3.1 Eigen vectors

The right eigen vectors for this system are shown in Table 7-8. A plot of these vectors is shown

in Figure 7-6.

Table 7-8 Right Eigen vectors for Kundur-pp-1038 system

Rotor	23.62 Hz Mode	20.22 Hz Mode	8.23 Hz Mode	15.18 Hz Mode
HP	1	-0.49422	1	-0.9212
LPC	-0.15693	-0.07506	0.859409	-0.48095
LPB	0.045615	0.526171	0.139315	1
LPA	-0.01861	-0.99879	-0.58708	0.106318
GENR	0.010776	1	-0.87799	-0.84163
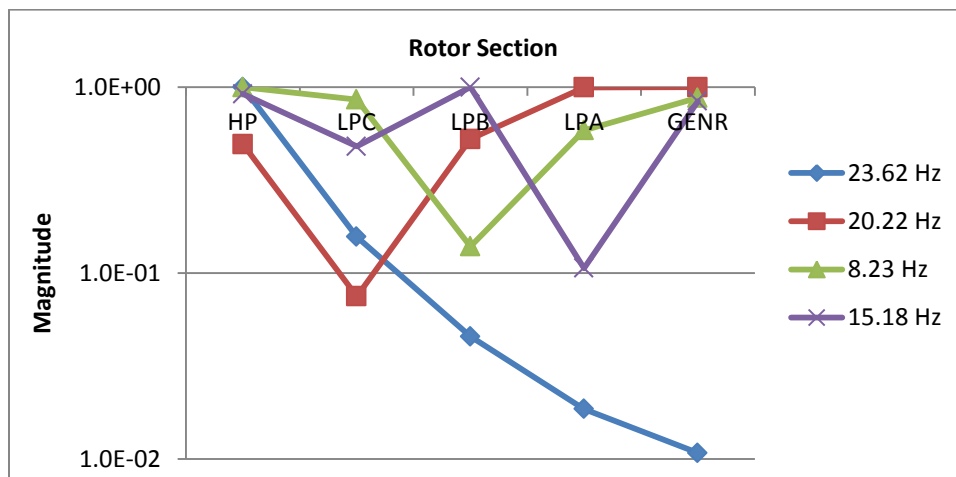
Figure 7-6 Kundur 1038 Right Eigen Vector Absolute Magnitudes Across Rotor Sections

85

The highest frequency mode (HFM) is 23.6 Hz. There is extensive variation in the right eigen vector (REV) of this mode across rotor section velocity states. Just like in the Kundur 1036 system, the smallest eigen vector value is about 100 times smaller than the largest value. Also, this smallest eigen vector value occurs in the generator rotor section velocity state. Although the variation in the rest of the mode shapes is considerable, they are smaller compared to that of the 23 Hz mode.

7.3.2 Participation Factors

The participation factors for this system are given in Table 7-9 and a plot of these factors is shown in Figure 7-7. It can be inferred from this figure that although the generator rotor section velocity state participates in lower frequency modes approximately uniformly, it has very little participation in the highest frequency mode (HFM) as indicated by the blue curve with the cross marker. The HFM participates very well in the HP rotor section velocity state, as indicated by the corresponding participation factor (4.09e-1), which is more than 1,000 times larger than the participation factor between the generator rotor section velocity and the 23 Hz mode (2.3e-4). Note that the participation factor between the 20 Hz mode and the HP rotor section velocity state is 100 times smaller than that of the participation factor between 20 Hz mode and the generator rotor section velocity state. However, it is not as small as the participation factor between 23 Hz mode and the generator rotor section velocity state, which is 1,000 times smaller than the participation factor between the 23 Hz mode and the HP rotor section velocity state. This establishes the HP rotor section velocity state as a better candidate to detect all the modes as compared to the participation factor between the 20 Hz mode and the generator rotor section velocity state. Recall that an identical conclusion was reached for the 1036 system earlier.

86

Table 7-9. Participation factors of Kundur-pp-1038 system

Rotor	23.62 Hz Mode	20.22 Hz Mode	8.23 Hz Mode	15.18 Hz Mode
HP	4.0986E-01	7.8448E-03	3.6368E-02	2.9411E-02
LPC	8.1835E-02	1.4673E-03	2.1778E-01	6.4998E-02
LPB	6.9192E-03	7.2146E-02	5.7270E-03	2.8120E-01
LPA	1.1511E-03	2.5996E-01	1.0170E-01	3.1785E-03
GENR	2.3498E-04	1.5858E-01	1.3842E-01	1.2121E-01
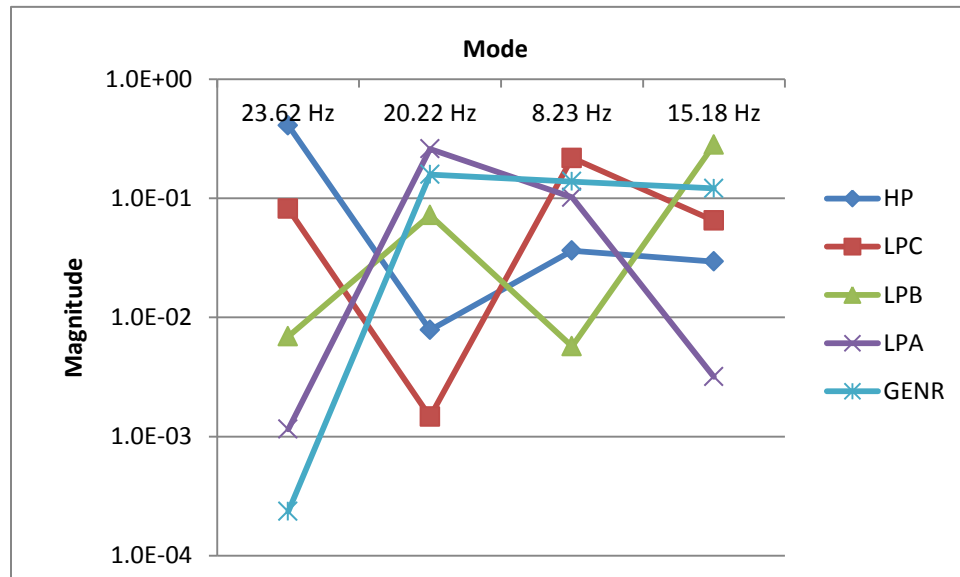
Figure 7-7 Kundur 1038 System's Participation Factors Across All Rotor Sections

7.3.3 Analysis of Impulse Response Modal Magnitudes

The impulse response modal magnitudes for this system are given in Table 7-10 and a plot of these magnitudes is shown in Figure 7-8. The curve for the generator rotor section velocity

87

indicates that all the modes show up equally well in the generator rotor section velocity signal, except for the 23 Hz mode whose magnitude is about 1,000 times smaller than the rest. However, if the HP rotor section velocity signal is chosen as the measurement signal, then all the modes appear approximately equally well. Moreover, these are relatively equal or higher than those detected in the generator rotor section velocity signal. Again, the observations in section 7.1 would imply that the 23 Hz mode would be even weaker in the instantaneous power, p(t), signal leading to the conclusion that the HP rotor section velocity signal is again a better candidate for modal extraction than the p(t) signal.

Table 7-10. Impulse Response Modal Magnitudes of Kundur-pp-1038 System

Frequency (Hz)	HP Magnitude	LPC Magnitude	LPB Magnitude	LPA Magnitude	GENR Magnitude
23.63	0.000333	5.23E-05	1.52E-05	6.2E-06	3.8E-06
20.21	0.001348	0.000206	0.001436	0.002725	0.00273
15.18	0.0026	0.001359	0.002816	0.0003	0.002371
8.235	0.003453	0.002968	0.000484	0.002024	0.003029
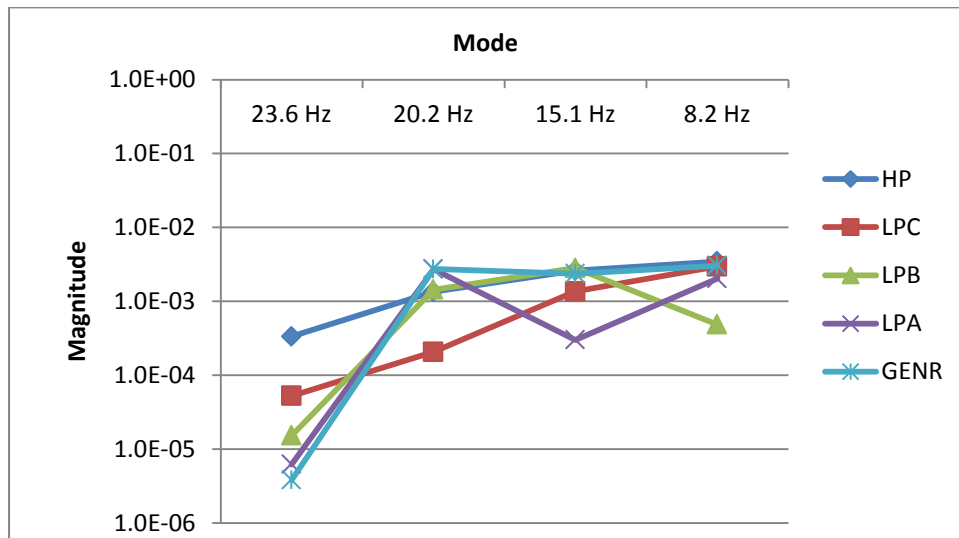
Figure 7-8. Kundur 1038 System Impulse Response Results

7.3.4 Conclusions

As observed previously in the Kundur 1036 system, here too the highest frequency mode (23HZ mode) participates very weakly in the generator rotor section velocity state, as validated by the impulse response measured magnitude in the generator rotor section velocity signal. In contrast, the measured magnitude of the 23 Hz mode in the HP rotor section velocity signal is much higher than in the generator rotor section velocity signal. Moreover, the magnitudes of all the modal components are sufficiently large enough to be detected in the HP rotor section velocity signal. This makes it a better candidate than the generator rotor section velocity signal and an even better candidate than the p(t) signal for detecting torsional modal components.

7.4 System 3: 191 MVA STG Shaft System from Kundur pp 1039

The third STG shaft system that will be studied is the Kundur 1039 system, whose data was presented in the previous chapter. For convenience the shaft configuration is presented here again in Figure 7-9. This system has four rotor sections and thus three torsional natural frequencies (22 Hz, 29 Hz and 52 Hz.)

7.4.1 Eigen vectors Analysis

The right eigen vectors for this system are shown in Table 6-6. A plot of these vectors is shown in Figure 7-10. The mode shape for the 52 Hz mode indicates that it shows up very insignificantly in the GNRSV signal, as compared to the rest of the rotor states. The mode shapes of the rest of the modes do not vary as much, indicating that they show up well in all the rotor section velocity states.
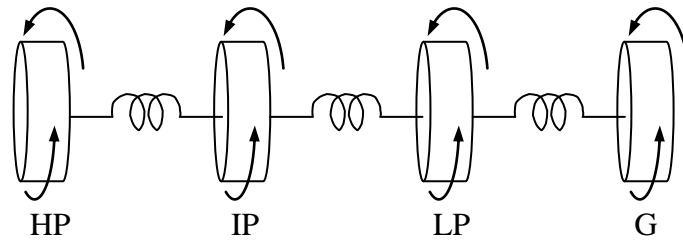
Figure 7-9 STG Shaft System Schematic for Kundur 1039 System
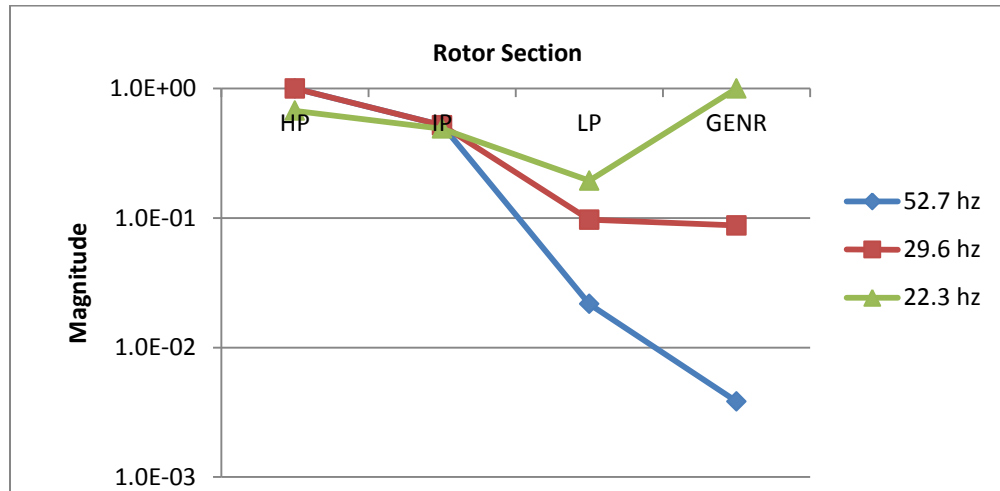
Figure 7-10 Kundur 1039 Right Eigen Vector Absolute Magnitudes Across Rotor Sections

7.4.2 Participation Factors

The participation factors for this system are given in Table 6-7, and a plot of these factors are shown in Figure 7-11.
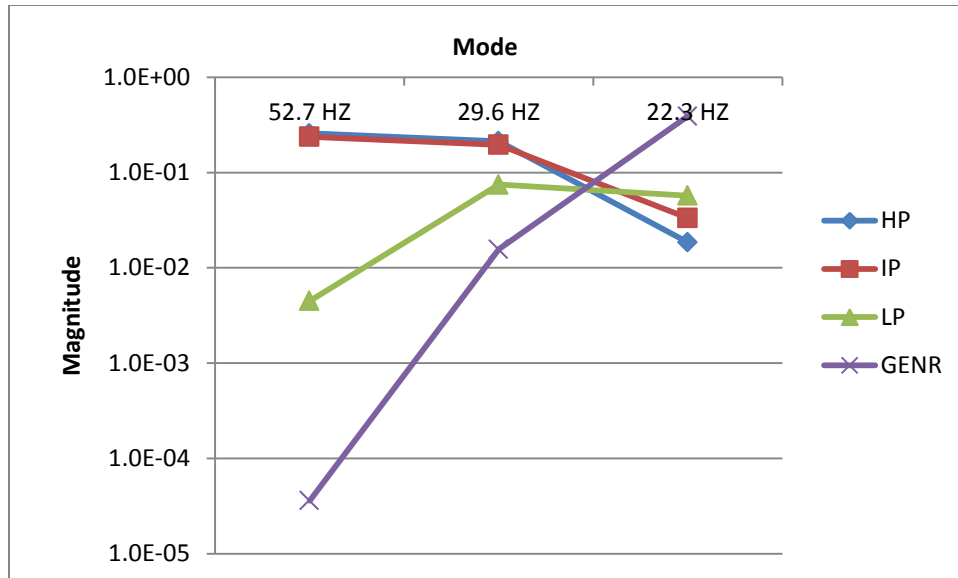
Figure 7-11 Kundur 1039 System's Participation Factors Across All Rotor Sections

From Figure 7-11, it can be inferred that the three modes participate very unevenly in the generator rotor section velocity state with the highest frequency mode (52 Hz) participating approximately 10,000 times weaker than the 22 Hz mode. Also, all the modes participate relatively equally and sufficiently in the HP rotor section velocity.

7.4.3 Analysis Using Impulse Response Modal Magnitudes

The impulse response modal magnitudes for this system are given in Table 6-8, and a plot of these factors is shown in Figure 7-12.
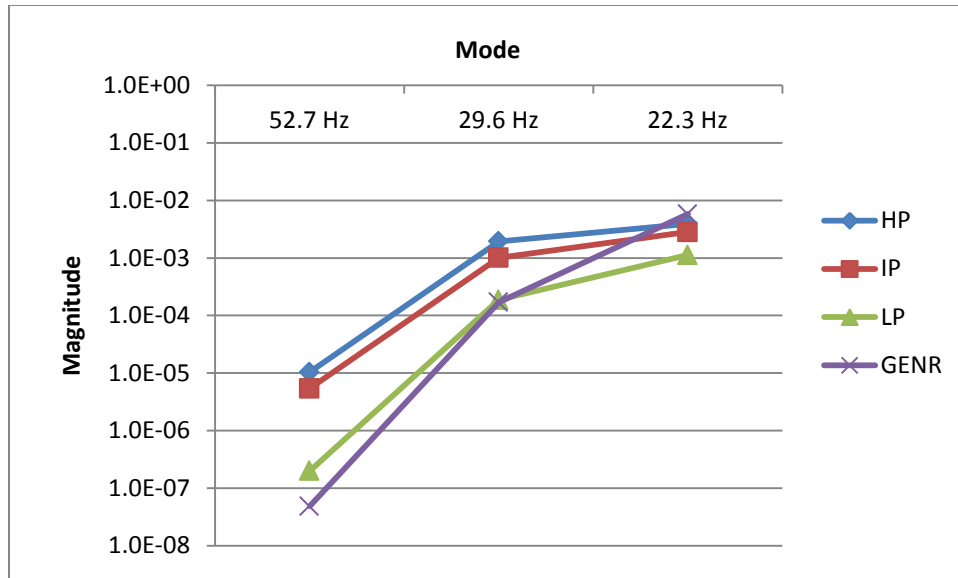
Figure 7-12. Kundur 1039 System Impulse Response Results

As predicted by the participation factors and the right eigen vectors, the 52 hz mode magnitude in the generator rotor section velocity state is very small (100 times smaller) compared to the measured magnitude in the HP rotor section velocity signal. Moreover, all the measured modal magnitudes are higher in the HP rotor section velocity signal than in the generator rotor section velocity signal. These facts again point to the conclusion that the HP rotor section velocity signal is a better candidate for detecting the torsional modes than the generator rotor section velocity signal. In addition, it is an even better candidate than the instantaneous power signal, $p(t)$, because of the reasons mentioned in section 7.1.

7.5 System 4: 892.4 MVA STG Shaft System From IEEE-FBM

The final test case is the so-called First Benchmark (FBM) case, a standardized test case, developed by the IEEE's SSR Task Force based on the Navajo Project [4] for the industry to analyze different models, compare their results and validate their simulation programs. It uses

data that belongs to actual generators and turbines, thus making the case more realistic. The shaft

system configuration and data are provided in Figure 7-13 and Table 7-11.
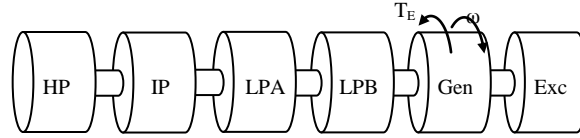
Figure 7-13 STG Shaft System for IEEE-FBM

Table 7-11. Rotor Spring Mass Parameters

Inertia		Spring Constant		
Mass	H (sec)	Shaft	K (p.u.)	p.u. torque / rad
HP	0.092897	HP-IP	7277	19.303
IP	0.155589	IP-LPA	13168	34.929
LPA	0.85867	LPA-LPB	19618	52.038
LPB	0.884215	LPA-GEN	26713	70.858
GEN	0.868495	GEN-EXC	1064	2.822
EXC	0.0342165			

7.5.1 Eigen vectors

The right eigen vectors for this system are shown in Table 7-12. A plot of these vectors is shown

in Figure 7-14.

Table 7-12 Right Eigen Vectors for IEEE-FBM System

Rotor	47.45 Hz Mode	32.28 Hz Mode	25.54 Hz Mode	15.71 Hz Mode	20.21 Hz Mode
HP	-0.7874	0.863783	1	-0.77714	-0.10989
IP	1	-0.0437	0.342151	-0.58376	-0.06464
LPA	-0.11328	-0.50271	-0.22972	-0.34244	-0.01499
LPB	0.021114	1	-0.09543	0.1117	0.039498
GENR	-0.00446	-0.62049	0.165974	0.373148	0.037344
EXCR	0.000945	0.376842	-0.25255	1	-1
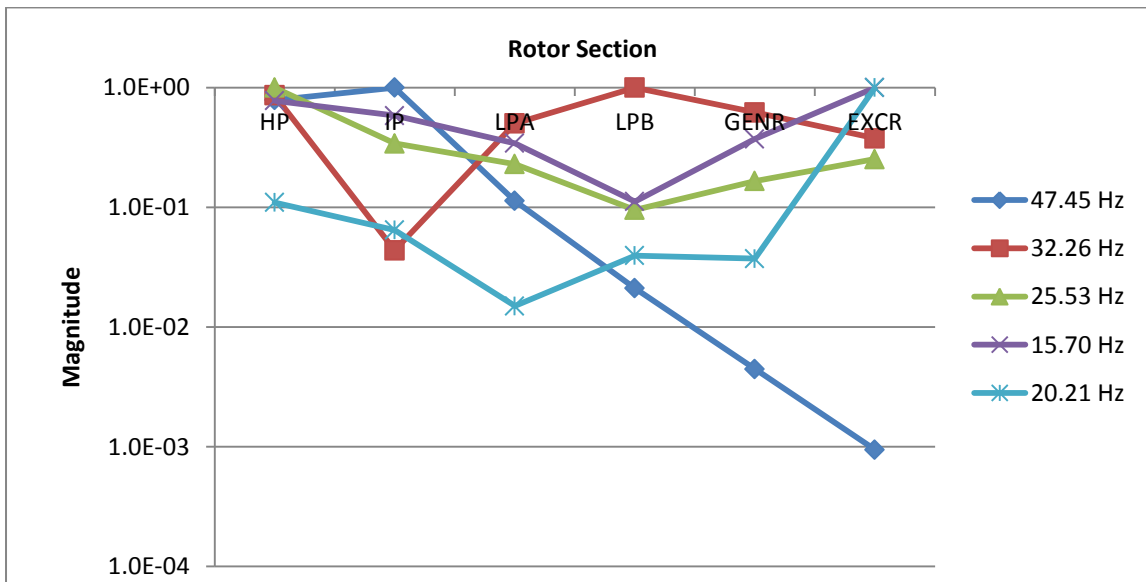
Figure 7-14 IEEE-FBM Right Eigen Vector Absolute Magnitudes Across Rotor Sections

Shown in the chart are mode shapes of the five modes with frequencies 15.7 Hz, 20 Hz, 25 Hz, 32 Hz and 47 Hz. The mode shape for highest frequency mode, i.e., the 47 Hz mode, indicates that this mode appears 200 times smaller in the generator rotor section velocity state than in the HP rotor section velocity state. Moreover, as mentioned in section 7.1, because the generator speed is not a measurable quantity because of the presence of the exciter on the end, these modes would have be detected in the instantaneous power signal, p(t). Again, as mentioned in section 7.1, it would be even harder to measure these modes as they would be even smaller, thus leading

94

to the conclusion that the HP rotor section velocity signal is the superior candidate of all these signals for torsional modal extraction.

7.5.2 Participation Factors Analysis

The participation factors for this system are given in Table 7-13, and a plot of these factors is shown in Figure 7-15.

Table 7-13. Participation Factors of IEEE-FBM Machine

Rotor	47.45 Hz Mode	32.28 Hz Mode	25.54 Hz Mode	15.71 Hz Mode	20.21 Hz Mode
HP	0.128211	0.02295	0.243714	0.074609	0.014467
IP	0.346346	9.84E-05	0.047785	0.070507	0.008383
LPA	0.024527	0.071851	0.118883	0.1339	0.00249
LPB	0.000877	0.292775	0.021125	0.014671	0.017789
GENR	3.85E-05	0.110717	0.062766	0.160812	0.015619
EXCR	6.81E-08	0.001609	0.005726	0.045502	0.441252
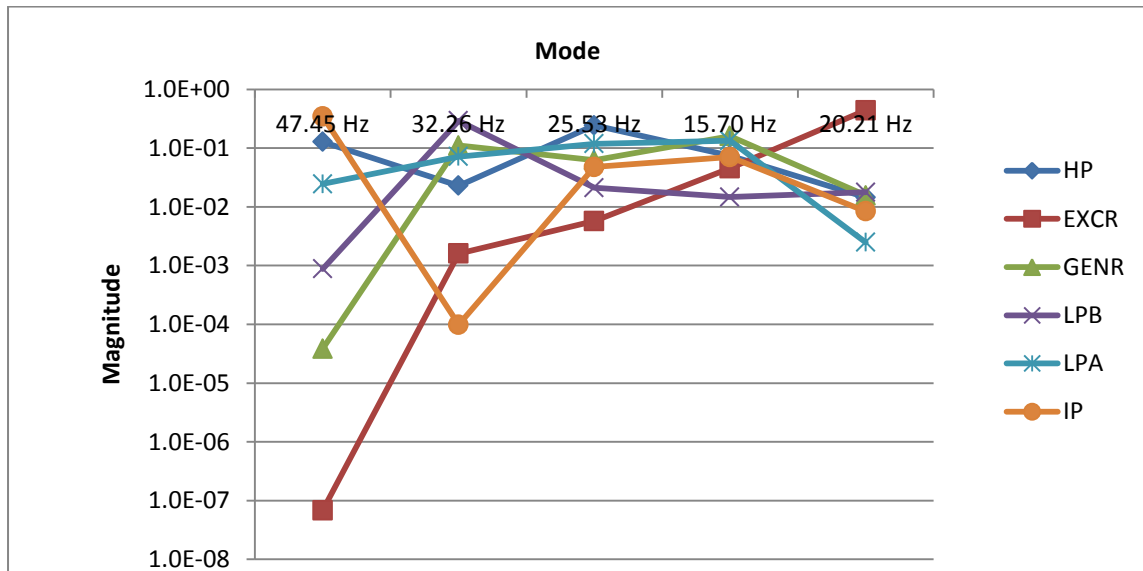
Figure 7-15 IEEE-FBM Participation Factors Across All Rotor Sections

95

For the sake of convenience, the two significant curves, participation factors of generator rotor section velocity and HP rotor section velocity states from Figure 7-15, are plotted in Figure 7-16. It can be inferred that although GNRSV participates equally and sufficiently among the 32 Hz, 25 Hz, 15.7 Hz and 20 Hz modes, its participation factor with respect to 47 Hz mode is extremely small, indicating that there is very slight likelihood that the 47 Hz mode will be detected in the generator rotor section velocity signal. Because these generator rotor section velocity signals are not measureable, the instantaneous power signal, p(t), would have to be used. Again, as mentioned in section 7.1, it would be even harder to measure these modes as they would be even smaller in p(t). However, observing the HP rotor section velocity participation factor curve, it is clear that it participates equally and sufficiently well in all the modes, dramatically increasing the likelihood of the 47 Hz mode being detected in its measured signal.
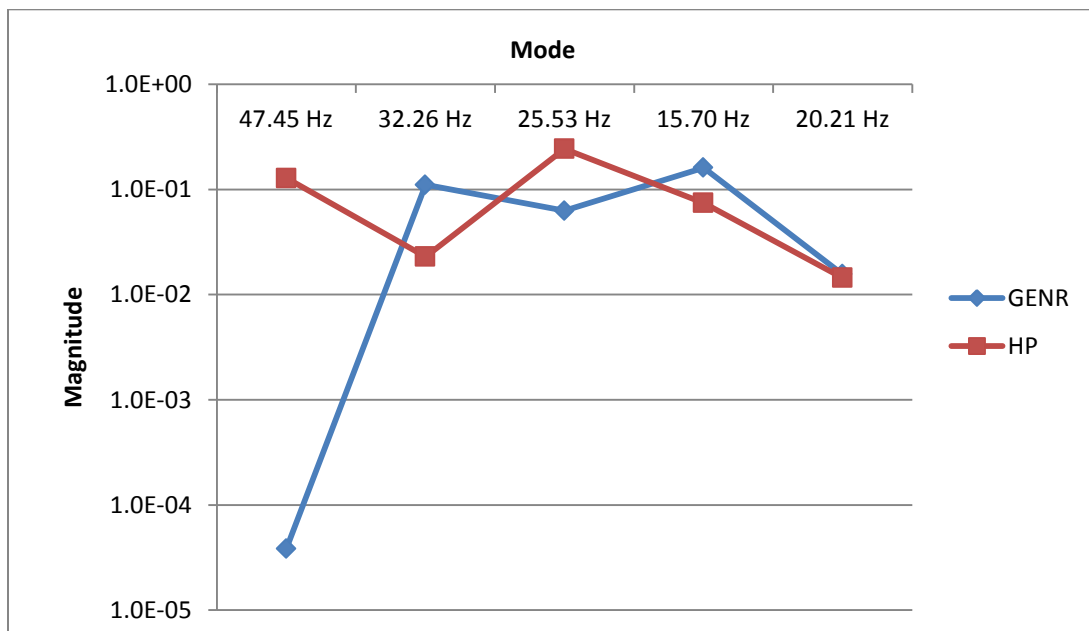
Figure 7-16 IEEE-FBM Participation Factors Across Generator and HP Rotor Sections

96

7.5.3 Impulse Response Modal Magnitudes

The impulse response modal magnitudes for this system are given in Table 7-14, and a plot of these factors is shown in Figure 7-17. As predicted earlier from eigen analysis, the 47 Hz mode magnitude is very small in the generator rotor section velocity signal as compared to the HP rotor section velocity signal. Also, all the modes appear well in the HP rotor section velocity signal.

Table 7-14. Impulse Response Modal Magnitudes of the IEEE-FBM System

Frequency (Hz)	HP	IP	LPA	LPB	GENR	EXCR
47.45727	8.19E-06	1.04E-05	1.18E-06	2.19E-07	4.63E-08	1.01E-08
32.26493	0.001562	7.88E-05	0.000909	0.001809	0.001121	0.000682
25.53284	0.005395	0.001846	0.001237	0.000515	0.000894	0.001364
15.70381	0.00649	0.004875	0.002861	0.000932	0.003117	0.00834
20.21083	0.00079	0.000464	0.000108	0.000284	0.000268	0.007197
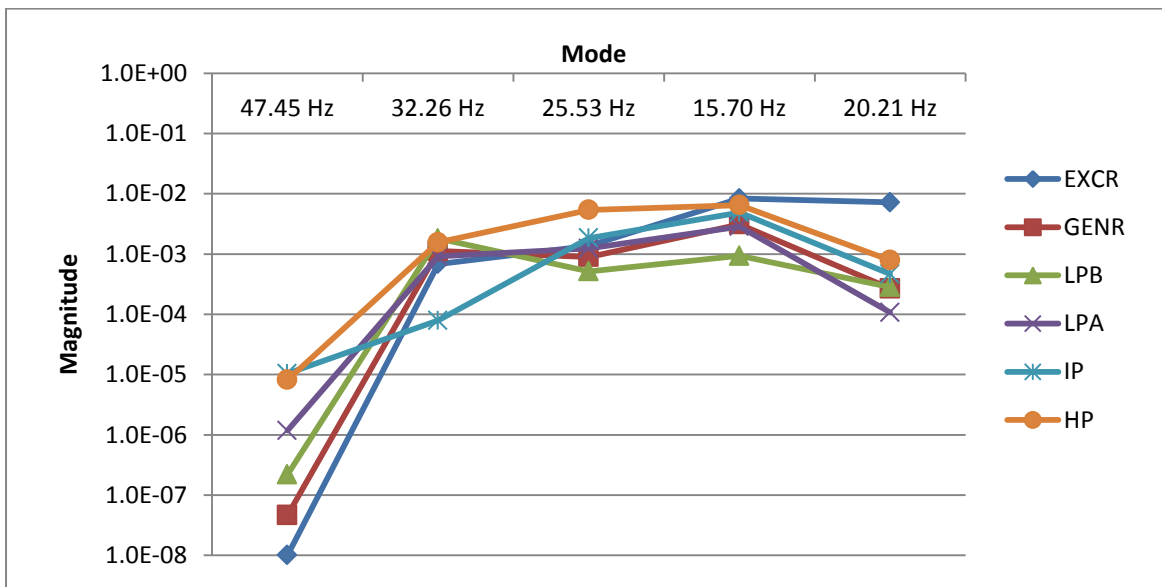
Figure 7-17 IEEE-FBM Impulse Response Results: Relative Magnitudes of Modes Measured in Different Rotor Section Speeds

7.6 General Conclusions from Right Eigen Vector Analysis of All Four Systems

For the sake of convenience, the mode-shapes (right eigen vectors) of the highest frequency modes of all four systems are plotted in a single chart in Figure 7-18. Because there are different numbers of rotor sections in these systems, the x-axis is not labeled. However, all the systems share a similar configuration in the sense that the HP rotor section is on the left hand side of the shaft system configuration and the exciter is on the right. Thus, we can choose to identify the x-axis unit labeled 1 as that of HP rotor section. Similarly, the unit labeled 4 corresponds to generator rotor section, except in the case of 1039 system where the unit labeled 4 corresponds to generator rotor section. Note that the exciter section of the FBM system is omitted for the sake of clarity. From these curves, it can be inferred that there is huge variation in all these mode-shapes and all the modal magnitudes tend to get extremely small in the generator rotor section velocity state as compared to the HP rotor section velocity state.
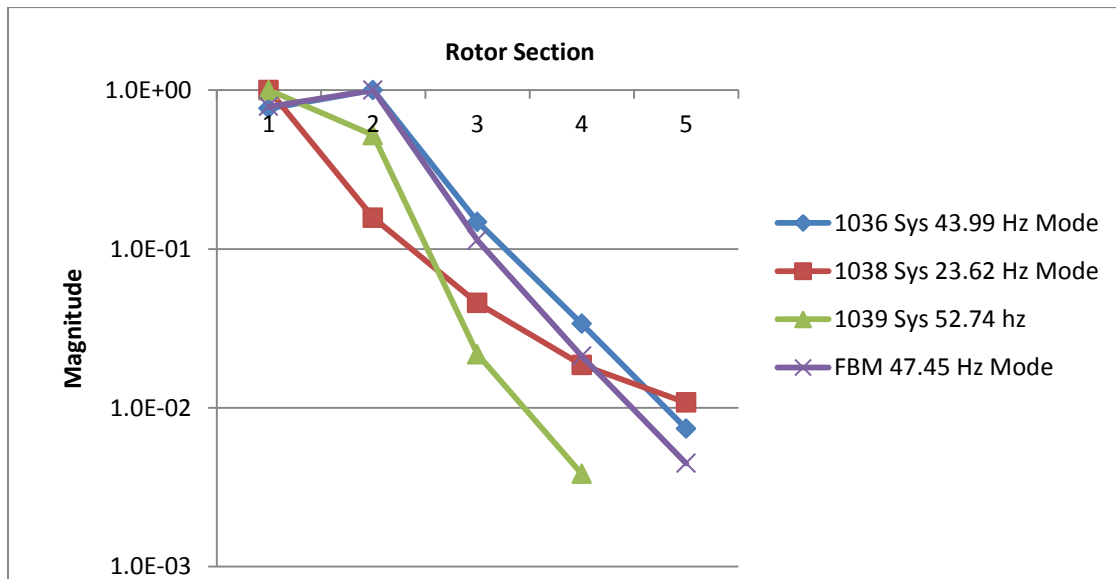
Figure 7-18 Comparison of Mode Shapes (Absolute Values) of Highest Frequency Modes

For the sake of convenience, the components corresponding to the HP rotor section velocity and generator rotor section velocity states of all the mode-shapes are separately plotted in Figure 7-19. These are normalized such that the right eigen vector component corresponding to the HP state is 1. From this figure, it can be inferred that there is a significant amount of attenuation of these modal magnitudes from the HP rotor section velocity to the generator rotor section velocity. As mentioned in section 7.1, these modes in the generator rotor section velocity signal would be even more attenuated in the instantaneous power, p(t), signal. To remedy this situation, it is recommended that the HP rotor section velocity signal be used instead of instantaneous power, p(t) signal.
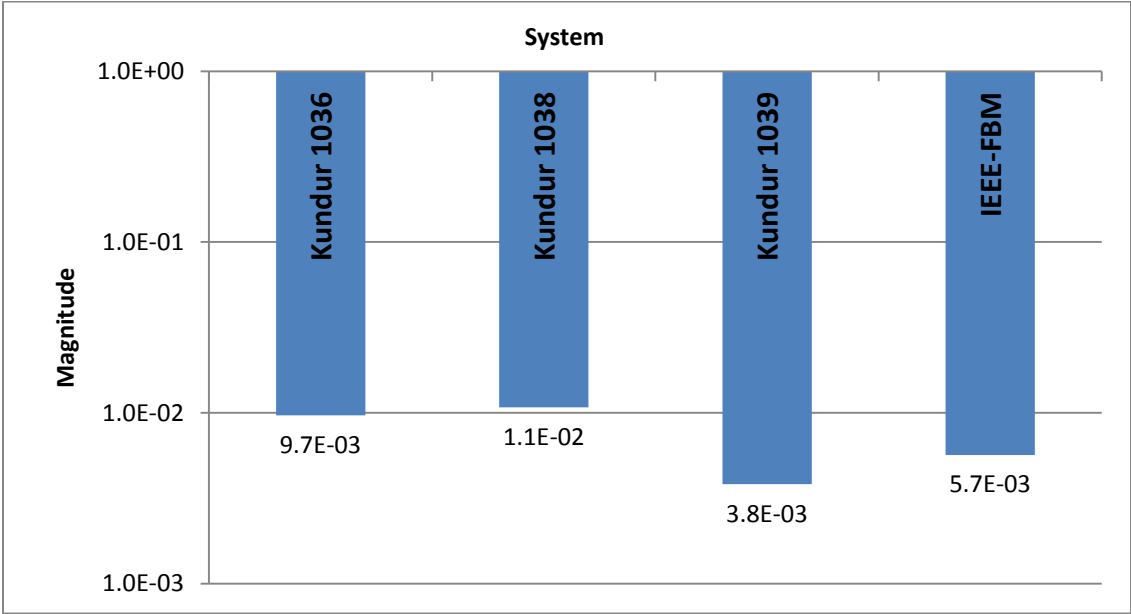
Figure 7-19 Comparison of Normalized (with respect to HP State) Right Eigen Vectors of Highest Mode in Generator State

Shown in Figure 7-20 is the improvement in magnitude of the highest frequency mode obtained by using the HP rotor section velocity signal instead of the generator rotor section velocity signal. It can be observed that there is a gain of approximately 100 in all the shaft systems.
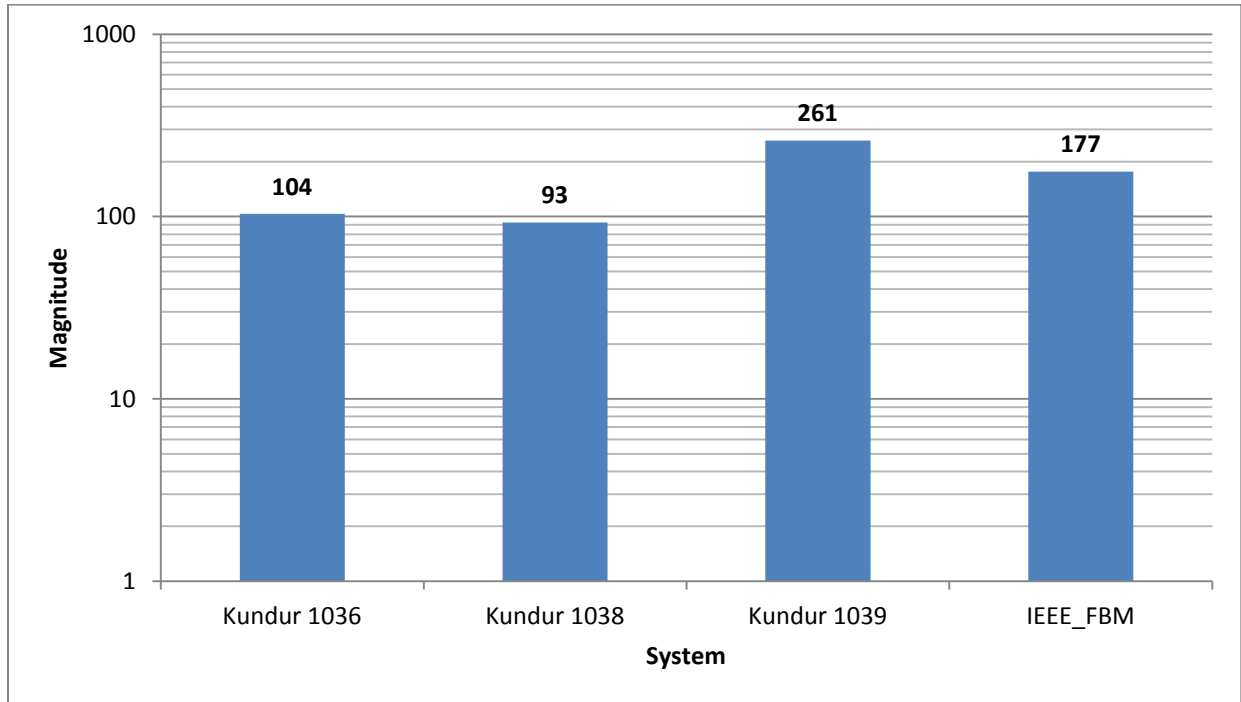
Figure 7-20 Improvement Attained using HP Rotor Section Speed Signal Instead of Generator Speed Signal for Measuring Highest Modal Component

Although using the HP rotor section velocity signal instead of the generator rotor section velocity yields enormous gains in the highest mode, we have to be careful to not let the other modes attenuate. Shown in Figure 7-21 is the plot of the lowest frequency mode which has the highest change compared to others. However, as observed from the figure, these do not attenuate for three of the systems and for the system that attenuates, it does so only modestly (gain = 0.67). This attenuation is miniscule compared to the attenuation (gain = 3.83e-3) that occurred in the same shaft system (Kundur 1039) for the highest mode when using the GNRSV signal instead of

the HPRSV signal. It can be concluded from this data that the HP rotor section velocity signal is again a much better candidate for detecting the modal components than the generator rotor section velocity signal or the associated p(t) signal because of the reasons mentioned in section 7.1.
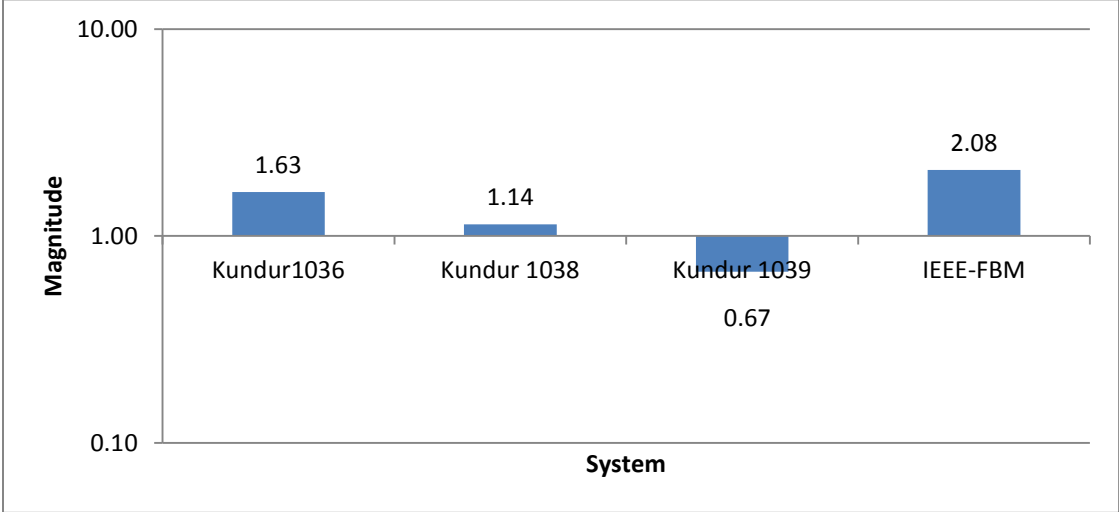
Figure 7-21 Normalized (With Respect To Generator Speed State) Right Eigen Vectors of Lowest Frequency Mode in HP Rotor Section Speed State

7.7 Overall Analysis and Conclusions Using Participation Factors

Show in Figure 7-22 is the comparison of participation factors between the four STGS systems for the highest frequency mode.
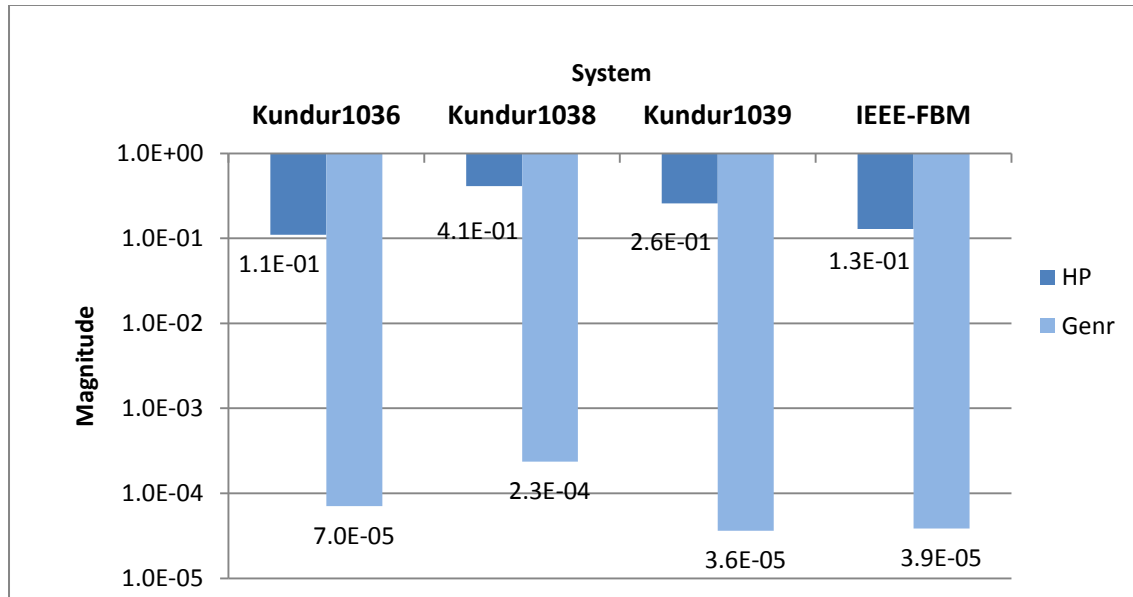
Figure 7-22 Comparison of Participation Factors of Highest Frequency Mode Between Generator and HP Rotor Section Speed States

The first set, labeled Kundur 1036, shows the comparison between participation factors of the highest frequency mode and the HP rotor section velocity state, and participation factors of the highest frequency mode and the generator rotor section velocity states. The maroon bar indicates that the highest frequency mode participates very weakly in the generator rotor section velocity state (7e-5). However, it participates relatively strongly in the HP rotor section velocity state i.e., approximately 1,000 times better. The same trend continues in the rest of the three shaft systems. Overall, it can be inferred that, in all the cases, the highest frequency mode participates very strongly in the HP rotor section velocity state compared to the generator rotor section velocity state. This again leads to the conclusion that the HP rotor section velocity signal is a better candidate for detecting modes than the generator rotor section velocity signal, or its associated instantaneous power signal, p(t).

7.8 Overall analysis using Impulse Response Analysis

The impulse response for all four STGS systems is shown in Figure 7-23. The first set, labeled Kundur 1036, indicates the measured magnitudes of the highest frequency modal component (44 Hz) as detected in the generator rotor section velocity and HP rotor section velocity signals in the Kundur 1036 system. This indicates that this mode appears extremely small in the generator rotor section velocity signal and the measured magnitude in the HP rotor section velocity signal is larger (about 100 times). The remaining sets of pairs show the same relationship for the rest of the three STGS systems.
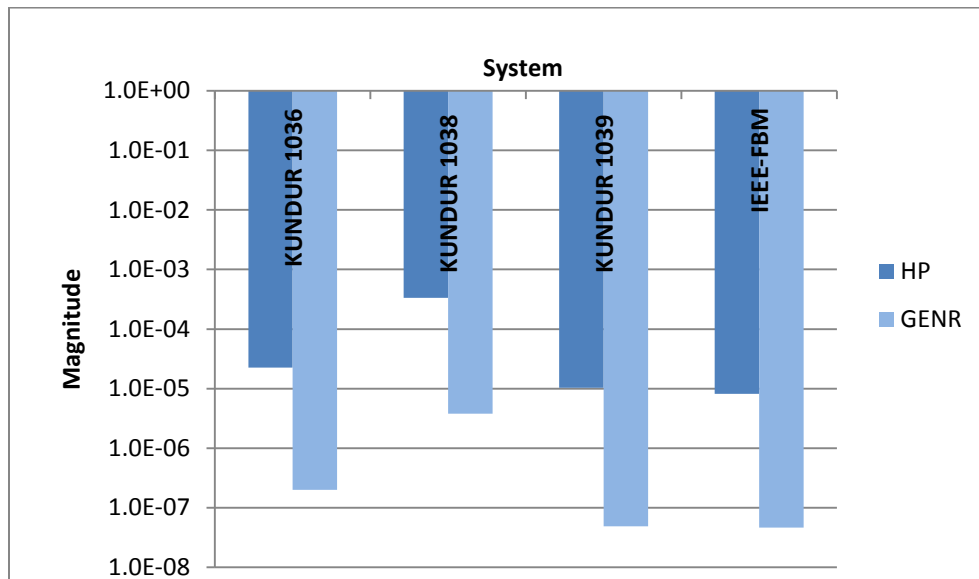
Figure 7-23 Comparison of Measured Values of Highest Modal Component Between Generator and HP Rotor Section Speed Signal

For the sake of convenience, this relationship is plotted in Figure 7-24. As shown in this figure there is a significant improvement, a gain of two orders of magnitude, in this modal magnitude when it is measured in the HP rotor section velocity signal instead of the generator rotor section velocity signal. It can also be inferred that the improvement occurs across all the shaft systems and in approximately similar amounts. This gain in modal magnitudes is going to

be even higher when using HP rotor section velocity signal, instead of the instantaneous power

signal, p(t), because of the reasons mentioned in section 7.1.
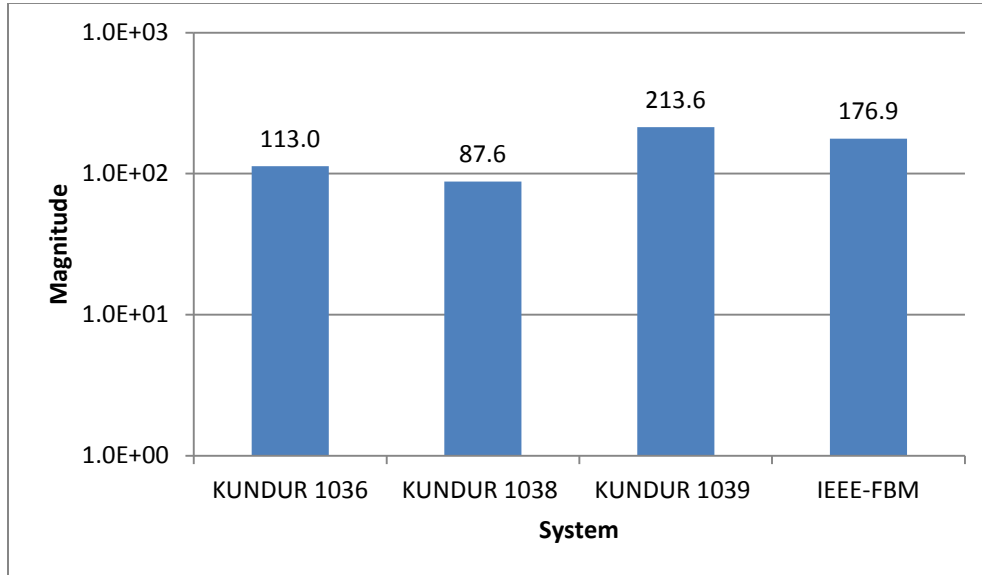
Figure 7-24 Improvement of Using HP Signal Instead of Generator Signal for Measuring Highest
Modal Component

7.9 Conclusions

In this chapter, four typical STG shaft systems were analyzed using three types of

analysis: right eigen vector analysis, participation factor analysis and the impulse response test.

All these shaft systems have a common configuration of rotor masses aligned linearly and

connected from one end (usually having the high-pressure turbine) to another end (usually

having the generator/exciter). The generator and the adjacently connected low-pressure turbine

usually tend to have the highest moments-of-inertia when compared to other rotors in the system.

In all four cases that were tested, it has been observed that the higher frequency modal

components tend to show up with much higher order magnitudes (approximately 100 times

stronger) in the HP rotor section's velocity signal than that of the generator. This could be

because the generator and adjacent rotor sections are considerably heavier than the HP and connected rotor sections. Moreover, all the modes' magnitudes were of similar order in the HP rotor section velocity state. This allows the option of choosing the HP rotor section velocity signal when the generator velocity signal or its associated instantaneous power signal, p(t) is insufficient to detect the required modal magnitudes. Thus, it can be concluded that the HP rotor section velocity signal is the more superior candidate for detecting STG shaft torsional modes than the generator rotor section velocity signal (which is not available for measurement in most cases) or its associated instantaneous power signal, p(t).

CHAPTER 8

IEEE-FBM FULL TEST SYSTEM APPLICATION AND ANALYSIS

In this chapter, two test cases, whose data have been provided in literature, will be utilized to illustrate and validate the proposed methodology. The first test case, the so called First Benchmark (FBM) case, is a standardized test case developed by the IEEE's SSR Task Force based on the Navajo Project [4] for the industry to analyze different models, compare their results and validate their simulation programs. All the data used in this case belongs to actual generators and turbines, thus making the case more realistic. Moreover, the authors have provided enough data to help validate the proposed method sufficiently. The second test case consists of a similar STG shaft system, whose torsional data and generator electrical parameters have been provided in [16]. However, because the electrical network data was not provided, the FBM system's electrical network configuration and parameters have been used. Both the systems have been built and simulated in ATPDraw software. The main concern is to apply the proposed method on this simulated model and validate it by verifying SSR frequencies and the shaft spring constant values.

8.1 Test Case 1: IEEE-FBM

This test case consists of a six-stage steam turbine-generator connected to a series capacitor compensated transmission line, which is connected to an infinite bus on the other end. The network and the transmission line parameters are shown in Figure 8-1.
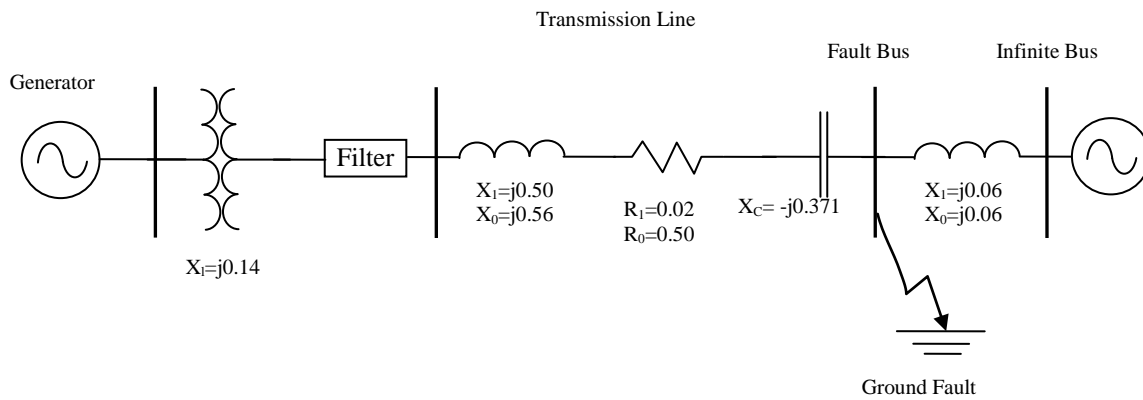
Figure 8-1 FBM Test Case's Network

The electrical parameters of the 892.4 MVA generator and the rotor masses and shaft spring constants of the six turbine sections are given in Tables 8-1, 8-2 and 8-3.

Table 8-1. Generator Impedances, Time Constants and Operating Conditions

Generator Impedances (p.u.)		Time Constants (sec)	
x_d	1.79	T'_{do}	4.3
x'_d	0.169	T''_{do}	0.032
x''_d	0.135	T'_{qo}	0.85
x_L	0.13	T''_{qo}	0.05
x_q	1.71	R_l	0
x'_q	0.228		
x''_q	0.2		

Generator Operating Condition	
power output	0.9 p.u.
power factor	0.9 lagging

Table 8-2. Rotor Circuit Parameters (p.u.)

Parameter	D-axis	Q-axis
R_f	0.00141	0.01406
X_f	0.062	0.326
R_k	0.0041	0.0082
X_k	0.0055	0.095
X_a	1.66	1.58
X_L	0.13	0.13

Table 8-3. Rotor Spring Mass Parameters

Inertia		Spring Constant		
Mass	H (sec)	Shaft	K (p.u.)	p.u. torque / rad
HP	0.092897	HP-IP	7277	19.303
IP	0.155589	IP-LPA	13168	34.929
LPA	0.85867	LPA-LPB	19618	52.038
LPB	0.884215	LPA-GEN	26713	70.858
GEN	0.868495	GEN-EXC	1064	2.822
EXC	0.0342165			

This linear system consists of six rotor masses connected by five shafts, as shown in Figure 8-2. Although this system would have five resonant frequencies, only four frequencies have been provided in [4]. These are shown in the first four rows of Table 8-4. However, because the rotor masses and shaft spring parameters are specified in [4], all five frequencies have been determined using eigen analysis as described in Chapter 6. The fifth frequency, shown in Table 8-4, is 47.45 Hz.
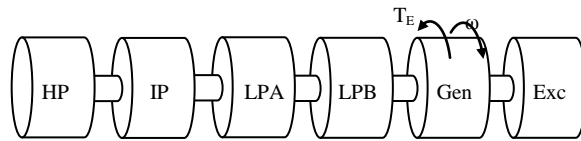
Figure 8-2 Lumped Spring Mass Model of the Steam Turbine

Table 8-4. List of SSR Frequencies

Frequency	Hz
1	15.71
2	20.21
3	25.55
4	32.28
5	47.45

8.1.1 Simulation in ATP/ATPDraw Software

The test case has been built and simulated in ATPDraw and ATP software, as shown in Figure 8-3.
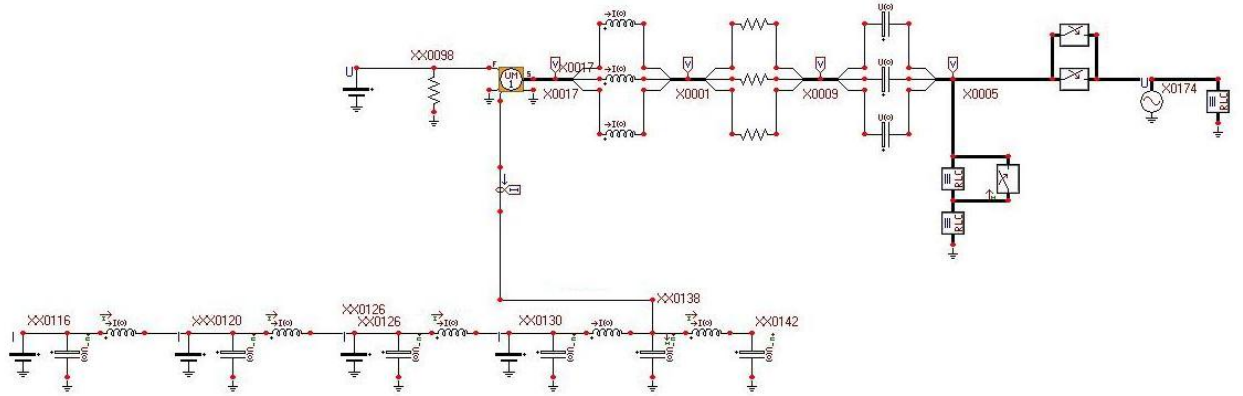
Figure 8-3 ATPDraw Schematic Showing the IEEE FBM System

The generator is simulated by the UM-1 model, which accommodates all electrical parameters of the generator. However, the mechanical rotor components have to be simulated external to the electrical model. The software simulates this mechanical system, which consists of rotor masses, shafts and torque inputs, with an electrical analog consisting of capacitors, inductors and constant current sources. A three-phase ground fault is applied for a duration of 0.02 seconds at the fault bus as shown in Figure 8-1. The instantaneous terminal power, *p(t)*, is shown in Figure 8-4.

8.1.2 Analysis of IEEE-FBM Simulation Results
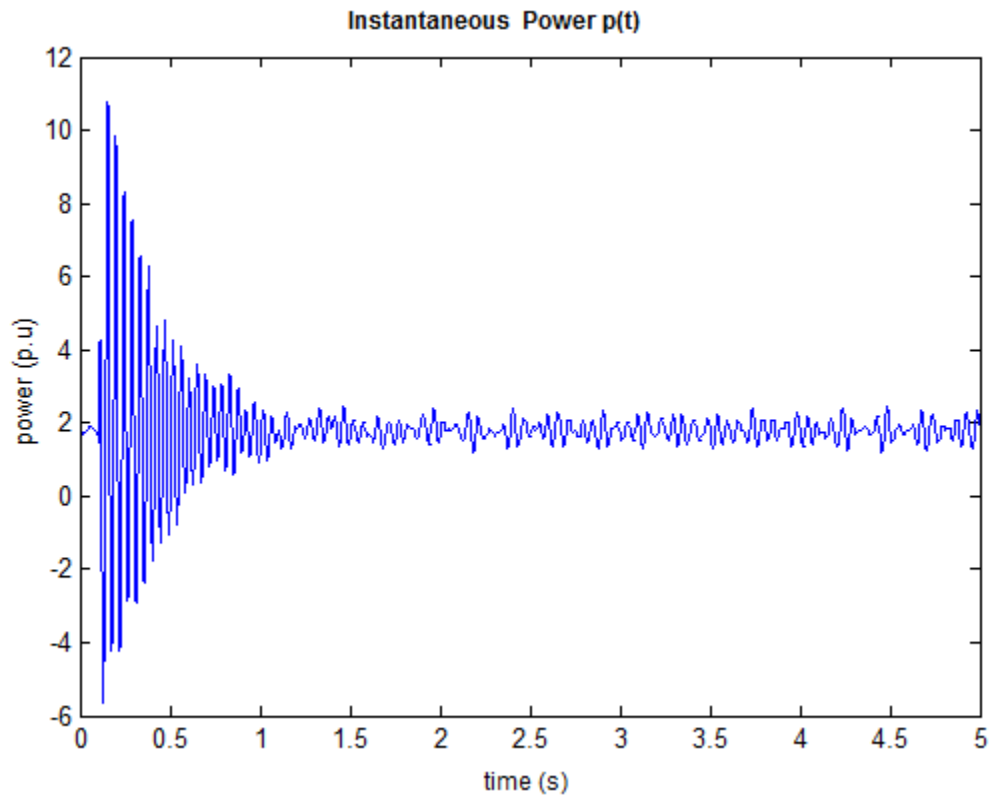
Figure 8-4. IEEE-FBM Systems' Instantaneous Power p(t)

Prony's method was used to estimate the constituent modal components in this signal. The resulting modes, sorted using the reordering algorithm discussed in Chapter 4, are shown in Table 8-5a. The input parameters for Prony's method are: $t_{min} = 3.50$, $t_{max} = 4.0$, numModes = 120 and nSkipSample = 12. A comparison of actual vs. estimated signal waveforms is shown in Figure 8-4b.

Table 8-5a. List of 10 Significant Constituent Modal Components in the IEEE-FBM System's Power Signal, p(t), Found Using Prony's Method

Magnitude	Exp-Decay	Frequency (Hz)	Phase (Rad)
0.276017667	0.0260722	15.8447405	2.1305827
0.180805621	0.0860599	20.2470613	0.5575678
0.094140055	0.0472314	11.9562734	0.8357333
0.086593703	-0.0594629	25.5213181	-0.035871
0.061468645	-7.4230014	3.2819871	1.4518369
0.007693741	-0.7214964	31.5658185	-0.4270126
0.021467517	-918.1780083	0	3.1415927
0.006047653	-4.0827177	35.8677556	-1.686961
0.009736733	-17.2561707	41.0963734	1.7500572
0.008595033	-145.1546038	416.6666783	3.1415927
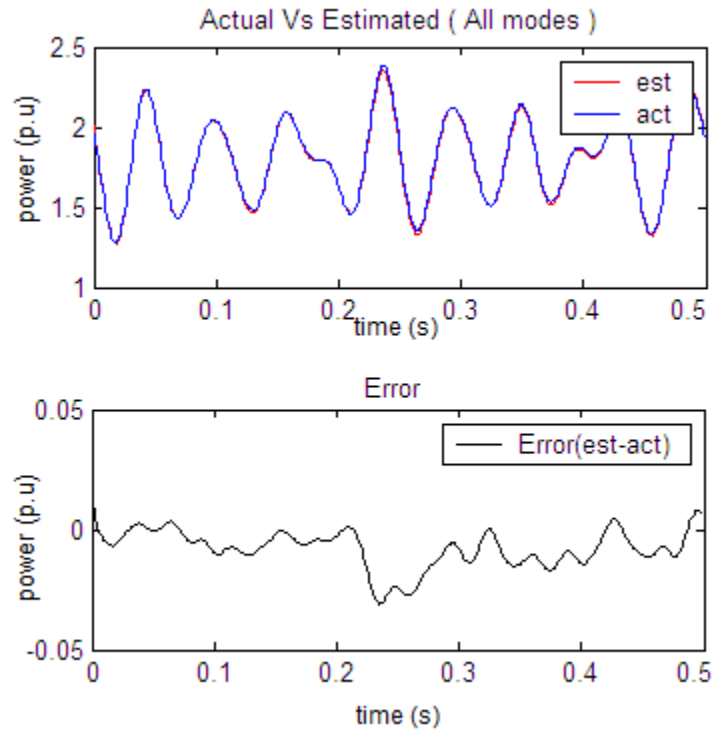
Figure 8-4b Comparison of Actual Vs. Estimated Instantaneous Power Signals of IEEE-

FBM System

113

It is to be noted that not all the modes in the list shown in Table 8-5a are shaft torsional modes. Most are noise modes that are generated by Prony's method because of the non-linear nature of p(t) signal as discussed in Chapter 3. However, it was observed that 11.9 Hz mode appeared consistently across multiple candidate data sets (defined by t_{min} and t_{max}). The existence of this mode could be attributed to the interaction of the series capacitance in the transmission line and other system components. For the sake of convenience, the list of shaft torsional modes are shown separately in Table 8-5b.

Table 8-5b. Estimated Shaft Torsional Frequencies Values in the IEEE-FBM System's Power Signal, p(t), Found Using Prony's Method

Magnitude	Exp-Decay	Frequency (Hz)	Phase (Rad)
0.276017667	0.0260722	15.8447405	2.1305827
0.180805621	0.0860599	20.2470613	0.5575678
0.086593703	-0.0594629	25.5213181	-0.035871
0.007693741	-0.7214964	31.5658185	-0.4270126

A comparison between the estimated frequencies and the FBM's frequencies is given in Table 8-6. It is clear from the small percentage errors that the estimated frequency values match the FBM's frequencies very closely.

Table 8-6. Comparison Between Estimated vs. IEEE-FBM System's Actual SSR frequencies

SSR frequencies (Hz)given in IEEE FBM paper	Estimated SSR frequency (Hz) values extracted from the power signal using Prony's method	Percentage Error
15.71	15.8447405	0.86
20.21	20.2470613	0.18
25.55	25.5213181	0.11
32.28	31.5658185	2.21

But, as shown in Table 8-5b, only four out of the five SSR frequencies could be extracted. The highest torsional frequency, 47 Hz, is missing. This is consistent with the results of our analysis provided in Chapter 6 using right eigen vectors, participation factors and impulse response tests on the IEEE-FBM shaft system. These analyses indicated that the highest frequency participated very weakly in the generator rotor velocity state. This causes it to show up even more weakly in the instantaneous power signal, p(t) resulting in it not being detected by the modal decomposition routine. Another reason might, among others, be the insufficient magnitude of the fault disturbance. To compensate for this, the process has been repeated, using the HP rotor section speed signal, as shown in Figure 8-5, in lieu of the power signal. It is to be noted from Chapter 7 analyses (Table 7-13) that the HP rotor section velocity state has a higher participation factor (0.128) with the 47 HZ mode compared to the generator section velocity state (3.85E-5).
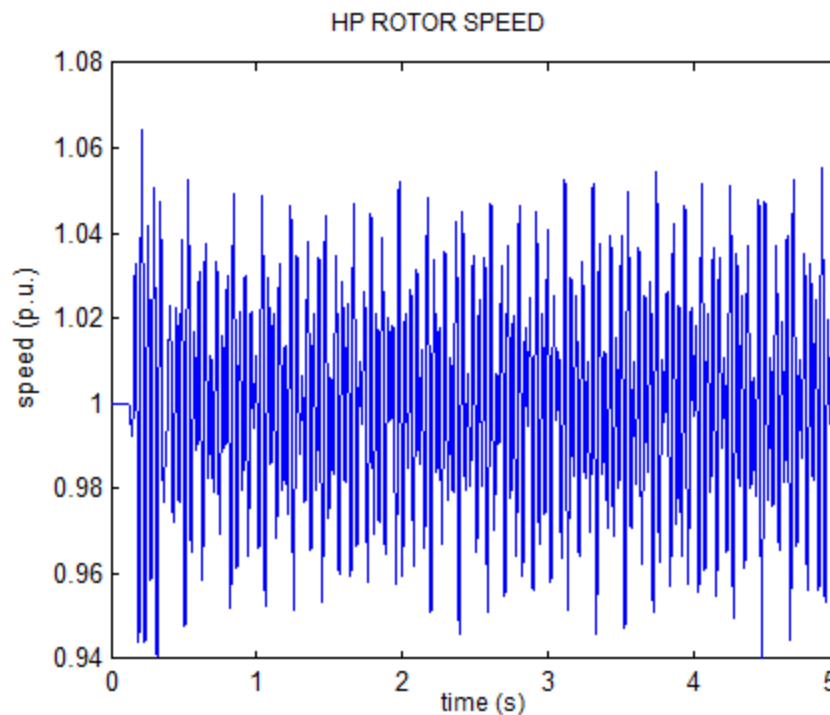
Figure 8-5. Speed Signal of the IEEE-FBM System's HP Rotor Section

Prony's method was used to estimate the constituent modal components in this signal. These modes, which also include the noise modes along with the shaft torsional frequencies, are shown in Table 8-7a. The input parameters for Prony's method are: $t_{min} = 3.5$, $t_{max} = 4.0$, numModes = 120 and nSkipSample = 10. For the sake of convenience, the list of shaft torsional modes are shown separately in Table 8-7b.

Table 8-7a. List of 10 Significant Constituent Modal Components in the HP Rotor Section Velocity Signal Found Using Prony's Method

Magnitude	ExpDecay	Frequency (Hz)	Phase (Rad)
0.028999	0.033513	25.49858	-1.57742
0.017561	0.048661	15.86501	0.541311
0.00898	0.045958	20.24075	-0.77257
0.0021	-0.03208	32.25314	0.850057
0.000353	-10.3972	2.218337	-2.57716
0.000238	-28.6691	0	0
5.11E-05	0.004753	47.45543	0.662151
6.08E-06	-3.96825	36.05672	2.404539
4.92E-05	-652.728	173.248	1.602849
5.72E-06	-42.2946	58.6955	1.433849

Table 8-7b. Estimated Shaft Torsional Modal Values in the Speed Signal Found Using Prony's Method

Magnitude	ExpDecay	Frequency (Hz)	Phase (Rad)
0.028999	0.033513	25.49858	-1.57742
0.017561	0.048661	15.86501	0.541311
0.00898	0.045958	20.24075	-0.77257
0.0021	-0.03208	32.25314	0.850057
5.11E-05	0.004753	47.45543	0.662151

A comparison of actual vs. estimated signal waveforms is shown in Figure 8-6. As seen in this figure, Prony's method was able to extract the underlying modal components with negligible error.
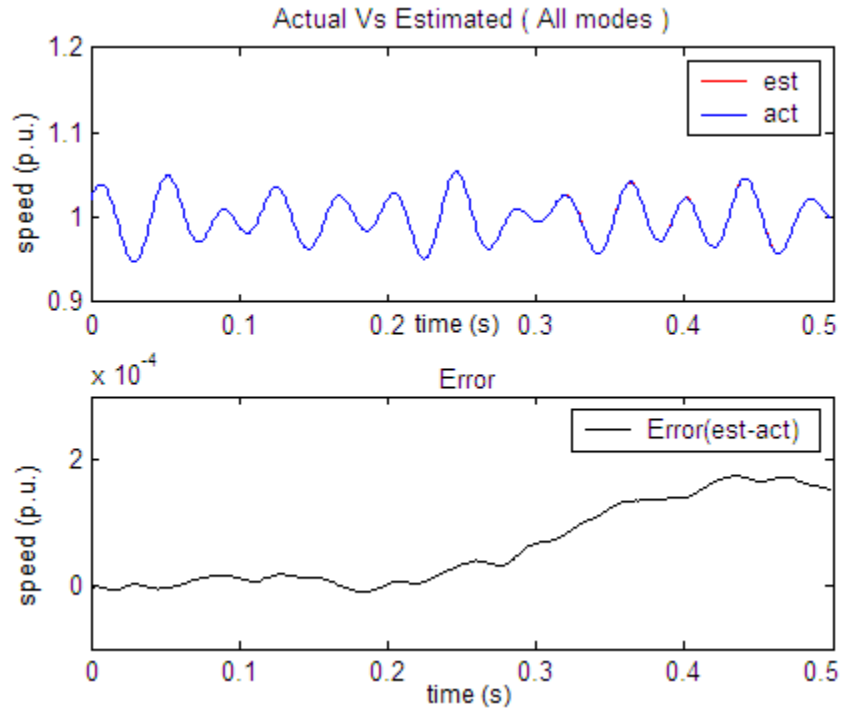
Figure 8-6. Waveform Comparison of IEEE-FBM System's Actual vs. Estimated HP signal

Moreover, all five SSR frequencies have been extracted successfully. These SSR frequency values and the rotor mass values were used in an iterative least squares method to estimate the shaft spring constants. The results of the least squares method are shown in Table 8-8. It can be seen that this method has been able to estimate the spring constants to within a maximum error of 5.6%.

Table 8-8. Comparison Between Estimated vs. IEEE-FBM System's Actual Shaft Spring

Constant Values (p.u.)

Estimated Shaft Spring Constants (found using Newton Raphson least squares method)	Actual FBM Shaft Spring Constants (values provided in paper)	Percentage Error
7193.975986	7276.96	1.14
13363.35297	13167.943	1.48
20711.43256	19617.974	5.57
25641.41227	26712.949	4.01
1063.86061	1063.991	0.012

On another note, shown in Table 8-7b, are the exponential decay values of the constituent SSR modal components along with the frequency values. Although these might indicate that the responses will increase exponentially to infinity, it may not necessarily be true. These damping values are simply the estimates determined by Prony's method for the signal for a particular chosen time interval. The aim of Prony's method is to minimize the error between the estimated and actual signal. These signals match closely with minimum error as seen in Figure 8-6. However, because these damping values are so small compared to the frequency values, they were not accurately determined.

8.2 Test Case 2: Kundur 1036 System

The second test case that will be used to validate the presented methodology is the Kundur 1036 system. The shaft system torsional and generator data for this system has been provided in Kundur [16]. This system consists of a steam turbine generator connected to a network similar to the one provided in FBM test case. The only exception is that the transmission line's series capacitances have been reduced such that instead of providing 70 percent compensation they provide 7 percent compensation. The shaft system consists of five

rotor masses as shown in Figure 8-7. The torsional data of the shaft system is provided in Table 8-9. The electrical parameters of the 2-pole, 555 MVA generator are given in Table 8-10.
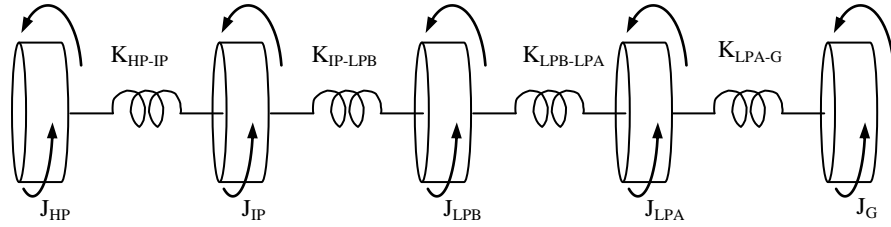
Figure 8-7 Kundur 1036 Shaft System Configuration

Table 8-9 Specifications for Kundur 1036 Shaft System Parameters

Rotor	H (MW.s/MVA)	Shaft	K (pu torque/rad)
HP	0.124	HP-IP	21.8
IP	0.232	IP-LPB	48.4
LPB	1.155	LPB-LPA	75.6
LPA	1.192	LPA-GENR	62.3
GENR	0.855		

Table 8-10 Kundur 1036 System's Generator Electrical Data

Paramter	p.u. value
Ll	0.15
Lad	1.66
Laq	1.61
Ld	1.81
Lq	1.76
Lafd	1.66
Lffd	1.825
Lfd	0.165
Ra	0.003
Rfd	0.0006

This shaft system has the following resonant frequencies as provided in the textbook: 16.3 Hz, 24.1 Hz, 30.3 Hz and 44.0 Hz. The schematic of the entire system consisting of the torsional system, the generator model and the connected electrical network, built in ATPDraw, is shown in Figure 8-8.

8.2.1 Simulation in ATP/ATPDraw Software
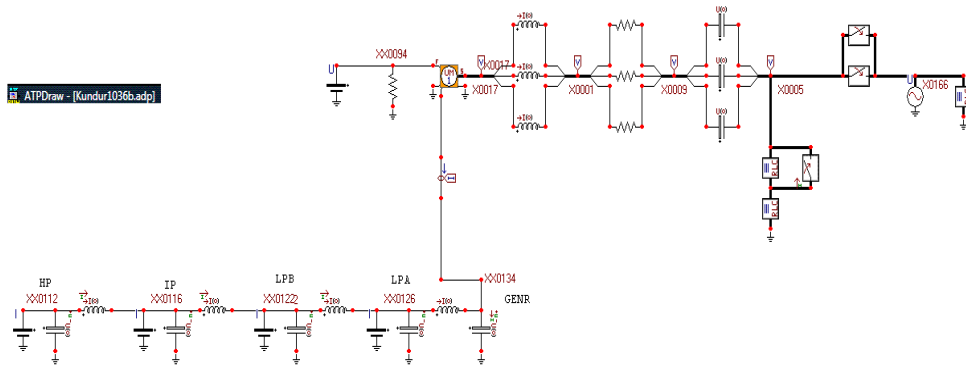
Figure 8-8 ATPDraw Schematic of the Kundur 1036 System

Similar to the FBM test case, a three-phase ground fault is applied at the other end of the transmission line for 20 milliseconds and removed. The resulting ring-down signals, generator instantaneous power p(t) and HP rotor velocity $\omega_{HP}(t)$, are recorded.

8.2.2 Analysis of Kundur 1036 System Simulation Results

Modal decomposition, based on Prony's method, is used to identify the underlying modal components in both these signals. Results of modal decomposition on the power signal p(t) are shown in Table 8-11a, which includes noise modes along with a subset of shaft torsional modes. The input parameters for Prony's method are: $t_{min} = 4.5$, $t_{max} = 5.0$, numModes = 180 and

nSkipSample = 10. For the sake of convenience, the list of shaft torsional modes are shown

separately in Table 8-11b. A comparison of actual vs. estimated signal waveforms is shown in

Figure 8-8b.

Table 8-11a. List of 10 Significant Constituent Modal Components in the Instantaneous
Power ,p(t), Signal Found Using Prony's Method

Magnitude	Exp-Decay	Frequency (Hz)	Phase (Rad)
0.100335294	-0.214798	1.0278007	1.4407871
0.026822201	-0.0268801	16.2915718	1.4259349
0.015395111	0.0635373	20.7025312	2.4360554
0.007576683	0.0101545	24.1168428	3.1185639
0.004403952	0.0200221	30.319575	-1.1807898
0.001614289	-12.5397531	18.5551256	3.1060812
0.000835548	-19.4412246	6.6322957	1.4899333
0.000137558	-0.6841653	37.1079194	-2.6494426
7.82391E-05	-3.971513	45.1327325	-1.1104041
3.55971E-05	-2.9137386	50.9898275	1.0545063

Table 8-11b. Estimated Shaft Torsional Modal Values in the Instantaneous
Power ,p(t), Signal Found Using Prony's Method

Magnitude	Exp-Decay	Frequency (Hz)	Phase (Rad)
0.026822201	-0.0268801	16.2915718	1.4259349
0.007576683	0.0101545	24.1168428	3.1185639
0.004403952	0.0200221	30.319575	-1.1807898
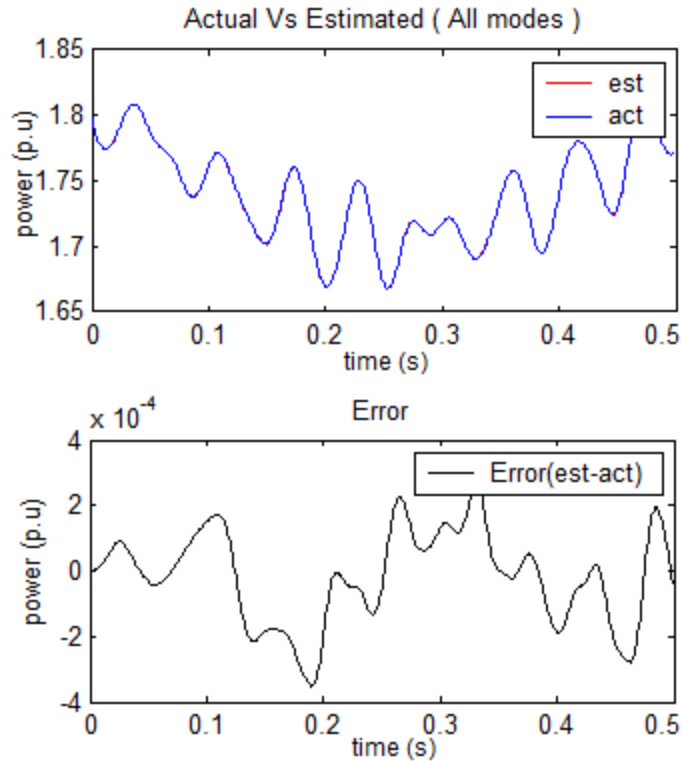
Figure 8-8b. Waveform Comparison of Kundur 1036 System Actual vs. Estimated p(t) signal

The 20.7 Hz mode shown in Table 8-11a was observed consistently across multiple candidate data sets (defined by t_{min} and t_{max}). Just as in the case of FBM system, the existence of this mode could also be attributed to the interaction of the series capacitance in the transmission line and other system components. As seen in Table 8-11b, the procedure was able to detect only three of the four resonant frequencies, just like in FBM case. The highest torsional frequency, 44 Hz, is missing. This is again consistent with the results of our analysis provided in Chapter 6 using right eigen vectors, participation factors and impulse response tests on the Kundur 1036 shaft system. These analyses indicated that the highest frequency participated very weakly (participation factor 7.05E-5) in the generator rotor section velocity state. This causes it

to show up even more weakly in the instantaneous power signal, p(t) resulting in it not being detected by the modal decomposition routine.

However, these same analyses-right eigen vectors, participation factors and impulse response tests-on the Kundur 1036 shaft system also indicated that all the modes participated strongly in the HP rotor section velocity state (participation factor = 1.1E-1). Therefore, modal decomposition has been performed on the HP rotor section velocity signal. The results are shown in Table 8-12a and Table 8-12b. The list of modal components in Table 8-12a includes both shaft torsional and noise modes. For the sake of convenience, the list of shaft torsional frequencies are shown separately in Table 8-12b. A comparison of actual vs. estimated signal waveforms is shown in Figure 8-8c.

Table 8-12a Results of Modal Decomposition on the HP Rotor Section Velocity Signal

Magnitude	Exp-Decay	Frequency (Hz)	Phase (Rad)
0.004919104	0.0004694	24.1010872	-1.7483499
0.004633141	-0.0040039	16.2908815	-0.2803303
0.001879906	0.0012081	30.324916	-2.9628608
0.000735043	-0.1783341	1.0251133	2.9835261
6.60606E-05	0.0004634	43.9975184	0.0776786
1.1878E-06	-16.5067852	17.756971	1.2672097
4.963E-07	-2679.291063	0	0
2.137E-07	-34.1110417	381.9555055	0.9443255
3.966E-07	-61.5138752	33.0911332	-3.008665
9.29E-08	-38.2153551	99.2265085	-1.957044

Table 8-12b Results of Modal Decomposition on the Kundur 1036 System's HP Rotor Section Velocity Signal

Magnitude	Exp-Decay	Frequency (Hz)	Phase (Rad)
0.004919104	0.0004694	24.1010872	-1.7483499
0.004633141	-0.0040039	16.2908815	-0.2803303
0.001879906	0.0012081	30.324916	-2.9628608
6.60606E-05	0.0004634	43.9975184	0.0776786
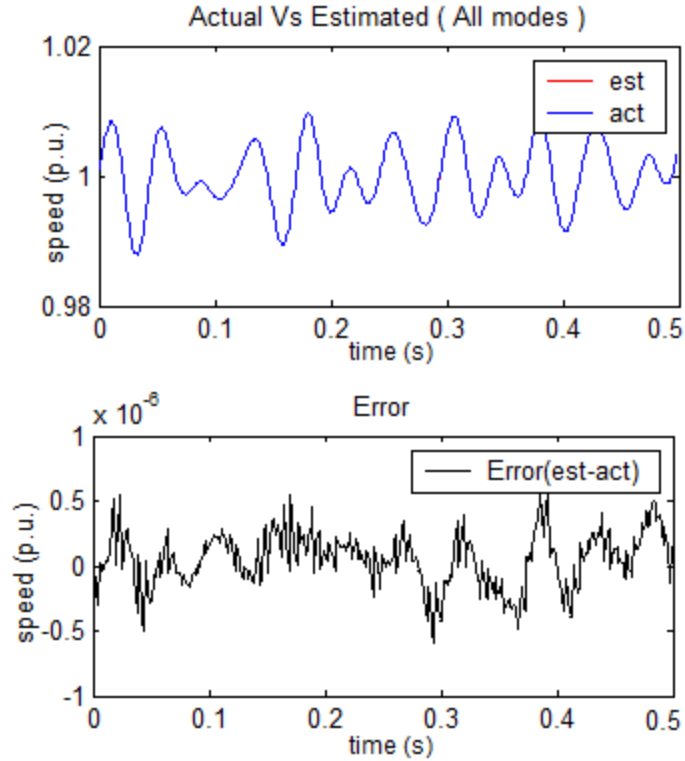
Figure 8-8c. Waveform Comparison of Kundur 1036 System's Actual vs. Estimated in HP Rotor Section Velocity Signal

As seen in Table 8-12b, all four frequencies have been extracted precisely. Next, these frequencies were fed into a non-linear Newton-Raphson based algorithm to estimate the shaft spring constants. The results are shown in Table 8-13. The units of the spring constants are Nm/mech-rad.

Table 8-13 Comparison Between Estimated and Kundur 1036 System's Actual Spring Constant Values

Estimated	Actual	Error %
30760262.08	32092838.2	4.152
74268733.87	71251989.39	4.234
112080995.1	111294429.7	0.707
92176056.7	91714854.11	0.503

124

These results show that two spring constants are estimated to within 1 percent. The maximum error in the estimated spring constant values is about 4.2 percent.

8.3 Conclusions

The results of time-domain simulations on two test cases were reviewed in this chapter. These test cases were built and simulated in ATPDraw software. The ring-down signals resulting from a three-phase ground fault on a transmission line were recorded. Modal decomposition on the instantaneous power signal revealed that most modes, except the highest one, were detected. This is to be expected as per the results of eigen analyses performed in Chapter 6. Consequently, alternative ring-down signals from other rotor sections were chosen as candidates for modal decomposition. These results of a modal decomposition on IEEE FBM's HP rotor section velocity and Kundur 1036 HP rotor section velocity were sufficient to detect all the torsional modes. These modal frequency values were used in a non-linear least squares algorithm to estimate, within reasonable (6 percent) error, all the shaft spring constants of the respective rotor shaft systems. In the next chapter, real data obtained from a steam turbine generator unit will be used for modal decomposition using Prony's method.

CHAPTER 9

REAL MEASUREMENT ANALYSIS

Up until now, Prony's method and its refinements, eigen analysis/tools and the behavior of typical steam turbine generator shaft (STGS) systems have been examined. In addition, in the previous chapter, the proposed methodology was tested using test systems that were simulated in ATP software and shaft spring constants were estimated using HP rotor section velocity (RSV) signals and not instantaneous power, p(t), signals. However, these data sets were simulated. In this chapter, real measurement data will be utilized to test the methodologies presented in previous chapters. The effects of the behavior of typical STG shafts, studied in Chapter 7, on the proposed methodology will also be examined.

This real data came from a steam turbine generator unit whose information will be kept confidential as requested by the plant owner. However, my advisory committee Chair, Dr. Mark Halpin, has full knowledge of the unit's STGS torsional frequencies and parameters. Note that in this dissertation work, the only type of field data available was three-phase instantaneous power at the generator terminals. Rotor section speed signals were not available.

9.1 Data Collection

A measurement device was placed for a few weeks on the premises to collect and record data whenever a disturbance occurred. The measurement device consists of an A/D convertor capable of reading six channels, three for instantaneous currents and three for instantaneous

voltages. Later these recorded quantities were converted to an instantaneous power signal, p(t) using (9.1).

$$p(t) = v_a(t)*i_a(t) + v_b(t)*i_b(t) + v_c(t)*i_c(t) \tag{9.1}$$

Because the reading of data from six channels occurred sequentially, there was a 180 Hz modulation frequency embedded in the p(t) signal which had to be removed using a filter. Whenever a disturbance occurred, a detection algorithm would trigger a procedure to record 30 seconds of instantaneous voltage and current quantities, which included 2 seconds of data prior to the occurrence of disturbance. The data was recorded at 1,920 samples per second corresponding to 32 samples per cycle. The collected data was written to an ascii file. All the data were in p.u.

9.2 Analysis of Data Set 1

A plot of the measured instantaneous power signal, p(t), from first data set is shown in Figure 9-1. The reason it looks like a strip of color instead of a single continuous curve is the aforementioned 180 Hz modulation frequency embedded in the p(t) signal. This is mainly because of the sequential sampling of three voltage quantities followed by three current quantities.
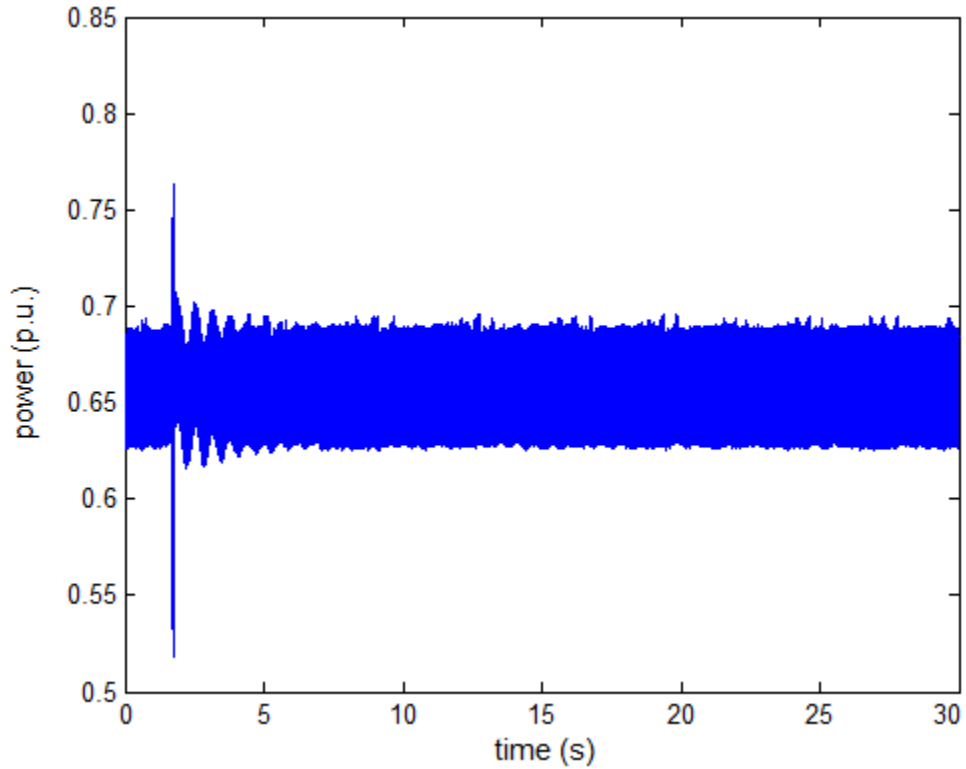
Figure 9-1 Plot of Actual p(t) Measurement Data

To remove this modulation, this data was filtered using a seventh order low-pass Butterworth filter with a cutoff-frequency of 59 Hz. A plot of the filtered data is shown in Figure 9-2. It depicts the ring-down signal as a result of a major disturbance event, which seems to begin at 1.7 seconds. To obtain a closer look at the data, the plot is zoomed as shown in Figure 9-3
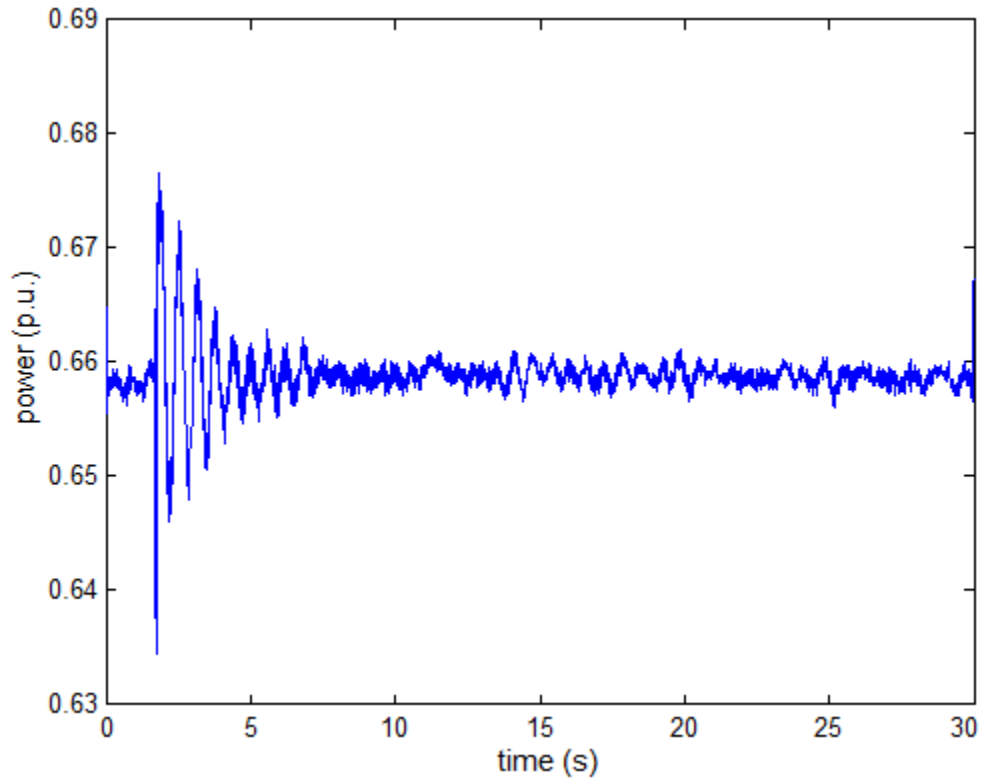
Figure 9-2 Plot of Filtered p(t) Signal from Data Set 1
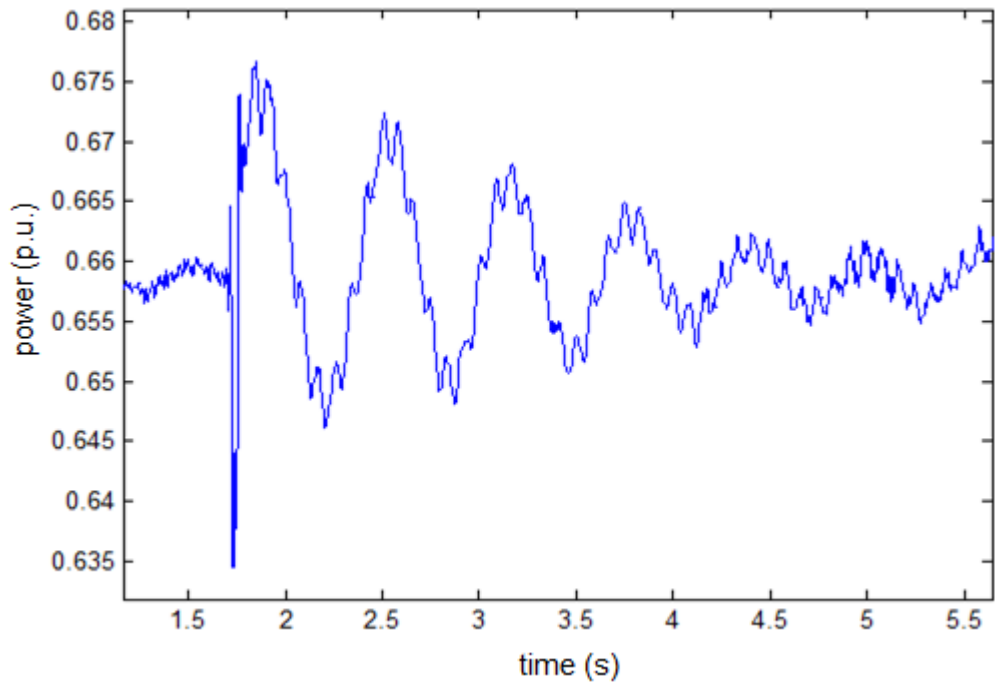
Figure 9-3 Zoomed-in Plot of the Disturbance Event in the p(t) Signal

The next task is to visually inspect the data and choose a proper candidate data set. The purpose of this visual inspection is to preclude any non-linear events such as sudden discontinuities. This would disqualify the data before 1.9 seconds (approximately) and after 4.5 seconds (approximately). A data window between 2 seconds and 3 seconds has been chosen and Prony's method has been applied to extract the underlying modal components. A plot of the data between 2 and 3 seconds is shown in Figure 9-4
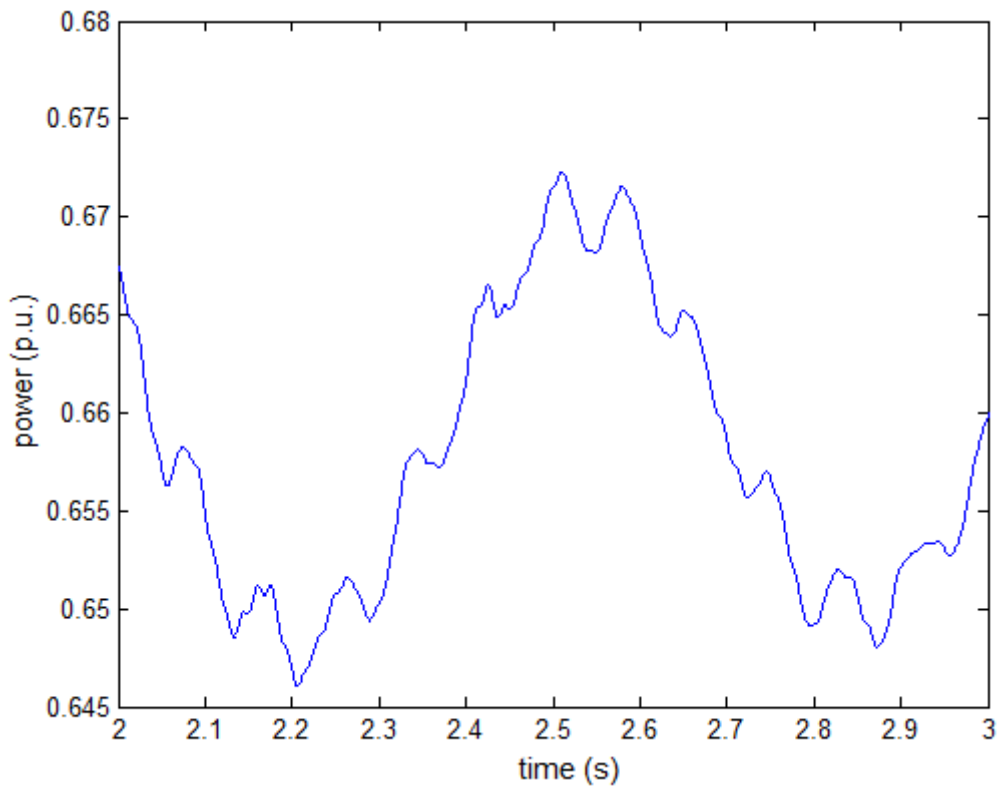
Figure 9-4 Plot of Proper Candidate Data Set for Prony's Method (Data Set 1)

To extract the correct underlying modal components, it necessary to select suitable algorithm parameters of Prony's method as discussed in Chapter 5. After gradually modifying the algorithm parameters and checking the results of Prony's method, it was found that suitable values for numModes and nSkipSample parameters were 90 and 5 respectively. The output of

Prony's method using these algorithm parameters is shown in table 9-1. Note that only the first 20 significant modes are shown. In addition, this list is ordered according to the LSE-based reordering algorithm presented in Chapter 4.

Table 9-1 Prony's Method's Output List of Constituent Modal Components for Data Set 1

Mode #	LSE	Magnitude	ExpDecay	Frequency(Hz)	Phase(rad)
1	0.145430301	0.012577665	-0.3309921	1.5488809	1.0758312
2	0.027445814	0.002169144	-0.2515075	12.0571053	-0.3224135
3	0.007599871	0.00032536	-0.0641375	16.335785	2.9754293
4	0.007306082	0.000376833	-0.7515305	20.8418966	2.1304798
5	0.006588591	0.000202878	-0.6714491	59.8825575	2.2886434
6	0.006550145	0.000184078	-0.5808247	24.952691	-3.086796
7	0.006499929	0.000460505	-6.4398204	38.9980768	2.0071578
8	0.006364739	0.000349181	-8.4033961	27.8239136	-0.5632267
9	0.006357859	0.00020614	-2.9386237	56.6811368	-0.2796263
10	0.006328438	0.000181467	-3.0516521	52.5733957	-2.0632532
11	0.006313769	0.000164204	-3.0921935	44.8612443	-0.6163595
12	0.006301417	0.000273349	-10.2966543	36.4077529	0.6941915
13	0.00629955	0.00024585	-8.5860998	32.7887102	0.7029586
14	0.006295845	0.000748658	-110.4579566	60.1552674	-1.030162
15	0.00629521	0.000112727	-1.9587407	48.0411351	-2.931303
16	0.006283306	0.000121469	-3.1095516	7.5468043	1.9888544
17	0.006279016	0.003337735	-592.1246285	152.0977954	1.7286927
18	0.006259379	5.57457E-05	-1.8085119	63.2491252	0.3082231
19	0.006254104	0.000176545	-73.2794058	0	0
20	0.006253283	4.86265E-05	-2.5630077	67.2675652	2.8706005

A comparison of the actual signal and reconstructed signal using all the constituent 90 modes is shown in Figure 9-5. Also shown in this figure is the difference between these two signals.
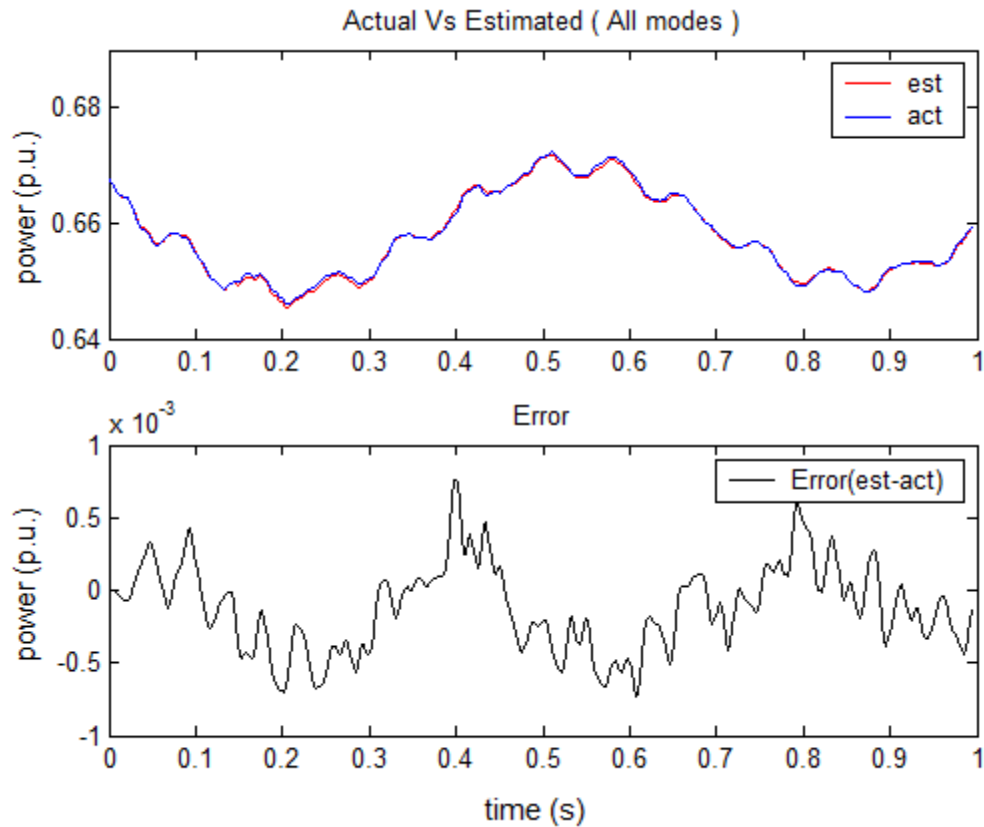
Figure 9-5 A Plot of Comparison Between the Actual and Reconstructed Signal Using the Output

Modes of Prony's Method for Data Set 1

The LSE-based reordering algorithm, presented in Chapter 4, had been successfully utilized in Chapter 7 for identifying the constituent modes in impulse response signals and in Chapter 8 for identifying torsional modes from output signals of systems simulated in the ATPDraw software. However, because of the poor quality of the actual signals in the present cases, it was found that LSE-based reordering algorithm was not effective in identifying these modes. However, in the absence of that, an alternative simpler method of identifying these torsional modes was chosen. It utilizes a selection criteria of { -4 < exponential-decay < 4 } and

{ 5 < frequency < 59 } to prune away the non-STGS torsional modes and noise modes. Any

constituent modes outside these bounds were excluded. In addition, because this method is not as

effective in identifying these torsional modes (because of appreciable measurement error and the

large number of cases involved), it was necessary to use a scatter plot to identify these modes.

This method is detailed in the following sections. Applying the selection criteria on the list of

modes in Table 9-1 gives a new list of modes as shown in Table 9-2.

Table 9-2. Selected List of Constituent Modes in the Signal Detected by Prony's Method

magnitude	Exp-Decay	Frequency(Hz)	Phase(rad)
0.000121	-3.10955	7.546804	1.988854
0.000113	-1.95874	48.04114	-2.9313
0.000164	-3.09219	44.86124	-0.61636
0.000181	-3.05165	52.5734	-2.06325
0.000206	-2.93862	56.68114	-0.27963
0.000184	-0.58082	24.95269	-3.0868
0.000377	-0.75153	20.8419	2.13048
0.000325	-0.06414	16.33579	2.975429
0.002169	-0.25151	12.05711	-0.32241

Note that as a result of using the selection criteria, Table 9-2 excludes the most dominant

mode in the signal, which has a frequency of about 1.54 Hz, as seen in row 1 of Table 9-1. It is

observed that this low-frequency mode, also known as the system mode [16], is present in most

STGS signals. In the system mode, the entire STGS system oscillates in unison against the power

system's electrical network. In most STGS signals, this mode lies in the frequency range of 1 to

2 Hz [16]. It was found that this mode is also present in most of the present measurement signals.

Because the main concern is extracting individual torsional frequencies, the selection criteria's

lower limit was set as 5 Hz so that this mode would be omitted in further results.

In this procedure, a sliding window analysis was used to detect constituent modes in the signal because it is necessary to use it to eliminate any noise modes present in the output list of modes. The first window began at 2.0 seconds and ends at 3.0 seconds. The next window was chosen to begin at 2.1 seconds and end at 3.1 seconds. The same algorithm parameters chosen earlier were chosen for this data window and the rest of the data windows in this analysis. The output modal list is shown in table 9-3. This procedure was repeated 10 times to obtain a total of 10 modal lists. The final list, starting at 3.0 seconds, of constituent modes is shown in Table 9-4.

Table 9-3. List of Constituent Modes in the Signal Detected by Prony's Method with Algorithm Parameters: tmin = 2.10 tmax = 3.10, numModes =   90 and nSkipSample =   5.

magnitude	Exp-Decay	Frequency(Hz)	Phase(rad)
0.000118	-2.66588	52.56122	-0.32567
0.000114	-3.59321	39.85057	0.6168
0.000239	-2.80993	7.612871	0.734371
0.000104	-1.79302	48.44691	1.229605
8.11E-05	-1.77031	44.98968	2.002963
0.000151	-2.99357	56.51658	-2.17675
0.000212	-0.67029	25.0694	-0.02513
0.000261	0.027198	20.92769	2.17706
0.000408	-0.44486	16.37496	0.524382
0.002154	-0.2917	12.06021	0.952535

Table 9-4. List of Constituent Modes in the Signal Detected by Prony's Method with Algorithm Parameters: tmin = 3.00 tmax = 4.00, numModes =   90 and nSkipSample =   5.

magnitude	Exp-Decay	Frequency(Hz)	Phase(rad)
0.000106	-3.62959	32.86421	-3.01986
0.000141	-1.94671	55.64619	-1.23221
0.000232	-3.7667	7.118301	2.090702
0.000325	-1.93688	25.08226	-2.77231
0.000264	-0.60996	16.37752	-2.04934
0.000235	-0.22158	20.80594	1.113286
0.001679	-0.19653	12.04989	0.031397

In the next step, the frequency data and exponential decay data from all 10 tables were chosen and combined into one list. The list is then sorted in ascending order according to frequency. The resulting list of modes is shown in Table 9-5.

Table 9-5 Combined list Modal Components showing only the Exponential Decay and Frequency parameters

Exp-Decay	Frequency(Hz)	Exp-Decay	Frequency(Hz)	Exp-Decay	Frequency(Hz)
-4.4149138	7.0914403	-1.2673978	20.7462942	-2.0158872	40.055229
-3.7667008	7.1183011	-0.2215773	20.8059387	-1.4376032	40.1428554
-4.7144464	7.1467739	-0.1764114	20.8198008	-2.2263055	44.8205265
-4.4628948	7.2519218	-0.7060205	20.8311284	-3.0921935	44.8612443
-1.0985038	7.3187341	-0.7515305	20.8418966	-4.2391012	44.9771431
-4.4055675	7.5183069	-0.8879877	20.8465696	-1.7703147	44.9896791
-1.714265	7.5407015	-0.563378	20.8829791	-3.6889312	45.0481237
-3.1095516	7.5468043	0.0271976	20.9276871	-0.2411489	45.1271992
-3.2565161	7.5586456	-0.891101	20.9488363	-3.8468226	45.1336808
-2.8099317	7.6128714	-1.2257292	20.9652567	-1.6546833	45.221385
-0.3113589	12.0355795	-0.5808247	24.952691	-1.4836504	45.2778428
-0.216627	12.0457647	-0.3921951	24.9758553	-1.9587407	48.0411351
-0.2209732	12.0474776	-1.0349055	25.0010154	-4.8350115	48.431882
-0.2157098	12.0491428	-1.4008373	25.0097467	-1.7930235	48.4469058
-0.1965312	12.0498854	-1.2242982	25.0582747	-4.1797655	48.6226286
-0.1737293	12.055951	-0.6702933	25.0694005	-1.6994487	48.625585
-0.2400201	12.0564182	-1.9368757	25.0822632	-0.2213687	52.105882
-0.2515075	12.0571053	-0.4763268	25.0870394	0.3564415	52.4073332
-0.2917031	12.0602059	-0.4124591	25.1296092	-3.7171471	52.4537301
-0.2497538	12.0619462	-0.8554051	25.1898511	-2.6658769	52.5612168
-0.235234	12.0674471	-0.875131	25.2777751	-3.0516521	52.5733957
-0.6734198	16.2825171	-4.8668484	32.062936	-4.6596633	52.5916038
-1.2011537	16.2919621	-3.8070836	32.2774069	-3.5227331	52.7169151
-1.4117868	16.2957412	-3.7041273	32.558519	-4.7201381	52.7376111
-0.7071557	16.3104169	-4.6223211	32.7482586	-3.211522	52.7600858
-1.2077944	16.3278117	-4.9038894	32.8445151	-1.9467082	55.6461888
-0.5884168	16.3301704	-3.6295861	32.8642094	-2.3711348	55.8850648
-0.0641375	16.335785	-4.4796474	36.197765	-2.0572016	55.9123034
-0.6497332	16.34294	-4.0538193	37.5258886	-3.1837891	55.9925392
-0.4901767	16.3680153	-4.727584	37.6079022	-3.2786228	56.0908796
-0.4448611	16.3749555	-2.8012967	37.8163192	2.6760975	56.0990834
-0.6099618	16.3775186	-3.5932084	39.8505682	-2.9935713	56.5165834
-0.5316564	20.732887	-2.2440638	39.8671388	-2.9386237	56.6811368

135

This list was then used to create a scatter plot as shown in Figure 9-6. From this figure it is obvious that there is are four clusters with large numbers of modal components, as illustrated in Figure 9-7, where these four clusters were marked and labeled. It appears that there are four dominant modal components in the signal with frequencies: 12 Hz, 16.3 Hz, 20.7 Hz and 25 Hz. To illustrate the number of occurrences in these clusters a histogram based on frequency components is shown in Figure 9-8.
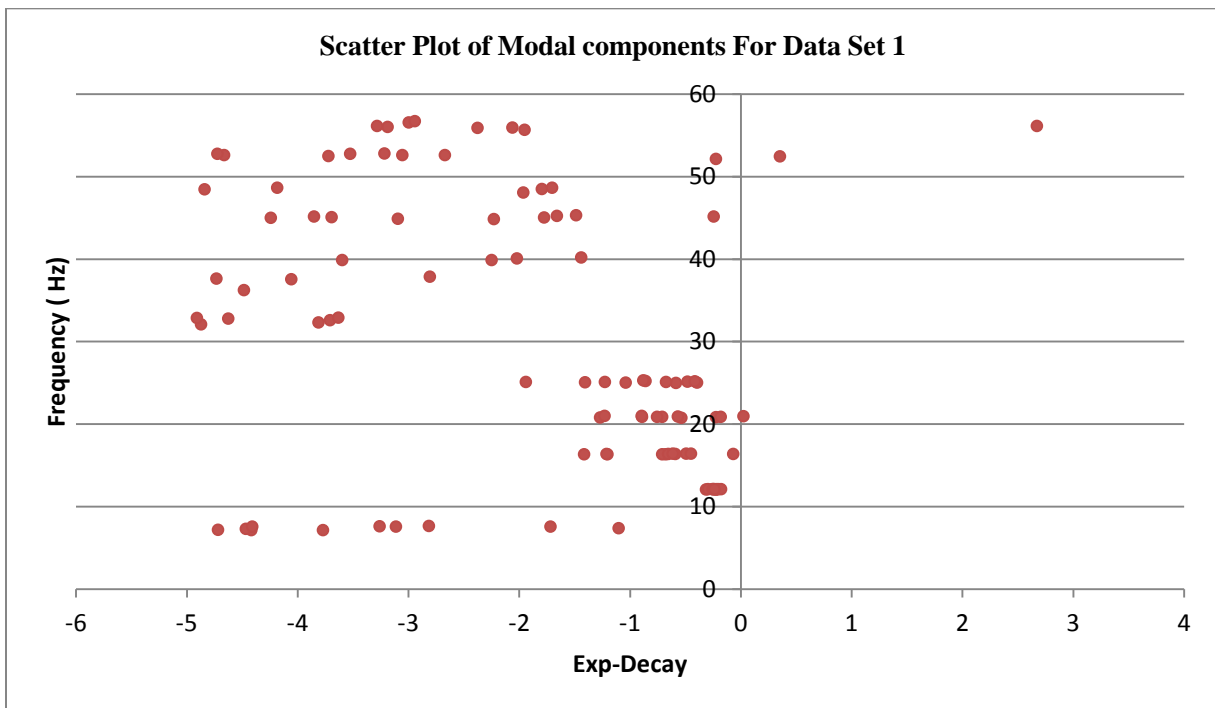

Figure 9-6 Scatter Plot of Constituent Modes of Data Set 1
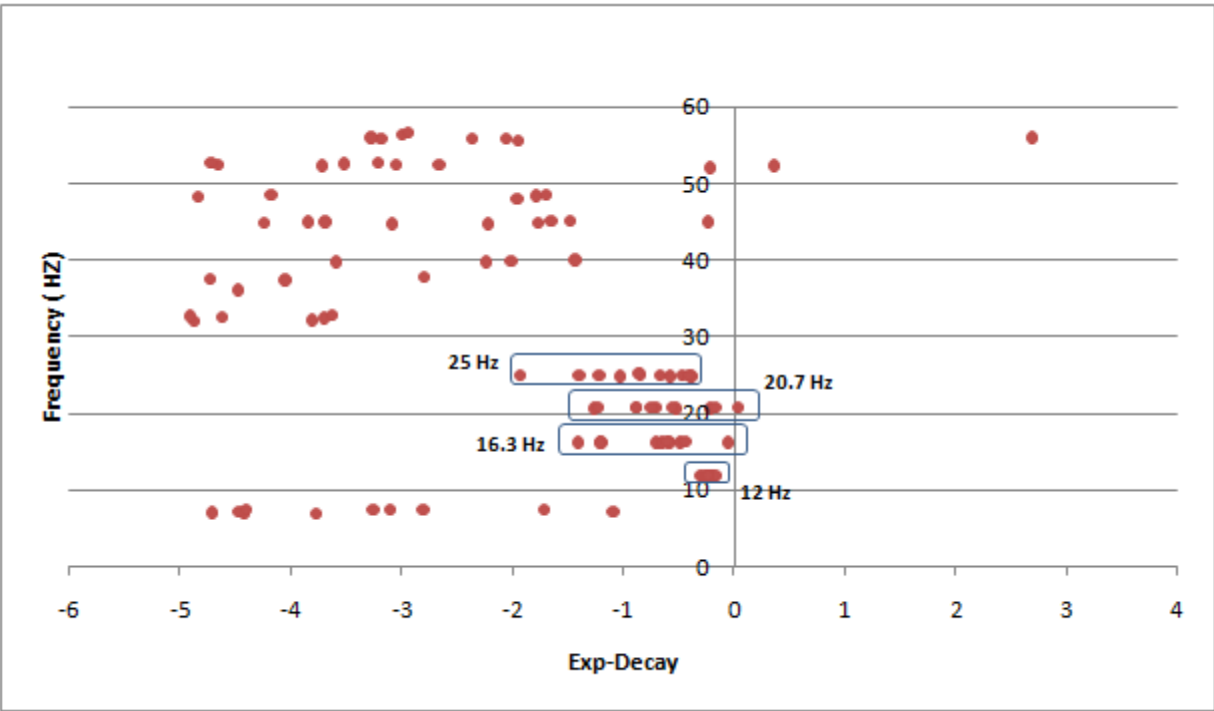
Figure 9-7 Scatter Plot of Constituent Modal Components with Major Clusters Demarcated to

Show the Four Dominant Modes
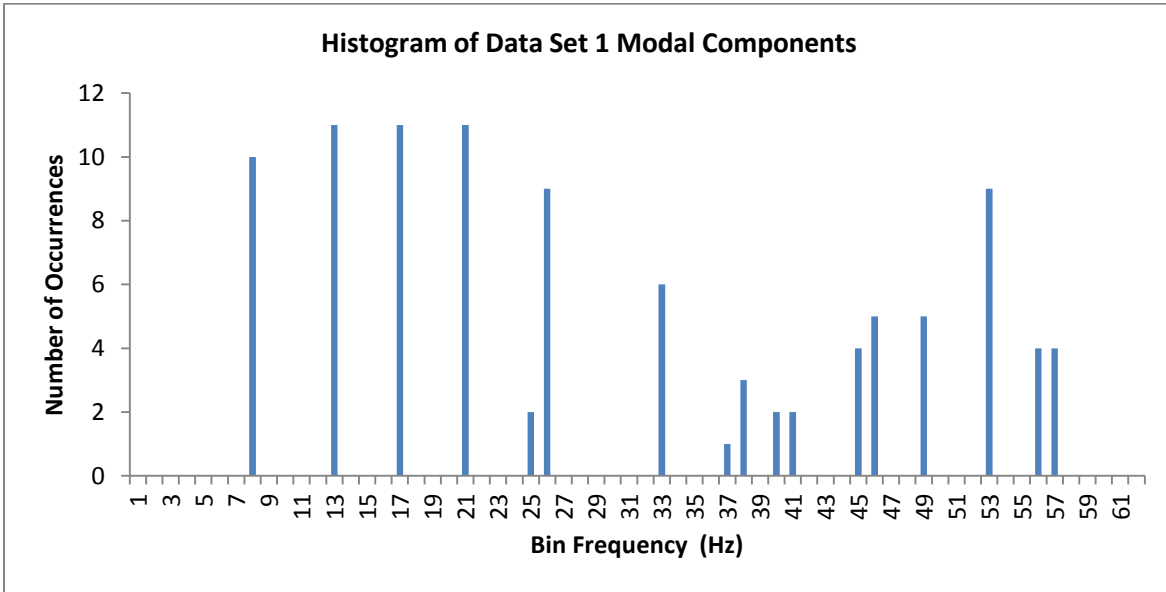
Figure 9-8. Histogram of Modal Components for Data Set 1 with Bin Width = 1 Hz

9.4 Analysis of Data Set 2

The above process was repeated on another measured instantaneous power signal, p(t), which consists of 30 seconds of measurement data. Just as in previous case, this data was filtered to remove the 180 Hz and other high frequency components. Shown in Figure 9-9 is a plot of the resulting waveform.
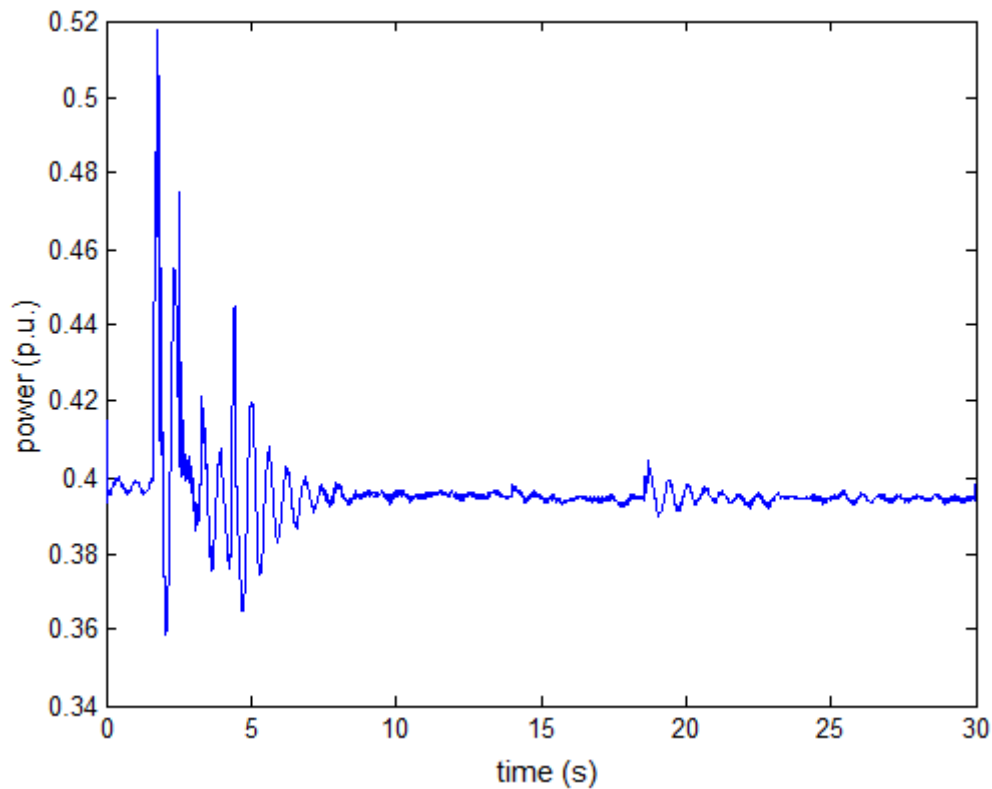
Figure 9-9 Plot of Filter p(t) signal from Data Set 2

After visually inspecting the data, a data window between 5.5 seconds and 6.5 seconds was chosen, shown in Figure 9-10, as the proper candidate for Prony analysis. Prony's method was then applied on this window, using the same algorithm parameters as used for data set 1 (numModes = 90 and nSkipSample = 5.) Shown in Figure 9-11 is a comparison of the specified signal and the reconstructed signal using the output modal list of Prony's method.

Figure 9-10 Plot of Proper Candidate Data Set for Prony's Method (Data Set 2)

Figure 9-11 A Plot of Comparison Between the Actual and Reconstructed Signal Using the

Output Modes of Prony's Method for Data Set 2

139

Shown in Table 9-6 are the first 20 constituent modes obtained from Prony's method. Note these are sorted in descending order of the LSE norms.

Table 9-6 Prony's Method's Output List of Constituent Modal Components for Data Set 2

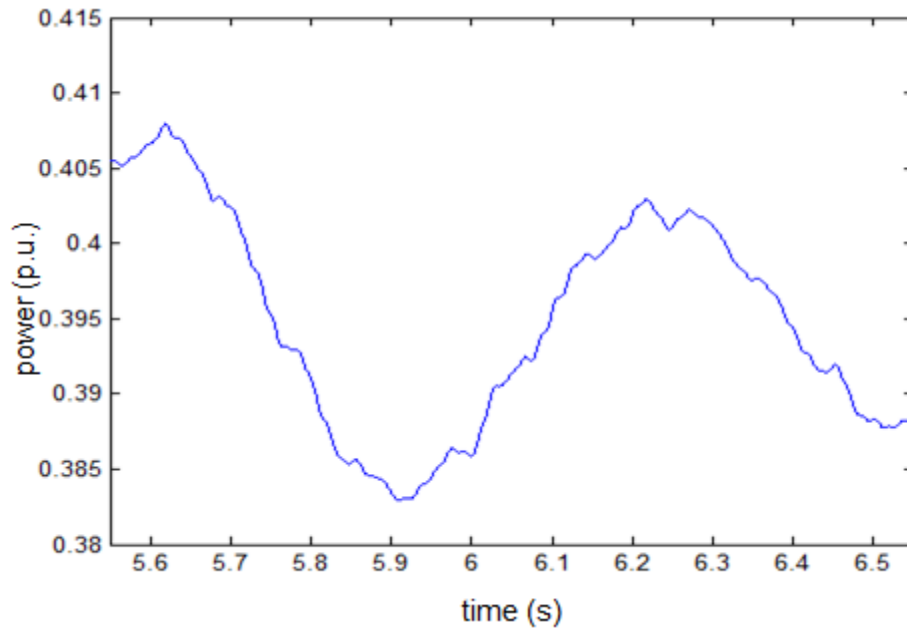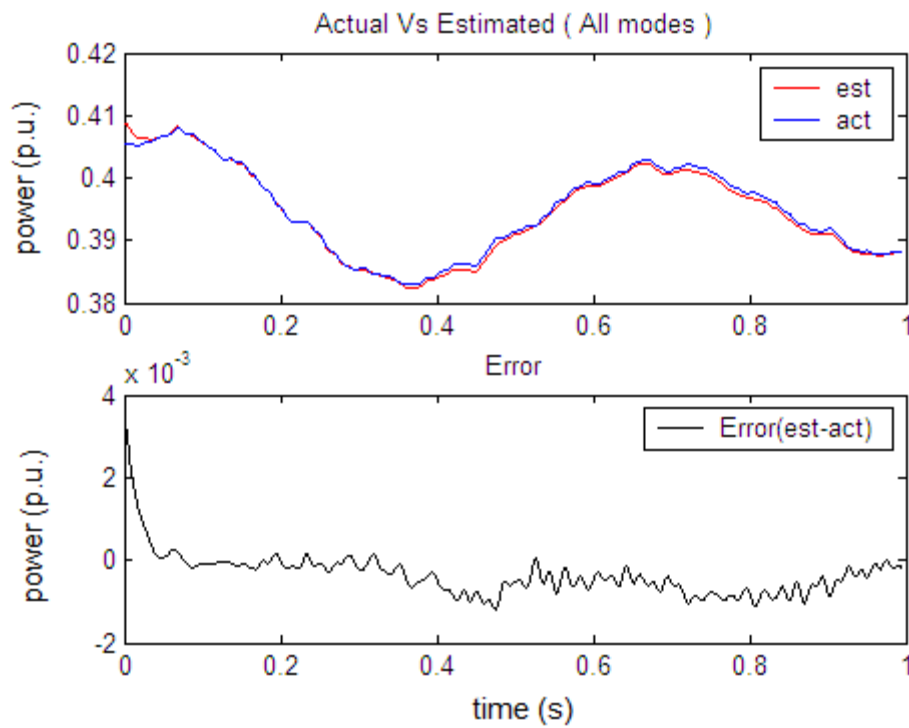| Mode #	LSE	Magnitude	Exp-Decay	Frequency(Hz)	Phase(Rad)
1	0.142834448	0.014368914	-0.8583511	1.5861547	-0.6056632
2	0.015434505	0.000837627	-0.4167396	12.0482712	0.4570315
3	0.014450656	0.001738426	-60.3963416	0	3.1415927
4	0.012976919	0.000968104	-15.3660889	50.958838	2.4137976
5	0.012738226	0.000274668	-1.1273558	25.1106227	1.2089022
6	0.012531351	0.000472737	-9.2393103	56.9428588	-2.827555
7	0.01251901	0.000348595	-6.6352855	43.1166366	0.9396941
8	0.012511692	0.000628562	-226.8675358	192	3.1415927
9	0.012493123	0.000226302	-0.4553859	21.1035697	-0.5255472
10	0.012452034	0.000123901	-4.7570831	47.119961	1.8736162
11	0.012438872	0.000271993	-3.3331461	52.8516535	-2.15545
12	0.012427474	0.000160298	-39.8492623	95.0812441	2.767976
13	0.012423201	0.000100095	-9.3272313	63.55788	1.7068752
14	0.01241987	0.000211142	-0.6739873	16.7001269	-0.261739
15	0.012418476	7.72883E-05	-5.2187667	67.0044016	2.4191549
16	0.012415291	6.00817E-05	-3.55913	29.0431211	1.086974
17	0.012399607	3.99114E-05	-20.1855681	115.7552143	2.8246925
18	0.012398451	7.39638E-05	-35.0501387	149.7066291	1.6086517
19	0.012395666	2.02879E-05	-6.8153595	79.0506098	-3.0683173
20	0.01239508	1.48799E-05	-11.7363145	111.638931	1.9637448

As discussed in the previous section, a selection criteria was applied to the entire list of constituent modes obtained from Prony's method to obtain the list of modes shown in Table 9-7.

Table 9-7 Selected List of Constituent Modes in the Signal Detected by Prony's Method

Magnitude	ExpDecay	Frequency (Hz)	Phase (rad)
6.00817E-05	-3.55913	29.0431211	1.086974
0.000211142	-0.6739873	16.7001269	-0.261739
0.000271993	-3.3331461	52.8516535	-2.15545
0.000123901	-4.7570831	47.119961	1.8736162
0.000226302	-0.4553859	21.1035697	-0.5255472
0.000274668	-1.1273558	25.1106227	1.2089022
0.000837627	-0.4167396	12.0482712	0.4570315

This process was repeated for a set of 14 sliding windows. The starting and ending position of each window was incremented by 0.05 seconds from one window to the next, with the final window beginning at 6.15 seconds and ending at 7.15 seconds. Each time Prony's method was applied to extract the constituent modes, the resulting output list was pruned according to parameters discussed in the previous section and stored in a separate list. Finally, the output list of 14 data windows were all combined together. As before, the exponential decay and frequency parameters were chosen and inserted into a scatter plot as shown in Figure 9-12
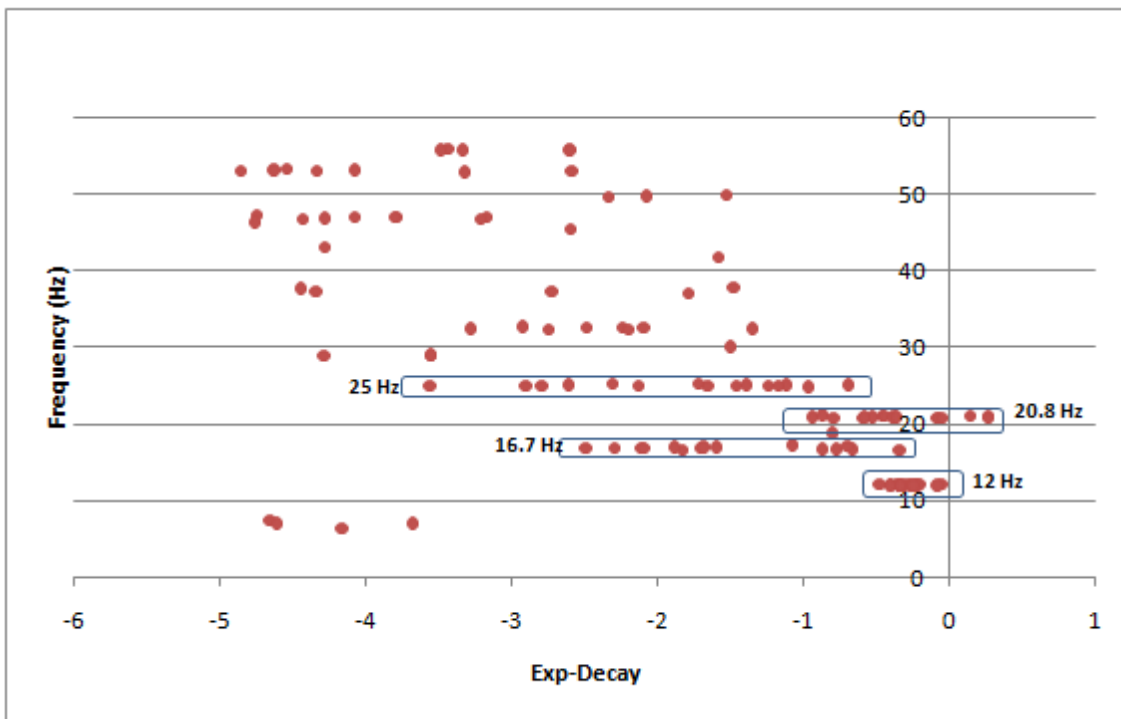
Figure 9-12 Scatter plot of Modal Components with Four Major Clusters Demarcated

Again, a histogram was plotted to identify the most frequent modes. Just as before, it was observed that there are four major clusters of modes as identified in Figure 9-13. It appears that there are four dominant modes with frequencies: 12 Hz, 16.7 Hz, 20.8 Hz and 25 Hz. in these clusters.
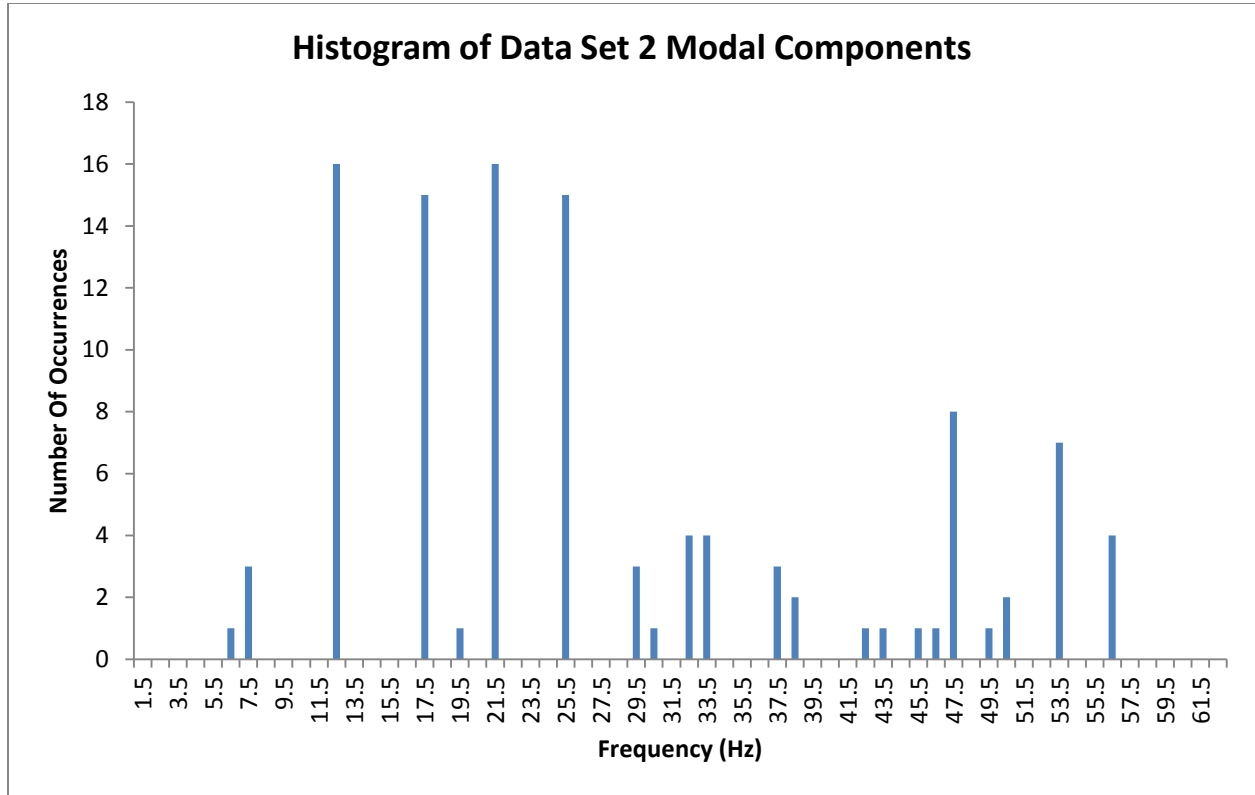
Figure 9-13 Histogram of Modal Components in Data Set 2 with Bin Width = 1 Hz

9.4 Comparison of Results and Analysis

Shown in the first two columns of table 9-8 are the lists of the four dominant modes extracted from the two given measurements. It appears that the results of both cases match very closely. Shown in the third column are the frequencies provided by the plant owner. As shown in

this table, the maximum percentage difference is less than 8 percent and the rest of the difference-percentages are under 4 percent. However, it is to be noted that these are differences, and not necessarily errors. There could be many reasons for these differences, including different operating conditions, i.e., the plant owner may have derived these figures based on design data.

Table 9-8 Results of Modal Decomposition using Prony's Analysis on the two data sets

Frequencies of Major Modal Constituents of Data Set 1 Signal	Frequencies of Major Modal Constituents of Data Set 2 Signal	Frequencies of the Shaft System Provided by the Plant Owner	Percentage Difference Between the Estimated (average) and Owner Specified Frequencies
12 Hz	12 Hz	13 Hz	7.69%
16.3 Hz	16.7 Hz	17 Hz	2.94%
20.7 Hz	20.8 Hz	21 Hz	1.19%
25 Hz	25 Hz	26 Hz	3.84%

This measurement data was obtained from a unit that had the STGS configuration shown in Figure 9-14, consisting of six rotor sections. This implies that this shaft system has five natural frequencies. However, we have found only 4 of the five frequencies: 12 Hz, 16.7 Hz, 20.8 Hz and 25 Hz. Prony's method was unable to detect and extract the fifth frequency. One of the reasons could be that there were too many non-linearities in the signal, in addition to noise in measurements, precluding Prony's method from detecting the fifth frequency. Another reason could be that the magnitude of disturbance was insufficient to excite the torsional modes significantly. However, a more probable reason could be the eigen behavior of the STGS system. Recall that all the analyses performed in Chapter 7 using right eigen vectors, participation factors and impulse response test, indicated that for typical STG shaft systems, the highest frequency

mode participates extremely weakly in the generator-section velocity state signal. This small magnitude signal, after passing through the generator stator & rotor circuits and the air-gap flux, gets even more attenuated, and thus appears indistinguishably small in the instantaneous power signal, p(t). The results obtained in this chapter appear to be consistent with the results of the analyses performed in Chapter 7 and lead to the hypothesis that HP rotor section velocity signal is a more superior candidate, compared to instantaneous power signal, for extracting the torsional modes of the steam turbine generator shaft system.
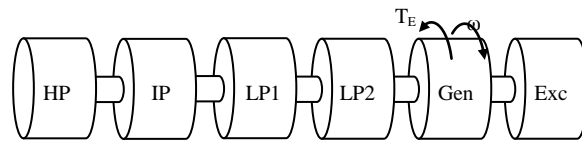
Figure 9-14 Steam Turbine Generator Shaft System Configuration of the Studied System

9.5 Conclusions

In this chapter, Prony's method was applied to extract the underlying modal constituents of actual instantaneous power measurements, p(t), of an actual STG unit. In the analyses of two separate p(t) signals of the same unit, it was found that there were four dominant modal components in the signal related to the STGS system. These frequencies matched closely (difference-percentage < 8%) those that were provided by the plant owner. It was known that the STGS system had six rotor sections, implying it had five natural frequencies. This meant that this procedure was not able to identify the fifth natural frequency of the STGS system. However, according to the analysis in Chapter 7 regarding eigen properties of typical STGS systems, this was to be expected. In that chapter it was found that the highest frequency mode always

144

participated very insignificantly in the generator velocity state, precluding it from being detected by Prony's method. This again emphasizes the previous finding that to estimate the shaft spring constants, it is highly recommended to use the HP rotor section velocity signal for modal decomposition.

CHAPTER 10

CONCLUSIONS

Over the past half century, power systems have grown tremendously which brought forth new problems in regard to shaft systems of steam turbine generator (STG) power plants (which contribute greater than 60 percent of generating capacity in the U.S.A.) interacting with long transmission lines consisting of series capacitors, causing potentially irreplaceable damage to these shaft systems. Current work presented here adds to a growing body of solutions and preventive measures developed by power industry professionals to address this problem by proposing a new methodology to estimate the shaft spring constants non-intrusively using measurement signals from the shaft systems.

This work uses Prony's method to identify the modal components in a given signal as it has many advantages over the FFT. The effect of various parameters of Prony's method - number of modes, number of samples and window position - have been thoroughly investigated. Also, an algorithm has been developed to reorder the resulting output modes of Prony's method to identify the power system modes.

In Chapters 6 and 7, a thorough analysis of four typical STG shaft systems presented in the literature using eigen analysis concepts and metrics, such a right eigen vectors and participation factors, was performed. Time domain simulations of impulse responses of the shaft systems have also been performed to further understand these LTI shaft systems' behavior. The purpose of this has been to bring forth the unique properties of STG shaft systems, with regards to the manner in which the modal components show up in different rotor velocity states. It has

been observed that high frequency modal components show up with lesser magnitudes in the generator and adjacent rotors section velocities relative to the high pressure (HP) turbine and adjacent rotor section velocities. It could be because the generator and adjacent rotors are considerably heavier than the HP and connected rotor sections. It has also been observed that all the modes show up well in the HP and connected rotor sections. This allows us options of choosing a proper rotor velocity signal to identify the modes. So far, the most suitable candidate for extracting modal components has been the HP rotor section velocity signal.

In Chapter 8 we have tested, using ATP simulation software, a fully connected IEEE-FBM model consisting of (1) an STG shaft system, (2) a generator d-q-o model and (3) an electrical network consisting of series capacitor, transmission line and infinite voltage source at the other end. After simulating a 20 millisecond ground fault disturbance on the line at the generator terminals, the resultant ring-down generator power output signal, p(t), and HP rotor velocity signal were analyzed using Prony's method. The results of the modal decomposition revealed that while four modes showed in the generator signal, all five modes show up in the HP velocity signal. Using the frequency values and specified rotor moment-of-inertia values, rotor shaft spring values were estimated using a non-linear Newton-Raphson based least squares algorithm, thus validating the developed algorithm.

An analysis of instantaneous power measurements, p(t), obtained from an STG unit, was presented in Chapter 9. The shaft system configuration consisted of six rotor sections, implying that it would have five natural frequencies. Prony's Method was applied, using the methodologies described in Chapters 3 and 5, to extract the underlying modal components. Four frequencies were identified from the list of the Prony's output modes by applying a simple selection criteria. Repeating this process on two separate data sets yielded a set of four frequencies that matched

closely with the manufacturer specified frequencies. However, it is be noted that the shaft system had six rotor sections, implying that it had five natural frequencies. Because the identification methodology was able to identify only four frequencies, it meant that it was unsuccessful in identifying the fifth frequency. But, this is not particularly surprising according to the analysis performed in Chapters 6 & 7. Recall that the mode corresponding to the highest natural frequency always participated very weakly in the generator and exciter rotor sections. It can be hypothesized that, in this case as well, the highest mode of this shaft system is participating very weakly in the generator section, thereby precluding it from being identified strongly in the instantaneous power, p(t), measurement signals.

In conclusion, an algorithm to estimate shaft spring constants non-intrusively using STG shaft measurements and an algorithm to reorder Prony's method's output modes have been presented in this work. Another significant contribution of this work has been in determining, after a thorough investigation of eigen properties of several steam turbine generator shaft systems, which of the non-intrusively available measurement signals is the best candidate to be used for extracting the shaft torsional modes. Taken together, these advances aim to assist the power engineer in designing better preventive measures and solutions to the complex and multifaceted subsynchronous resonance problem in power systems.

BIBLIOGRAPHY

[1]   IEEE Subsynchronous Resonance Working Group, "Terms, Definitions And Symbols For Subsynchronous Oscillations," IEEE Transactions on Power Apparatus and Systems, Vol. PAS-104, No. 6, June 1985.

[2]   M. C. Hall and D. A. Hodges, "Experience with 500 kV Subsynchronous Resonance and Resulting Turbine Generator Shaft Damage at Mohave Generating Station," IEEE Publication 76 CH1066-PWR. New York IEEE Press, 1976. pp 22-29.

[3]   IEEE Subsynchronous Resonance Working Group, "Proposed Terms And Definitions For Subsynchronous Oscillations," IEEE Transactions on Power Apparatus and Systems, Vol. PAS-99, No.2 March/April 1980.

[4]   IEEE Subsynchronous Resonance Task Force of the Dynamic System Performance Working Group, Power System Engineering Committee, "First benchmark model for computer simulation of subsynchronous resonance," IEEE Transactions on Power Apparatus and Systems, Vol. 96, No. 5, pp. 1565-1572, September 1977.

[5]   IEEE Subsynchronous Resonance Task Force of the Dynamic System Performance Working Group, Power System Engineering Committee, "Second benchmark model for computer simulation of subsynchronous resonance," IEEE Transactions on Power Apparatus and Systems, Vol. PAS-104, No. 5, pp. 1057-1066, May 1985.

[6]   Butler, J.W.; Concordia, C., "Analysis of Series Capacitors Application Problem", AIEE Transactions, Vol. 56, pp. 975-988, 1937.

[7]   Carter, G.K.; Concordia, C.;, "Negative Damping of Electrical Machinery", AIEE Transactions, Vol. 60, pp. 116-119, March 1941.

[8]   Ramey, D.G.; Sismour, A.C.; Kung, G.C.; , "Important Parameters in Considering Transient Torques on Turbine-Generator Shaft Systems," IEEE Transactions on Power Apparatus and Systems, vol.PAS-99, no.1, pp.311-317, Jan. 1980.

[9]   "Introduction to numerical analysis," by Hildebrand, F. B. New York, McGraw-Hill, pp. 457-462, 1956.

[10]   Hauer, J.F.; Demeure, C.J.; Scharf, L.L.; , "Initial results in Prony analysis of power system response signals ," IEEE Transactions on Power Systems, vol.5, no.1, pp.80-89, Feb 1990.

[11]   Kay, S.M.; Marple, S.L., Jr.; , "Spectrum analysis—A modern perspective," Proceedings of the IEEE , vol.69, no.11, pp. 1380- 1419, Nov. 1981.

[12]   G.R.B. Prony, "Essai experimental et analytic ...," J. l'Ecole Polytech. (Paris), vol. 1, pp. 24-76, 1795.

[13]   Kumaresan, R.; Feng, Y., "FIR Prefiltering improves Prony's method," IEEE Transactions on Signal Processing, Vol. 39, No. 3, pp. 736 – 741, March 1991.

[14]   Pitstick, G.M.; Cruz, J.R.; Mulholland, R.J., "A novel interpretation of Prony's method," Proceedings of the IEEE, Vol. 76, No. 8, pp. 1052 - 1053, August 1988.

[15]   "Subsynchronous Resonance in Power Systems," by Anderson, P.; Agrawal, B.; Ness, J.; IEEE Press, 1990.

[16]   "Power System Stability and Control," by Kundur, P. McGraw-Hill, 1993.

[17]   "Modern Control Theory," by Brogan, W.L.; Prentice Hall, 1990.

[18]   Kumaresan, R.; Tufts, D.W.; Scharf, L.L.; , "A Prony method for noisy data: Choosing the signal components and selecting the order in exponential signal models," Proceedings of the IEEE , vol.72, no.2, pp. 230- 233, Feb. 1984.

[19]   Zivanovic, R.; Schegner, P.; , "Pre-filtering improves Prony analysis of disturbance records," Developments in Power System Protection, 2004. Eighth IEE International Conference on , vol.2, no., pp. 780- 783 Vol.2, 5-8 April 2004.

[20]   J. V. Milanovic, "The influence of shaft spring constant uncertainty on torsional modes of turbogenerator," IEEE Transactions on Energy Conversion, Vol. 13, No. 2, June 1998.

[21]   Subsynchronous Resonance Working Group of the System Dynamic Performance Subcommittee, "Reader's Guide To Subsynchronous Resonance," IEEE Transactions on Power Systems. Vol. 7, No. 1, February 1992.

[22]   Katz, E.; Tang, J.; Bowler, C.E.J.; Agrawal, B.L.; Farmer, R.G.; Demcko, J.A.; Selin, D.A.; Cruz, C.; Sims, J.; , "Comparison of SSR calculations and test results," IEEE Transactions on Power Systems, vol.4, no.1, pp.336-344, Feb 1989.

[23] Members of the Bibliography Group of the Subsynchronous Resonance Task Force of the Dynamic Performance Working Group of the IEEE Power System Engineering Committee, "A bibliography for the study of subsynchronous resonance between rotating machines and power systems," Power Apparatus and Systems, IEEE Transactions on , vol.95, no.1, pp. 216- 218, Jan. 1976.

[24] Bibliography Group of the Subsynchronous Resonance Task Force of the Dynamic Performance Working Group of the IEEE Power Systems Engineering Committee.; , "First Supplement to a Bibliography for the Study of Subsynchronous Resonance Between Rotating Machines and Power Systems," IEEE Transactions on Power Apparatus and Systems, vol.PAS-98, no.6, pp.1872-1875, Nov. 1979.

[25] Bibliography Task Force of the Subsynchronous Resonance Working Group of the Dynamic System Performance Subcommittee of the IEEE Power Systems Engineering Committee, "Second Supplement to A Bibliography For the Study Of Subsynchronous Resonance Between Rotating Machines And Power Systems," IEEE Transactions on Power Apparatus and Systems, vol.PAS-104, no.2, pp.321-327, Feb. 1985.

[26] IEEE Subsynchronous Resonance Working Group, "Third Supplement to a Bibliography for the Study of Subsynchronous Resonance Between Rotating Machines and Power Systems," IEEE Transactions on Power Systems, vol.6, no.2, pp.830-834, May 1991.

[27] Iravani, M.R.; Agrawal, B.L.; Baker, D.H.; Bowler, C.E.J.; Farmer, R.G.; Hedin, R.A.; Larsen, E.H.V.; Tang, J.F. , "Fourth Supplement to a Bibliography for the Study of Subsynchronous Resonance Between Rotating Machines and Power Systems," IEEE Transactions on Power Systems, vol.12, no.3, pp.1276-1282, Aug 1997.

[28] G. C. Verghese, I.J. Perez-Arriaga, and F.C. Schweppe, , "Selective Modal Analysis with Applications to Electric Power Systems, PART I: Heuristic Introduction, Part II: The Dynamic Stability Problem," IEEE Transactions on Power Apparatus and Systems, vol.PAS-101, No. 9, pp.3117-3134, September 1982.